NUWC-NPT Technical Report 11,284
20 December 2001

Use of Quadratic Time-Frequency Representations to Analyze Cetacean Mammal Sounds

Antonia Papandreou-Suppappola
University of Rhode Island

Lynn T. Antonelli
NUWC Division Newport

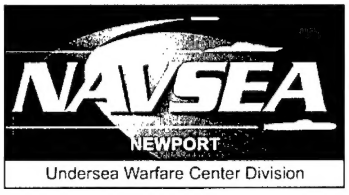

Naval Undersea Warfare Center Division
Newport, Rhode Island

PREFACE

This document contains the Technical Report for Task A, entitled "Use of Quadratic Time-Frequency Representations to Analyze Cetacean Mammal Sounds," for the project study "Biological Signal Analysis, Detection, and Estimation Using Quadratic Time-Frequency Representations," conducted from December 1996 through December 1997. This report was written and submitted to NUWC Division Newport by Antonia Papandreou-Suppappola of the Department of Electrical and Computer Engineering at the University of Rhode Island under NUWC contract number N66604-96-C-A336. The contract was initiated by Code 8215 in December 1996. Lynn T. Antonelli (Code 2141) acted as point of contact and coordinator for the documentation effort.

The study was initiated and commissioned by Kenneth M. Walsh (Code 824), James E. Ensminger (Code 8241), and Gerard H. Martineau (Code 8215) in response to Broad Agency Announcement 94-01A.

The SOUND Database of Marine Animal Vocalizations Structure and Operations, containing the cetacean mammal sounds analyzed in this manuscript, was provided by W. A. Watkins of the Woods Hole Oceanographic Institution.

The technical reviewer for this report was Kenneth M. Walsh (Code 824).

Reviewed and Approved: 20 December 2001

Paul M. Dunn
Head, Torpedo Systems Technology Department

REPORT DOCUMENTATION PAGE

Form Approved
OMB No. 0704-0188

1. AGENCY USE ONLY *(Leave blank)*	2. REPORT DATE	3. REPORT TYPE AND DATES COVERED
	12-20-01	

4. TITLE AND SUBTITLE

Use of Quadratic Time-Frequency Representations to Analyze Cetacean Mammal Sounds

5. FUNDING NUMBERS

6. AUTHOR(S)

Antonia Papandreou-Suppappola
Lynn T. Antonelli

7. PERFORMING ORGANIZATION NAME(S) AND ADDRESS(ES)

Naval Undersea Warfare Center Division
1176 Howell Street
Newport, RI 02841-1708

8. PERFORMING ORGANIZATION REPORT NUMBER

TR 11,284

9. SPONSORING/MONITORING AGENCY NAME(S) AND ADDRESS(ES)

10. SPONSORING/MONITORING AGENCY REPORT NUMBER

11. SUPPLEMENTARY NOTES

12a. DISTRIBUTION/AVAILABILITY STATEMENT

Approved for public release; distribution is unlimited.

12b. DISTRIBUTION CODE

13. ABSTRACT (Maximum 200 words)

The research presented in this report outlines the time-frequency characterization of mammalian click and whistle sounds. Analysis of the group delay structure of the mammalian vocal communication signals was matched to the appropriate quadratic time-frequency class for proper signal processing with minimal skewing of the results. The presented material includes a discussion of the recorded mammalian data recordings from the Woods Hole Oceanographic Institution, and a mathematical introduction into quadratic time-frequency classes, properties, and mathematical structure. This report determines the computational formulations appropriate for analyzing underwater mammalian vocal sounds using quadratic time-frequency representations. Once the proper quadratic time-frequency representations were identified for use in the analysis of clicks and whistles, a large selection of sound files was analyzed to characterize the time-frequency structure. The time duration and bandwidth of the clicks and whistles of various genera of dolphins and whales are presented in this report.

14. SUBJECT TERMS

Cetacean Mammal Sounds
Quadratic Time-Frequency Representation
Signal Processing

15. NUMBER OF PAGES
142

16. PRICE CODE

17. SECURITY CLASSIFICATION OF REPORT	18. SECURITY CLASSIFICATION OF THIS PAGE	19. SECURITY CLASSIFICATION OF ABSTRACT	20. LIMITATION OF ABSTRACT
Unclassified	Unclassified	Unclassified	SAR

EXECUTIVE SUMMARY

Quadratic time-frequency representations (QTFRs) are used in this report to analyze the time-frequency structure of cetacean mammal sounds. The nature of the signals and their properties were determined, and the types of QTFRs that are best suited for analyzing these biological signals based on their properties were investigated. Analysis of the group delay structure of the mammalian vocal signals was matched to the appropriate quadratic time-frequency class for proper signal processing with minimal skewing of the results.

This report includes a discussion of the mammalian data recordings from the Woods Hole Oceanographic Institution (WHOI) and an introduction to quadratic time-frequency classes, properties, and mathematical structure. It also determines the appropriate computational formulations for analyzing underwater mammalian vocal communications using quadratic time-frequency representations.

There are two main marine mammal sounds: short broadband clicks, which are the sounds used by dolphins and whales for echolocation, and whistles, which are continuous, frequency-modulated, narrowband signals used by dolphins and whales primarily for communication. It has been determined that the broadband clicks can be analyzed using constant time-shift covariant QTFRs, such as the Wigner distribution and the spectrogram, as these QTFRs are matched to signals with constant or linear group delay characteristics. On the other hand, it has been determined that whistles have characteristic time-frequency structures that may be matched to the generalized time shift preserved by the generalized warped QTFRs. These QTFRs can be obtained by appropriately warping the constant time-shift covariant QTFRs of Cohen's class or the affine class. For example, it was observed that long-finned pilot whales emit whistles with a characteristic hyperbolic time-frequency structure. Thus, they were well analyzed using hyperbolic QTFRs, since these QTFRs preserve hyperbolic group delay changes on the analysis signals. The hyperbolic QTFRs are obtained by hyperbolically warping corresponding QTFRs of Cohen's class. Due to the large sampling rate of the data provided by WHOI, the whistles extend over a large number of samples, resulting in a high computational intensity in the existing algorithms. Therefore, short-time time-frequency techniques and short-time adaptive time-frequency techniques were used to provide an adequate analysis of the whistles.

A large selection of sound files from the WHOI database was analyzed and the time-frequency structure characterized. The time duration and bandwidth of the clicks and whistles of various genera of dolphins and whales are provided in this report.

TABLE OF CONTENTS

Section		Page
	LIST OF ILLUSTRATIONS	iv
	LIST OF TABLES	v
	LIST OF ABBREVIATIONS AND ACRONYMS	v
	FOREWORD	vii
1	INTRODUCTION	1
2	MARINE MAMMAL SOUNDS	5
2.1	SOUND Database	5
2.2	Click and Whistle Sounds	11
3	CONSTANT TIME-SHIFT COVARIANT QTFRs	15
3.1	Cohen's QTFR Class	15
3.2	Affine QFTR Class	18
4	GENERALIZED TIME-SHIFT COVARIANT QTFRs	21
4.1	Generalized Warped Cohen's Class	23
4.2	Generalized Warped Affine Class	30
5	IMPLEMENTATION OF GENERALIZED TIME-SHIFT COVARIANT QTFRs, INCLUDING POWER CLASS QTFRs	37
6	TIME-FREQUENCY ANALYSIS OF SONAR CLICKS	41
7	TIME-FREQUENCY ANALYSIS OF WHISTLES	49
7.1	Spectrogram Analysis of Whistles	50
7.2	Other Cohen's Class QTFRs Analysis of Whistles	74
7.3	Hyperbolic Class QTFRs Analysis of Whistles	81
7.4	Power Class QTFRs Analysis of Whistles	86
7.5	Adaptive Optimal Kernal QTFR Analysis of Whistles	91
8	CONCLUSIONS	93
	REFERENCES	R-1
	APPENDIX – MATLAB PROGRAMS	A-1

LIST OF ILLUSTRATIONS

Figure **Page**

1 A Single Sonar Click of a White-Sided Dolphin from Data File 75001012.kay: (a) Signal in the Time Domain and (b) Fourier Transform of the Signal 12
2 The Single Sonar Click of the White-Sided Dolphin from Data File 75001012.kay from Figure 1: (a) Signal in the Time Domain, (b) Wigner Distribution, and (c) Spectrogram of the Click 44
3 Click Trains of a Long-Finned Pilot Whale from Data File 75010001.kay: (a) Signal in Time, (b) Wigner Distribution, and (c) Pseudo-Wigner Distribution 45
4 Spectrogram of Spotted Dolphin Whistles from Data File 83006023.kay Demonstrating Power and Linear (Rise and Fall) Time-Frequency Characteristics 51
5 Spectrogram of Spotted Dolphin Whistles from Data File 9002709d.kay Demonstrating Sinusoidal (Rise, Fall, and Rise) Time-Frequency Characteristics 52
6 Spectrogram of Long-Finned Pilot Whale Whistles from Data File 7703500w.kay Demonstrating Hyperbolic Time-Frequency Characteristics 53
7 Spectrogram of White-Sided Dolphin Whistles from Data File75001016.kay Demonstrating Linear Fall and Power Time-Frequency Characteristics 54
8 Spectrogram of Striped Dolphin Whistles from Data File 7200700f.kay Demonstrating Various Types of Time-Frequency Characteristics 55
9 Spectrogram of a Spotted-Dolphin Whistle from Data File 8300603c.kay 73
10 Direct SPWD of a Long-Finned Pilot Whale Whistle from Data File 7703500w.kay 77
11 Direct SPWD of a Spotted-Dolphin Whistle from Data File 9002709d.kay 78
12 Short-Time SPWD of a Spotted Dolphin Whistle from Data File 83035024.kay 80
13 Time-Frequency Analysis of the Sum of Two Hyperbolic Impulses: (a) Wigner Distribution, (b) Smoothed Pseudo-Wigner Distribution, (c) Altes Q-Distribution, and (d) Smoothed Pseudo-Altes Q-Distribution 82
14 Short-Time SPAD of Long-Finned Pilot Whale Whistles from Data File 77035011.kay 85
15 Power Class Analysis of Two Power Impulses: (a) Power Wigner Distribution with $\kappa = 3$, (b) Smoothed Pseudo-Power Wigner Distribution with $\kappa = 3$, (c) Wigner Distribution; (d) Affine Smoothed Pseudo-Wigner Distribution of a Two-Component Signal Consisting of Two Windowed Power Impulses with $\kappa = 3$, (e) Power Wigner Distribution with $\kappa = 3$, and (f) Smoothed Pseudo-Power Wigner Distribution with $\kappa = 3$ of a Two-Component Signal Consisting of Two Windowed Power Impulses with $\kappa = 4$ 87
16 Short-Time Power Smoothed Pseudo-Wigner Distribution with $\kappa = 2$ of a Spotted-Dolphin Whistle from Data File 83035024.kay 90
17 Short-Time Adaptive Radially Gaussian Kernel QTFR of Long-Finned Pilot Whale Whistles from Data File 77035011.kay 92

LIST OF TABLES

Table		Page
1	Example of a SOUND Database Record	6
2	Explanation of the Various Fields in the SOUND Database Record in Table 1	7
3	Marine Mammals and Some Typical Sounds Present in the Database Provided by the Woods Hole Oceanogaphic Institution	9
4	Examples of QTFR Classes from the Generalized Warped Cohen's Class with Associated Function $\xi(b)$, Generalized Time Shift $\tau(f)$, and Covariance Operators Corresponding to Equations (13) – (14) and (20) – (21)	30
5	Examples of QTFR Classes from the Generalized Warped Affine Class with Associated Function $\xi(b)$, Generalized Time Shift $\tau(f)$, and Covariance Operators Corresponding to Equations (13) – (14) and (29) – (30)	33
6	Comparison of Various Statistics of Marine Mammal Click Bursts	46
7	Comparison of Various Statistics of Marine Mammal Whistles	56
8	Whistle Statistics for Long-Finned Pilot Whales	68
9	Whistle Statistics for White-Sided Dolphins	69
10	Whistle Statistics for Spotted Dolphins	70
11	Whistle Statistics for Striped Dolphins	71

LIST OF ABBREVIATIONS AND ACRONYMS

AD	Altes Q-distribution
AOK	Adaptive optimal kernel
FFT	Fast-Fourier transform
GA	Generalized warped affine class
GC	Generalized Cohen's class
GWWD	Generalized warped Wigner distribution
LAF	Local autocorrelation function
PAD	Pseudo-Altes Q-distribution
PSPWD	Power smoothed psuedo-Wigner distribution
PWD	Pseudo-Wigner distribution
QTFR	Quadratic time-frequency representations
SPAD	Smoothed pseudo-Altes Q-distribution
SPEC	Spectrogram
SPWD	Smoothed pseudo-Wigner distribution
STAF	Short-time ambiguity function
WD	Wigner distribution
WHOI	Woods Hole Oceanographic Institution

FOREWORD

The research presented in this report outlines the time frequency characterization of mammalian click and whistle sounds. Analysis of the group delay structure of the cetacean mammalian vocal signals was matched to the appropriate quadratic time-frequency class for proper signal processing with minimal skewing of the results.

The time duration and bandwidth of the clicks and whistles of various genera of dolphins and whales are provided in this report. These data are useful as a comparison guide to other recorded sonar data to aid in the identification of recorded signals of unknown origin that may belong to ocean dwelling mammals via the time duration and bandwidth structure of the recorded signals. This information is also useful for areas where mammal sounds interfere with human-generated sonar transmissions and when noise characterization is required for signal processing. The characterized mammalian noise can be useful for signal processing algorithms that may benefit undersea acoustic communications. This report also outlines the correct mathematical formulations for analysis of underwater mammalian sounds with quadratic time-frequency representations.

USE OF QUADRATIC TIME-FREQUENCY REPRESENTATIONS TO ANALYZE CETACEAN MAMMAL SOUNDS

1. INTRODUCTION

The analysis of marine mammal sounds has been a subject of considerable interest for many years, as marine mammals such as dolphins and whales have complicated acoustics and communications systems. Marine mammal sound emissions can be classified into two broad categories: sonar signals called clicks, used for echolocation[1-7] and non-echolocation signals called whistles, used for communication.[8-14] Sonar clicks are short-duration, broadband, transient-like pulses that are used by marine mammals to detect, localize, discriminate, and recognize various objects of interest such as prey, obstacles, and predators.[1] Marine mammals emit bursts of clicks, called click trains, when searching for targets. The number of clicks and the time interval between clicks depend on various factors, such as the distance of interest, the difficulty in detecting a target, the presence or absence of a target of interest, and the mammal's expectation of finding a specific target. Whistles are long-duration, narrowband, frequency-modulated, continuous tonal sounds, often referred to as squeaks, squawks, and squeals,[1] that are not used for active sonar searches. They vary in frequency, duration, and in the shape of the whistle time-frequency structure, depending on the nature of the signal's frequency modulation. The whistles are used mainly for communication between the animals.

Marine mammal sounds are nonstationary signals, i.e., signals whose frequency content changes with time; thus, they have time-frequency characteristics that can be seen by a sonogram or spectrogram.[15-17] The Fourier transform is of limited use for the analysis of mammal sounds, since it does not provide easily accessible information about the time localization of a given frequency component in a signal. Analysis tools of choice are the quadratic time-frequency representations (QTFRs), as they are potentially capable of displaying the temporal localization of the signal's spectral components.[18-21] Some well-known QTFRs include the Wigner

distribution,[18, 22] the spectrogram,[23, 24] the Choi-Williams distribution,[20, 25] the scalogram,[19, 26] and the Altes-Q distribution.[27-29] Although many QTFRs have been proposed in the literature, no one QTFR exists that can be used effectively in all possible applications. The choice of a QTFR depends on a specific application as well as the QTFR properties that are desirable for that application. Thus, QTFRs may be classified based on various properties that they satisfy.

Some important QTFR properties include the covariance properties. A QTFR is said to satisfy a covariance property provided that the QTFR preserves (i.e., is covariant to) various time-frequency changes in the signal. For example, if a signal is shifted in time, then a QTFR satisfies the constant (nondispersive) time-shift covariance property if the QTFR preserves the exact time shift information of the signal.[18] A useful QTFR classification is based on the grouping of various covariance properties that the QTFRs satisfy. In particular, Cohen's class[20, 30] consists of QTFRs (with signal-independent kernels) that satisfy the constant time-shift and the constant frequency-shift covariance properties. The affine class QTFRs[19, 26, 31, 32] preserve constant time shifts and dilations (scale changes) on the analysis signal. The hyperbolic class QTFRs[29, 33-36] are covariant to hyperbolic time shifts and dilations on the signal. Other covariant QTFR classes include the power classes,[36-40] the exponential class,[41, 42] and the power exponential classes.[43, 44] These QTFR classes satisfy different covariance properties and, as a result, are used for different types of applications.

The aim of this project was to analyze the time-frequency structure of marine mammal sounds in order to ascertain the type and properties of the signal. Various types of QTFRs were investigated to determine those QTFRs that are best suited for analyzing biological signals based on the signal's properties. Some QTFRs types, for example Cohen's class of time-frequency shift covariant QTFRs, have been used to analyze dolphin whistles;[17, 45] however, this report provides analysis of other types of QTFRs that match the characteristic time-frequency structure of marine mammal sounds to a particular group delay curve in the time-frequency plane. The MATLAB code for some of the QTFRs already exists, such as the code for some of Cohen's class, affine class, and hyperbolic class QTFRs, and new MATLAB code was written for those QTFRs that are considered well matched for analysis of marine mammal sounds. The results are summarized in the following sections.

This report is organized as follows: Section 2 describes the marine mammal sound data files provided by the Woods Hole Oceanographic Institution (WHOI)[46] and provides the MATLAB code necessary to access the data for processing. Section 3 discusses some well-known QTFR classes (Cohen's class and the affine class) that preserve constant time shifts on the analysis signal. The constant time-shift covariant QTFRs, including the Wigner distribution and the spectrogram, are ideal for analyzing signals with constant or linear time-frequency characteristics, such as dolphin and whale clicks. Section 4 presents the generalized time-shift covariant QTFR classes that preserve the signal's changes in group delay. These QTFRs include hyperbolic QTFRs, such as the Altes Q-distribution, and power QTFRs, such as the power Wigner distribution that are better matched to the frequency-modulated narrowband whistles of dolphins and whales. Section 5 describes the implementation technique of the generalized time-shift covariant QTFRs, such as power class QTFRs, using the warping approach. Section 6 provides an analysis of sonar clicks and click trains. Clicks can be successfully analyzed using Cohen's class QTFRs, such as the Wigner distribution and its smoothed versions, due to the click's broadband nature. Section 7 analyzes various dolphin and whale whistles, and provides tables to summarize the results.

Whistles may be matched to hyperbolic class QTFRs and power class QTFRs depending on their characteristic time-frequency structure. As the sampling rate of the sounds provided is relatively large, the long-duration whistles consist of many samples; as a result, the present algorithms developed to compute hyperbolic and power QTFRs are not computationally efficient. Thus, short time-frequency techniques were developed to analyze longer sections of the data in an on-line fashion for both hyperbolic and power QTFRs.

2. MARINE MAMMAL SOUNDS

2.1 SOUND DATABASE

The marine mammal sounds analyzed in this report were provided by WHOI's SOUND database. This database contains descriptive information about each of the sound recordings and is accompanied by a set of digital sound-cut files whose filenames match the text database record. These cuts are sequences of sound from the repertoire of vocalizations of the different species of marine mammals that are selected from the original underwater recordings and are digitized. The digitized sound cuts are stored as independent files in the tapes provided, and are accompanied by an ASCII file that contains the corresponding database records. The organization of the database records in various fields, together with the SOUND database field description, is provided in the Woods Hole Oceanographic Institution Technical Report[1] WHOI-92-31,* entitled "SOUND Database of Marine Animal Vocalizations Structure and Operations," by W. A. Watkins, K. Fristrup, M. A. Daher, and T. Howald.[46] Thus, for each digitized file, there is information regarding, for example, the sample rate, the cut (record) size, the identification of the vocalizing mammal, and the species code of the mammal. Similar indexing information is also included in the first 512 bytes of each file. An example of a record file from the SOUND database is provided in table 1. The record chosen is 72007001.kay, which consists of clicks and whistles from striped dolphins (Stenella coeruleoalba). Also present in the record is ambient noise from the ship or from ice (transient X), and the other species present during the recording (sperm whales (Physeter catodon)). An explanation of the various fields in the record is given in table 2. Additional information[46] on the structure of the database, with a listing of species, common mammal names, and geographical locations of the recordings are also provided in the report.

*Two additional Woods Hole Oceanographic Institution Technical Reports, WHOI-92-04[47] and WHOI-94-13,[48] were also available for reference.

Table 1. Example of a SOUND Database Record

Record 72007001.kay
RN 72007001
CU 1063 B7:00.000 18:00.692
NC 41B
SR 166666
CS 1.918
PL Pemtek 301/ K-H L0.02 H50.0
SC OTF
GS Stenella coeruleonalba BD15C
; Transient X
GA ANWBD15C ANWX
OD 4-Aug-1972 BD15C X
; AugBD15C 1972BD15C
; AugX 1972X
NT BD15C X N37 42' W73 01'. Clicks and whistles. Water splashes.
OS Physeter catodon BA2A
NA 50 + BD15C
GB Delaware BD15C X
GC N37BD15C W073BD15C
; N37X W073X
AU WAW

Table 2. Explanation of the Various Fields in the SOUND Database Record in Table 1

Field Label	Example
RN 72007001	Retrieval Number of Record (Year/Tape#/Cut#) Year: 1972/ Tape #: 007/ Cut #: 001
CU 1063 B7:00.000 18:00.692	Cue or time (min:sec) on tape at signal end, (B) analyzer buffer size (min:sec), and decimal time (sec) from the start of the Kay buffer to the cursor at the beginning of the sound.
NC 41B	# of channels recorded (first digit). # of channels multiplexed (second digit), Channel ID letters.
SR 166666	Sample rate (Hz).
CS 1.918	Cut size (sec).
PL Pemtek 301/K-H L0.02 H50.0	Playback recorder/filter type settings in kHz, L=low (for HP), H=high (for LP).
SC OTF	Signal class (S=Signature, M=Mimic, V=Variant, D=Deletion, U=Uncharacteristic, C=Calf), quality (1 to 5-best). O=Overlap in T (time) or F (frequency)
GS Stenella coeruleoalba BD15C ; Transient X	Genus and species of vocalizing animal, scientific names, species code.
GA ANWBD15C ANWX	Geographic location area code (first 3 letters), species code.
OD 4-Aug-1972 BD15C X ; AugBD15C 1972BD15C ; AugX 1972X	Observation date for original, species code, e.g., for BD15C, month=August, year=1972.
NT BD15C X N37 42' W73 01'. Clicks and whistles. Water splashes.	Species code, Comments, Recording detail.
OS Physeter catodon BA2A	Other species present, species codes.
NA 50 + BD15C	Number of animals vocalizing, species codes.
GB Delaware BD15C X	Geographical location area name, species code.
GC N37BD15C W073BD15C ; N37X W073X	Geographical location latitude (N or S and 2 digits) Geographical location longitude (E or W and 3 digits), species codes.
AU WAW	Author, originator of recording.

In order to easily access the various types of marine mammal sounds from the SOUND database for analysis, a shorter, simplified database was created for easier access to the required information. For each digitized data record chosen, this database contains the retrieval number of the record and the various types of sounds present, together with the common names and species codes of the marine mammals that created the sounds. For example, the entry in the new database for the record in table 1 that corresponds to striped dolphin sounds is simply:

72007001.kay – Striped dolphin BD15C, transient X
(other species: sperm whale BA2A)
Clicks and whistles. Water splashes.

Based on the simplified database, the main marine mammals present in the sound cuts were grouped together with some types of recorded sounds, as outlined in table 3. Some of the more interesting artifacts in the data include a 12-kHz pinger, water splashes and droplets, reverberation, ship engine noise, and hydrophone bumps. It is also possible to audibly observe the data and to hear the time-frequency structure of the whistles that are present. In order to access the data from the digitized files, a MATLAB function (see section A.1 in the appendix) was written to extract the header of each file and read the data.

Table 3. Marine Mammals and Some Typical Sounds Present in the Database Provided by the Woods Hole Oceanographic Institution

Striped Dolphin (Stenella coeruleoalba) Other mammal present: Sperm Whale (Physeter catodon)
• Clicks and whistles. Water splashes.
• Clicks and whistles.
• Clicks, pulsed clicks, and whistles.
• Clicks and whistles. Water droplet.
• Clicks and whistles. About 4 sp. whale clicks present on cut.

White-Sided Dolphin (Lagenorhynchus acutus) Other mammal present: Finback Whale (Balaenoptera physalus)
• Clicks, pulsed click burst 12-kHz pinger present.
• Clicks, pulsed click burst.
• Clicks.
• Clicks and whistles.
• Clicks and whistles. Reverberation.
• Clicks, pulsed clicks. Reverberation.
• Clicks and a whistle. Maruffa ship noise-crack.
• Clicks and 3 whistles. Reverberation.
• Clicks. Reverberation present.
• Clicks, pulsed clicks, and a whistle.

Spotted Dolphin (Stenella attenuata)
• Whistle. Water splash.
• Clicks.
• Whistle and clicks.
• Clicks and whistle. Water splash.
• Clicks, pulsed clicks, and whistle.
• Clicks, pulsed clicks, and whistle.
• Clicks; pulsed clicks.

Table 3. Marine Mammals and Some Typical Sounds Present in the Database Provided Provided by the Woods Hole Oceanographic Institution (Cont'd)

Spotted Dolphin (Stenella attenuata) Other mammals present: Humpback Whale (Megaptera novaeangliae) and Sperm Whale (Physeter catodon)
• Many overlapping clicks; whistle.
• Ship's engine noise throughout.
• Many overlapping clicks, ship.
• Many overlapping clicks; pulsed clicks; whistle engine.

Long-Finned Pilot Whale (Globicephala melaena) Other mammal present: Sperm Whale (Physeter catodon)
• Fast click series.
• Fast click series. Ship noise (clunk).
• Clicks and whistles. Water splash.
• Clicks and whistles.
• Clicks, pulsed clicks, and whistles.
• Clicks, burst pulsed clicks, and whistles.
• Sperm whale clicks. Pilot whale clicks and whistles. Hydrophone bumps.
• Pilot whale clicks and whistles. Hydrophone bumps.
• Sperm whale clicks. Pilot whale clicks, pulsed clicks, and whistles. Splashes.
• Sperm whale clicks – skipped beats. Pilot whale clicks and whistles.
• Pilot whales – clicks, fast series of clicks, and whistles.
• Whistles.
• Chirps, whistles. Hydrophone bumps.
• Whistles. Hydrophone bumps.
• Chirps.
• Whistles. Water splash.
• Whistles and clicks.
• Whistles, pulsed clicks, chirps. Hydrophone bumps.
• Chirps; pulsed clicks.

2.2 CLICK AND WHISTLE SOUNDS

Time-frequency techniques were used in this report to analyze clicks and whistles that were present in the data provided by WHOI. These were the main sounds produced by dolphins and whales; some characteristics of the sounds are given below.

- **Clicks**: Clicks are sonar signals that are used by marine mammals for echolocation.[1-7] Using its active and passive sonar capabilities in the form of click sounds, a marine mammal such as a dolphin or a whale can effectively probe its underwater environment for the purpose of navigation, obstacle and predator avoidance, and prey detection. Clicks consist of short-duration, broadband, transient-like pulses that are used by marine mammals to detect, localize, discriminate, and recognize various objects of interest such as prey, obstacles, and predators. Experiments have shown that a click has a short duration of 40 – 600 μs and a 3-dB bandwidth of 4 – 60 kHz, depending on the species of the marine mammal.[1] For example, the Pacific bottlenose dolphin has a 3-dB bandwidth of 30 – 60 kHz. As the data sampling rate is 166.666 kHz for the data provided, the broadband clicks extend over the full bandwidth of the data. Marine mammals emit bursts of clicks, called click trains, when searching for targets. The number of clicks and the time interval between clicks depend on various factors, such as the distance of interest, the difficulty in detecting a target, the presence or absence of a target of interest, and the mammal's expectation of finding a specific target. For example, it has been recorded that for the Atlantic bottlenose dolphin, the lag time between clicks ranged from 2.5 ms to 20 ms for a target range of 0.4 m to 40 m.[1] An example of a single sonar click in the time domain of a white-sided dolphin from data file 75001012.kay is shown in figure 1(a). The click occurs at approximately 1.2396 s and has a duration of about 60 μs. The Fourier transform (frequency domain) of the data segment is shown in figure 1(b), where the spectrum has large magnitude values over a broad range of frequencies. Indeed, the click is of short duration and is relatively broad band.

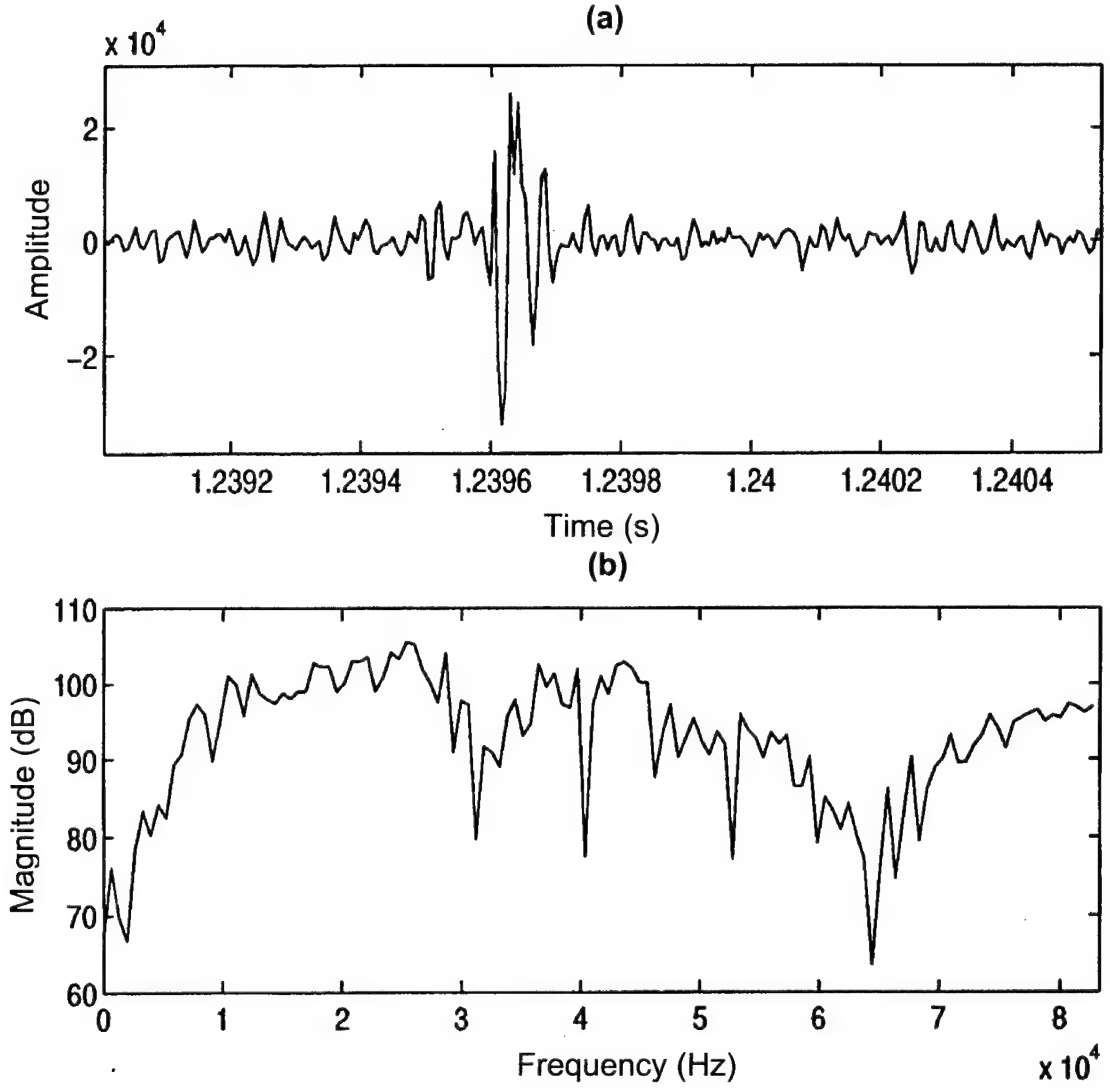

Figure 1. A Single Sonar Click of a White-Sided Dolphin from Data File 75001012.kay: (a) Signal in the Time Domain and (b) Fourier Transform of the Signal

- **Whistles:** Whistles are non-echolocation signals that are predominantly emotional and communication sounds.[8-14] They are long-duration, narrowband, frequency-modulated, continuous tonal sounds that are not used for active sonar searches. Whistles vary in frequency, duration, and in the shape of the whistle time-frequency structure depending on the nature of the signal's frequency modulation. For example, the frequency range of the dolphin whistles varies from 5 kHz to 15 kHz, and their duration varies from 0.5 s to 2 s. The whistles are used mainly for communication between the mammals in order to establish vocal contact. There are disputes as to whether each signature whistle identifies one animal from another. Studies have shown that dolphins in isolation have a characteristic signature whistle. When dolphins are in groups, however, they make various types of whistles, as they may have the ability to mimic each other's signature whistle.[9] The frequency modulation in the whistle has a large variation between the different mammals, as the dominant frequency as a function of time changes in various ways. The characteristic whistle time-frequency structure may show a rise or a fall in frequency, it may be flat (no change in frequency), it may be falling hyperbolically (as 1/frequency), or it may be changing sinusoidally or as a function of some power.[13] In many cases, the time-frequency structure may consist of a combination of various frequency modulation changes. As a result, the whistle's group delay time-frequency structure may change from mammal to mammal. Various classes of quadratic time-frequency representations are examined in this report for use as analysis tools for clicks and whistles.

3. CONSTANT TIME-SHIFT COVARIANT QTFRS

3.1 COHEN'S QTFR CLASS

A QTFR of a signal *x(t)*, with Fourier transform defined as $X(f) = \int_{-\infty}^{\infty} x(t)e^{-j2\pi tf}dt$, is a two-dimensional function of time *t* and frequency *f* denoted as $T_X(t, f)$. Cohen's class[20, 30] contains all QTFRs, denoted as $T_X^{(C)}(t, f)$ (the superscript *(C)* in the QTFR indicates that the QTFR is a member of Cohen's class), that satisfy the time-shift covariance and the frequency-shift covariance properties.[18] The time-shift covariance property is defined as

$$(S_\eta X)(f) = e^{-j2\pi\eta f}X(f) \Rightarrow T_{S_\eta X}^{(C)}(t,f) = T_X^{(C)}(t-\eta,\ f), \tag{1}$$

where S_η is an operator that causes the signal to be shifted in time by an amount η, and the double arrow implies the transformation from the analysis signal to the QTFR. Note that $T_{S_\eta X}^{(C)}(t, f)$ stands for $T_Y^{(C)}(t, f)$, with $Y(f) = (S_\eta X)(f)$. Thus, equation (1) states that if a signal $X(f)$ is time-shifted by an amount η, then a Cohen's class QTFR $T_X^{(C)}(t, f)$ is also shifted along the time axis by the same amount $T_X^{(C)}(t-\eta, f)$. The frequency-shift covariance property is defined as

$$(M_\nu X)(f) = X(f-\nu) \Rightarrow T_{M_\nu X}^{(C)}(t,f) = T_X^{(C)}(t, f-\nu), \tag{2}$$

where M_ν is an operator that causes the signal to be shifted in the frequency domain. Both the time-shift and frequency-shift covariance properties are important in applications where the signal needs to be analyzed at all time-frequency points with fixed time-frequency resolution. As a result, the QTFRs in Cohen's class exhibit analysis characteristics that do not change with time and frequency (constant bandwidth analysis), and preserve the signal's time and frequency shifts. This is important in applications such as speech analysis, narrowband Doppler systems, and multipath environments.

Based on these two covariance properties, any member of Cohen's class can be written as

$$T_X^{(C)}(t,f) = \int_{-\infty}^{\infty}\int_{-\infty}^{\infty}\Gamma_T^{(C)}(f-f_1,\ f-f_2)X(f_1)X^*(f_2)e^{j2\pi t(f_1-f_2)}df_1 df_2, \tag{3}$$

$$= \int_{-\infty}^{\infty}\int_{-\infty}^{\infty}\Phi_T^{(C)}(f-\hat{f},\ \nu)U_X(\hat{f},\nu)e^{j2\pi t\nu}d\hat{f}\,d\nu, \tag{4}$$

where $\Phi_T^{(C)}(f,\ \nu) = \Gamma_T^{(C)}\left(f-\frac{\nu}{2},\ f+\frac{\nu}{2}\right)$ is a two-dimensional function (or kernel) that uniquely characterizes the Cohen's class QTFR $T^{(C)}$, and the signal product is defined as

$$U_X(f,\ \nu) = X\left(f+\frac{\nu}{2}\right)X^*\left(f-\frac{\nu}{2}\right).$$

The Wigner distribution[18, 22] is an important member of Cohen's class, as it satisfies many desirable QTFR properties. It is defined as

$$WD_X(t,f) \triangleq \int_{-\infty}^{\infty}X\left(f+\frac{\nu}{2}\right)X^*\left(f-\frac{\nu}{2}\right)e^{j2\pi t\nu}d\nu = \int_{-\infty}^{\infty}U_X(f,\nu)e^{j2\pi t\nu}d\nu, \tag{5}$$

and has the kernel $\Phi_{WD}^{(C)}(f,\ \nu) = \delta(f)$ in equation (4). The Wigner distribution exhibits high time-frequency localization for signals such as sinusoids, impulses, and linear chirps. However, due to its quadratic nature, the Wigner distribution suffers from interference or cross terms when multicomponent signals are analyzed. Cross terms may impede signal analysis depending on the application. In particular, the Wigner distribution of an N component signal $X(f) = \sum_{i=1}^{N}X_i(f)$ is given by

$$WD_X(t,f) = \sum_{i=1}^{N}WD_{X_i}(t,f) + 2\sum_{p=2}^{N}\sum_{q=1}^{p-1}Re\{WD_{X_p,X_q}(t,f)\}, \tag{6}$$

where $WD_{X_p,\,X_q}(t,f)$ is the cross-Wigner distribution of $X_p(f)$ and $X_q(f)$ (defined in equation (5)), with X and X^* replaced by X_p and X_q^*, respectively.[49] Thus, the Wigner distribution of the multicomponent signal $X(f)$ consists of the sum of N auto terms and the sum of $\frac{N(N-1)}{2}$ cross terms.

In practical applications, the cross terms in equation (6) can be attenuated by smoothing the Wigner distribution. Note that any member of Cohen's class can be written as a smoothed Wigner distribution using

$$T_X^{(C)}(t,f) = \int_{-\infty}^{\infty}\int_{-\infty}^{\infty}\psi_T^{(C)}(t-\hat{t},f-\hat{f})\,WD_X(\hat{t},\hat{f})\,d\hat{t}\,d\hat{f}\,, \tag{7}$$

where $\psi_T^{(C)}(t,f) = \int_{-\infty}^{\infty}\Phi_T^{(C)}(f,v)e^{j2\pi tv}dv$. Thus, the cross terms in equation (6) can be reduced by choosing the kernel $\psi_T^{(C)}(t,f)$ in equation (7) accordingly. Specifically, the spectrogram[23, 24] $SPEC_X(t,f)$ uses an analysis window $\Gamma(f)$ to reduce cross terms. The kernel of the spectrogram in equation (7) is the Wigner distribution of the smoothing window $\Gamma(f)$, i.e., $\psi_{SPEC}^{(C)}(t,f) = WD_\Gamma(-t,-f)$. Inserting this kernel in equation (7), the spectrogram can be defined as a smoothed Wigner distribution

$$SPEC_X(t,f) = \int_{-\infty}^{\infty}\int_{-\infty}^{\infty}WD_\Gamma(\hat{t}-t,\hat{f}-f)\,WD_X(\hat{t},\hat{f})\,d\hat{t}\,d\hat{f} = \left|\int_{-\infty}^{\infty}X(\hat{f})\Gamma^*(\hat{f}-f)e^{j2\pi t\hat{f}}d\hat{f}\right|^2. \tag{8}$$

Note that equation (8) shows that the spectrogram can also be defined as the squared magnitude of the short time-Fourier-transform, linear time-frequency representation.[18]

As the smoothing kernel of the spectrogram is the Wigner distribution of a window, the spectrogram cannot simultaneously provide a small amount of smoothing in both the time and frequency directions. On the other hand, the smoothed pseudo-Wigner distribution uses two windows to provide independent time and frequency smoothing. The smoothed pseudo-Wigner distribution $SPWD_X(t, f)$ uses a separable kernel $\psi^{(C)}_{SPWD}(t, f) = g(t)H(f)$ in equation (7), where $g(t)$ and $H(f)$ are two analysis windows; it is defined as

$$SPWD_X(t,f) = \int_{-\infty}^{\infty}\int_{-\infty}^{\infty} g(t-\hat{t})\,H(f-\hat{f})\,WD_X(\hat{t},\hat{f})\,d\hat{t}\,d\hat{f}. \tag{9}$$

3.2 AFFINE QTFR CLASS

The affine class[19, 26, 31, 32] contains all QTFRs ($T^{(A)}_X(t, f)$) that satisfy the time-shift covariance property in equation (1), and the scale covariance property defined as

$$(C_a X)(f) = \frac{1}{\sqrt{|a|}} X\left(\frac{f}{a}\right) \Rightarrow T^{(A)}_{C_a X}(t,f) = T^{(A)}_X\left(at, \frac{f}{a}\right). \tag{10}$$

The scale covariance property is important for multiscale analysis, scale covariant systems, the wideband Doppler effect, and detecting short-duration transients. Thus, affine QTFRs are used in applications such as image enlargement and data compression, where it is desirable to preserve dilations or scale changes on the analysis signal. Many affine QTFRs are used for constant-Q time-frequency analysis, where the analysis bandwidth is proportional to the analysis frequency. This provides an alternative to the constant bandwidth analysis achieved by Cohen's class QTFRs.

Based on the time-shift covariance property and the scale covariance property, any affine class QTFR can be written as

$$T_X^{(A)}(t,f) = \frac{1}{|f|}\int_{-\infty}^{\infty}\int_{-\infty}^{\infty}\Gamma_T^{(A)}\left(\frac{f_1}{f},\frac{f_2}{f}\right)X(f_1)X^*(f_2)e^{j2\pi t(f_1-f_2)}df_1 df_2, \tag{11}$$

$$= \frac{1}{|f|}\int_{-\infty}^{\infty}\int_{-\infty}^{\infty}\Phi_T^{(A)}\left(-\frac{\hat{f}}{f},\frac{\nu}{f}\right)U_X(\hat{f},\nu)e^{j2\pi t\nu}d\hat{f}\,d\nu, \tag{12}$$

where $\Phi_T^{(A)}(b,\beta) = \Gamma_T^{(A)}\left(-b+\frac{\beta}{2},-b-\frac{\beta}{2}\right)$ is a two-dimensional kernel that uniquely characterizes the affine QTFR $T^{(A)}$ and the signal product $U_X(f, \nu)$ that is defined in equation (4). The Wigner distribution in equation (5) is also a member of the affine class. Another important member of the affine class is the scalogram, which is defined as the squared magnitude of the wavelet transform.[19, 26]

4. GENERALIZED TIME-SHIFT COVARIANT QTFRs

The generalized time-shift covariant QTFR classes[36, 38, 41, 44, 50, 51] consist of QTFRs that are covariant to frequency-dependent time shifts $\tau(f)$ that can be selected to match the group delay function of the analysis signal. The generalized time-shift covariance property is important for analyzing signals passing through systems with dispersive characteristics corresponding to specific group delay functions. For QTFR $T_X(t,f)$, the generalized time-shift covariance property is defined as

$$T_{D_c^{(\xi)}X}(t,f) = T_X(t - c\tau(f), f), \tag{13}$$

where the generalized time-shift covariance operator is given by

$$(D_c^{(\xi)}X)(f) = e^{-j2\pi c\xi(\frac{f}{f_r})}X(f). \tag{14}$$

Here, $\xi(b)$ is a one-to-one phase function, the time shift or group delay $\tau(f) = \frac{d}{df}\xi\left(\frac{f}{f_r}\right)$ is the derivative of the phase function, and $f_r > 0$ is a fixed reference frequency. Different generalized time shifts are obtained by fixing $\xi(b)$ and $\tau(f)$ in equations (13) and (14). Some special cases of generalized time shifts include:

- constant (nondispersive) time shifts* in Cohen's class or the affine class when $\xi(b) = b$ and $\tau(f) = \frac{1}{f_r}$
- hyperbolic time shifts in the hyperbolic class when $\xi(b) = \ln b$ $(b > 0)$ and $\tau(f) = \frac{1}{f}$

*Note that $D_c^{(\xi)}$ in equation (14) simplifies to S_η in equation (1) when $\xi(b) = b$ and $\eta = \frac{c}{f_r}$.

- κth power time shifts in the κth power class, $\kappa \neq 0$, when $\xi(b) = \xi_\kappa(b) = \mathrm{sgn}(b)|b|^\kappa$, where $\mathrm{sgn}(b)$ is -1 for $b < 0$, 1 for $b > 0$, and 0 for $b = 0$, and

$$\tau(f) = \tau_\kappa(f) = \frac{\kappa}{f_r}\left|\frac{f}{f_r}\right|^{\kappa - 1}$$

- exponential time shifts in the exponential class when $\xi(b) = e^b$ and $\tau(f) = \frac{1}{f_r} e^{\frac{f}{f_r}}$.

Thus, generalized time-shift covariant QTFRs unify existing QTFR classes, such as Cohen's class, the affine class, the hyperbolic class, the power classes, and the exponential class. They are important QTFR classes for analyzing signals passing through dispersive systems and are specifically suited for signals whose group delay is proportional to the time shift $\tau(f)$.

Generalized time-shift covariant QTFR classes can be obtained by warping existing constant time-shift covariant classes such as Cohen's class and the affine class.[36, 38, 41, 44, 50-55] The form of the warping is fixed by the choice of $\xi(b)$ in the desirable generalized time-shift covariance property in equations (13) and (14).[38, 41, 50] The QTFR warping is given by

$$T_X^{(G\ class)}(t, f) = T_{W_\xi X}^{(class)}\left(\frac{t}{f_r \tau(f)},\ f_r \xi\left(\frac{f}{f_r}\right)\right), \tag{15}$$

where the generalized time-shift warping operator is defined as

$$(W_\xi X)(f) = \frac{1}{\sqrt{\left|\xi'(\xi^{-1}(\frac{f}{f_r}))\right|}} X\left(f_r \xi^{-1}\left(\frac{f}{f_r}\right)\right). \tag{16}$$

Here, the inverse function $\xi^{-1}(b)$ is such that $\xi^{-1}(\xi(b)) = b$ and $\xi'(b) = \frac{d}{db}\xi(b)$. The superscript (*class*) indicates which QTFR class undergoes the warping in equation (15). When (*class*) = (*C*),

corresponding to Cohen's class, then Cohen's class QTFRs $T_X^{(C)}(t,f)$ are warped using equation (15) to obtain the generalized warped Cohen's class QTFRs $T_X^{(GC)}(t,f)$. Similarly, when (*class*) = (*A*), corresponding to the affine class, then affine class QTFRs $T_X^{(A)}(t,f)$ are warped using equation (15) to obtain the generalized warped affine class QTFRs $T_X^{(GA)}(t,f)$. The generalized warped QTFRs always satisfy the generalized time-shift covariance in equation (13) for a given one-to-one function $\xi(b)$ because the warping maps the constant time-shift operator $S_{\frac{c}{f_r}}$ in equation (1) of Cohen's class or the affine class to the generalized time-shift operator D_c^{ξ} in equation (14) using $W_\xi^{-1} S_{\frac{c}{f_r}} W_\xi = D_c^{(\xi)}$, where W_ξ^{-1} is such that $(W_\xi^{-1} W_\xi X)(f) = X(f)$. The generalized warped QTFRs also satisfy an additional covariance property that depends on $\xi(b)$.[50]

4.1 GENERALIZED WARPED COHEN'S CLASS

4.1.1 Generalized Warped Cohen's Class Formulation and Covariance Properties

The generalized warped Cohen's class (*GC*) is obtained by warping Cohen's class QTFRs[20, 30] using equation (15) with (*class*) = (*C*). Applying the warping in equation (15) to Cohen's class QTFR formulation in equations (3) and (4), any *GC* QTFR can be expressed as[36, 38, 41, 44, 50, 51]

$$T_X^{(GC)}(t,f) = \int_{-\infty}^{\infty}\int_{-\infty}^{\infty} \Gamma_T^{(GC)}\left(\xi\left(\frac{f}{f_r}\right) - \xi\left(\frac{f_1}{f_r}\right), \xi\left(\frac{f}{f_r}\right) - \xi\left(\frac{f_2}{f_r}\right)\right)\sqrt{|\tau(f_1)\tau(f_2)|}$$
$$\cdot X(f_1)X^*(f_2)e^{j2\pi\frac{t}{\tau(f)}\left[\xi\left(\frac{f_1}{f_r}\right) - \xi\left(\frac{f_2}{f_r}\right)\right]} df_1 df_2, \tag{17}$$

$$= \int_{-\infty}^{\infty}\int_{-\infty}^{\infty} \Phi_T^{(GC)}\left(\xi\left(\frac{f}{f_r}\right) - b, \beta\right) V_X(b,\beta) e^{j2\pi\frac{t}{\tau(f)}\beta} db\, d\beta, \tag{18}$$

where $\Phi_T^{(GC)}(b,\beta) = \Gamma_T^{(GC)}\left(b-\frac{\beta}{2},\ b+\frac{\beta}{2}\right)$ is a two-dimensional kernel function that uniquely characterizes the *GC* QTFR $T^{(GC)}$. The signal function $V_X(b,\beta)$ in equation (18) is given by

$$V_X(b,\beta) = f_r U_{W_\xi X}(f_r b, f_r \beta) = f_r (W_\xi X)\left(f_r b + f_r \frac{\beta}{2}\right)(W_\xi X)^*\left(f_r b - f_r \frac{\beta}{2}\right),$$

$$= f_r \left|\xi'\left(\xi^{-1}\left(b+\frac{\beta}{2}\right)\right)\xi'\left(\xi^{-1}\left(b-\frac{\beta}{2}\right)\right)\right|^{-\frac{1}{2}} X\left(f_r \xi^{-1}\left(b+\frac{\beta}{2}\right)\right) X^*\left(f_r \xi^{-1}\left(b-\frac{\beta}{2}\right)\right), \quad (19)$$

where the signal product $U_X(f,\nu)$ is given in equation (4) and the warped signal $W_\xi X(f)$ is defined in equation (16). Note that the *GC* formulation in equations (17) and (18) generalizes Cohen's class since, when $\xi(b) = b$, equations (17) and (18) simplify to Cohen's class formulation in equations (3) and (4) with $\Gamma_T^{(GC)}(b_1,b_2) = f_r \Gamma_T^{(C)}(f_r b_1, f_r b_2)$ and $\Phi_T^{(GC)}(b,\beta) = f_r \Phi_T^{(C)}(f_r b, f_r \beta)$, respectively.

Due to the warping, the constant time-shift covariance property in equation (1) and the frequency-shift covariance property in equation (2) in Cohen's class are transformed into two new covariance properties in the *GC*. As a result, any *GC* QTFR $T_X^{(GC)}(t,f)$ satisfies the generalized time-shift covariance property in equations (13) and (14), and the generalized warped frequency-shift covariance property defined as

$$T_{y_\nu^{(\xi)}X}^{(GC)}(t,f) = T_X^{(GC)}\left(t\frac{\tau(f_r y(f,\nu))}{\tau(f)}, f_r y(f,\nu)\right), \quad (20)$$

where $y(f,\nu) = \xi^{-1}\left(\xi\left(\frac{f}{f_r}\right) - \frac{\nu}{f_r}\right)$. The covariance property in equation (20) follows from the mapping of the frequency shift operator (M_ν in equation (2)) in Cohen's class to $W_\xi^{-1} M_\nu W_\xi = Y_\nu^{(\xi)}$, which transforms the signal as

$$(y_v^{(\xi)}X)(f) = \sqrt{\frac{\left|\xi'\left(\frac{f}{f_r}\right)\right|}{\left|\xi'(y(f,v))\right|}}X(f_r y(f,v)). \tag{21}$$

The covariance property in equations (20) – (21) may or may not be useful in a particular application, depending on the choice of $\xi(b)$. For $\xi(b) = \ln b$ and $\nu = f_r \ln a$, the covariance property in equation (20) simplifies to the scale covariance property in equation (10), which is an important property for multiresolution analysis. Furthermore, the operator in equation (21) simplifies to the scale operator in equation (10), since $\left(y_{f_r \ln a}^{(\ln)}X\right)(f) = \left(C_a X\right)(f)$ and the corresponding *GC* is the hyperbolic class[34, 35] (see table 4).

4.1.2 Generalized Warped Cohen's Class Members

GC QTFRs can be obtained by warping Cohen's class QTFRs using equation (15), and are defined by fixing the kernel $\Phi_T^{(GC)}(b,\beta)$ in equation (18). An important *GC* member that satisfies many desirable QTFR properties is the generalized warped Wigner distribution (GWWD) $WD_X^{(\xi)}(t,f)$. The GWWD is obtained by warping the well-known Wigner distribution in equation (5) using equation (15). Thus, the GWWD is defined as

$$WD_X^{(\xi)}(t,f) = WD_{W_\xi X}\left(\frac{t}{f_r\tau(f)}, f_r\xi\left(\frac{f}{f_r}\right)\right) = \int_{-\infty}^{\infty} V_X\left(\xi\left(\frac{f}{f_r}\right),\beta\right)e^{j2\pi\frac{t}{\tau(f)}\beta}d\beta, \tag{22}$$

and its kernel in equation (18) is $\Phi_{WD^{(\xi)}}^{(G,C)}(b,\beta) = \delta(b)$. Note that equation (22) simplifies to the Wigner distribution in equation (5) when $\xi(b) = b$ and $\tau(f) = \frac{1}{f_r}$. The GWWD provides good time-frequency resolution for various analysis signals[36] and is ideally matched to signals whose group delay equals the generalized time shift that is preserved by the GWWD.[56, 57] The generalized impulse is a nonstationary signal defined in the frequency domain as

$$I_c^{(\tilde{\xi})}(f) = \sqrt{|\tilde{\tau}(f)|}e^{-j2\pi c\tilde{\xi}\left(\frac{f}{f_r}\right)}, \tag{23}$$

with phase function $\tilde{\xi}(b)$ and group delay function $c\tilde{\tau}(f) = c\frac{d}{df}\tilde{\xi}\left(\frac{f}{f_r}\right)$. When the one-to-one function $\xi(b)$ of the GWWD equals the phase function $\tilde{\xi}(b)$ of the generalized impulse, the GWWD of the generalized impulse is simply a Dirac delta function centered along the impulse's group delay, i.e.,

$$WD_{I_c^{(\xi)}}^{(\xi)}(t,f) = |\tau(f)|\delta(t - c\tau(f)) \text{ if, and only if, } \xi(b) = \tilde{\xi}(b). \tag{24}$$

Thus, the GWWD is ideally matched to generalized impulses as it provides high time-frequency localization along the signal's group delay characteristics. Just like the Wigner distribution, the GWWD suffers from cross terms when multicomponent signals are analyzed. For example, if the signal consists of the sum of two generalized impulses $X(f) = I_{c_1}^{(\xi)}(f) + I_{c_2}^{(\xi)}(f)$, then the GWWD results in the sum of two auto terms and one cross term. The auto terms $WD_{I_{c_1}^{(\xi)}}^{(\xi)}(t,f)$ and $WD_{I_{c_2}^{(\xi)}}^{(\xi)}(t,f)$ are defined in equation (24). The cross term

$$C_{I_{c_1},I_{c_2}}^{(\xi)}(t,f) = 2\cos\left(2\pi(c_1 - c_2)\xi\left(\frac{f}{f_r}\right)\right)|\tau(f)|\delta\left(t - \frac{c_1 + c_2}{2}\tau(f)\right) \tag{25}$$

is centered along the group delay curve $t = \frac{c_1 + c_2}{2}\tau(f)$ and oscillates at a frequency that increases as the parameter difference $(c_1 - c_2)$ increases.

In many practical applications, it is important to reduce cross terms by means of smoothing the GWWD. Specifically, any member of the *GC* can be written as a smoothed version of the GWWD ($WD_X^{(\xi)}(t,f)$ in equation (22)) using a smoothing kernel $\psi_T^{(GC)}(c,b)$, i.e.,

$$T_X^{(GC)}(t,f) = \int_{-\infty}^{\infty}\int_{-\infty}^{\infty}\psi_T^{(GC)}\left(\frac{t}{\tau(f)}-\frac{\hat{t}}{\tau(\hat{f})},\ \xi\left(\frac{f}{f_r}\right)-\xi\left(\frac{\hat{f}}{f_r}\right)\right)WD_X^{(\xi)}(\hat{t},\hat{f})\,d\hat{t}\,d\hat{f},$$

where $\psi_T^{(GC)}(c,b) = \int_{-\infty}^{\infty}\Phi_T^{(GC)}(b,\beta)e^{j2\pi c\beta}d\beta$ (equation (18)). A *GC* QTFR that applies smoothing to reduce cross terms in the time-frequency plane is the generalized warped spectrogram that is obtained by warping the spectrogram in equation (8) using equation (15). This generalized warped spectrogram uses a window to reduce cross terms. More smoothing is provided by the generalized warped smoothed pseudo-Wigner distribution that is obtained by warping the smoothed pseudo-Wigner distribution in equation (9) using equation (15). This is because the generalized warped smoothed pseudo-Wigner distribution uses two windows that can smooth out cross terms independently along the time direction and along the group delay $\tau(f)$ direction.

4.1.3 Generalized Warped Cohen's Class Examples

Different *GC* QTFR classes can be obtained simply by choosing a one-to-one, differentiable, and invertible function $\xi(b)$ in equations (17) or (18). Depending on $\xi(b)$, the covariance properties in equations (13) and (20) may be useful depending on the analysis application at hand. Examples of the generalized warped Cohen's class are the hyperbolic class and the κth-power warped Cohen's class; these are listed below and, together with some additional examples, are summarized in table 4.

1. **Hyperbolic class**: When $\xi(b) = \ln b$ and $\tau(f) = \frac{1}{f}$, $f > 0$, the corresponding *GC* in equation (18) is the hyperbolic class.[29, 33-36] Thus, any member of the hyperbolic class $T_X^{(H)}(t,f)$ can be written as

$$T_X^{(H)}(t,f) = \int_{-\infty}^{\infty}\int_{-\infty}^{\infty} \Phi_T^{(H)}\left(\ln\frac{f}{f_r} - b, \beta\right) V_X^{(H)}(b,\beta) e^{j2\pi t f \beta} db\, d\beta ,$$

where $\Phi_T^{(H)}(b,\beta) = \Phi_T^{(GC)}(b,\beta)$(equation (18)) is a two-dimensional kernel that uniquely characterizes the hyperbolic QTFR $T^{(H)}$, and $V_X^{(H)}(b,\beta)$ is the signal product $V_X(b,\beta)$ in equation (18) when $\xi(b) = \ln b$. Any member of the hyperbolic class satisfies two covariance properties that are special cases of the two covariance properties satisfied by all *GC* QTFRs. Specifically, the generalized time-shift covariance of the *GC* in equation (13) simplifies to the hyperbolic time-shift covariance of the hyperbolic class defined as $T_{H_c X}^{(H)}(t,f) = T_X^{(H)}\left(t - \frac{c}{f}, f\right)$, since $W_{1n}^{-1} S_{\frac{c}{f_r}} W_{1n} = D_c^{(1n)} = H_c$ (note that $W_{\ln}$ is the warping operator W_ξ in equation (16) when $\xi(b) = \ln b$, and $D_C^{(ln)}$ is defined in equation (14) with $\xi(b) = \ln b$). The generalized warped frequency-shift covariance in equations (20) and (21) simplifies to the scale covariance in equation (10), since $W_{1n}^{-1} M_v W_{1n} = y_v^{1n} = C_e^{\frac{v}{f_r}}$; thus, hyperbolic class QTFRs preserve hyperbolic time shifts and scale changes on the analysis signal. An important member of the hyperbolic class is the Altes Q-distribution[27-29] which corresponds to the generalized warped Wigner distribution in equation (22) when $\xi(b) = \ln b$. The Altes Q-distribution is defined as

$$AD_X(t,f) = f\int_{-\infty}^{\infty} X(fe^{\frac{\beta}{2}}) X^*(fe^{\frac{-\beta}{2}}) e^{j2\pi t f \beta} d\beta , \qquad (26)$$

and is ideal for analyzing signals with hyperbolic group delay characteristics such as Doppler-invariant signals that are similar to the signals used by bats for echolocation.[58] For example, the Altes Q-distribution of a hyperbolic impulse, defined in the frequency domain as $X(f) = \frac{1}{\sqrt{f}} e^{-j2\pi c \ln \frac{f}{f_r}}$ for $f > 0$, is a Dirac delta function centered at the signal's group delay function, i.e., $AD_X(t, f) = \frac{1}{f}\delta\left(t - \frac{c}{f}\right)$, $f > 0$. Note that this is a special case of equations (23) and (24) when $\xi(b) = \ln b$ and $\tau(f) = \frac{1}{f}$.

2. **κth-power warped Cohen's class**: When $\xi(b) = \xi_\kappa(b) = sgn(b)|b|^\kappa$, $\kappa \neq 0$, and $\tau(f) = \tau_\kappa(f) = \frac{\kappa}{f_r}\left|\frac{f}{f_r}\right|^{\kappa - 1}$, the *GC* in equation (18) is the κth power warped Cohen's class.[36, 41, 50] The generalized time-shift covariance of the *GC* in equation (13) simplifies to the κth power time-shift covariance defined as $T^{(GC)}_{D_c^{(\xi_\kappa)}X}(t, f) = T^{(GC)}_X(t - c\tau_\kappa(f), f)$, since $W^{-1}_{\xi_\kappa} S_{\frac{c}{f_r}} W_{\xi_\kappa} = D_c^{(\xi_\kappa)}$ (where $D_c^{(\xi_\kappa)}$ and W_{ξ_κ} are defined in equations (14) and (16), respectively, with $\xi(b) = \xi_\kappa(b)$), but equation (20) does not simplify to any known covariance. Members of this class include the κth power Wigner distribution and the power spectrogram.[41, 50]

Table 4. Examples of QTFR Classes from the Generalized Warped Cohen's Class with Associated Function $\xi(b)$, Generalized Time Shift $\tau(f)$, and Covariance Operators Corresponding to Equations (13) – (14) and (20) – (21)

Characteristic Class Functions	**Examples of Generalized Warped Cohen's Class**			
	Cohen's Class	**Hyperbolic Class**	**κth Power Warped Cohen's Class**	**Exponential Warped Cohen's Class**
Function $\xi(b)$	b	$\ln b$	$\xi_{\kappa}(b)$	e^{b}
Generalized Time Shift $\tau(f)$	$\frac{1}{f_r}$	$\frac{1}{f}$	$\tau_{\kappa}(f)$	$\frac{e^{\frac{f}{f_r}}}{f_r}$
Covariance Operator $D_c^{(\xi)}$ in Equation (14)	$S_{\frac{c}{f_r}}$	$H_c = D_c^{(\ln)}$	$D_c^{(\xi_{\kappa})}$	$\varepsilon_c = D_c^{(\exp)}$
Covariance Property in Equation (13)	Constant Time-Shift	Hyperbolic Time-Shift	Power Time-Shift	Exponential Time-Shift
Covariance Operator $y_{\nu}^{(\xi)}$ in Equation (21)	M_{ν}	$C_{e^{\frac{\nu}{f_r}}}$	$y_{\nu}^{(\xi_{\kappa})}$	$y_{\nu}^{(\exp)}$
Covariance Property in Equation (20)	Frequency-Shift	Scale	Power Warped Frequency-Shift	Exponential Warped Frequency-Shift

4.2 GENERALIZED WARPED AFFINE CLASS

4.2.1 Generalized Warped Affine Class Formulation and Covariance Properties

The generalized warped affine class (*GA*) is obtained by warping the time-shift and scale covariant affine QTFR class[19, 26, 31, 32] using equation (15) with (*class*) = (*A*). Similar to the generalized warped Cohen's class, the *GA* is a generalized time-shift covariant class, since both the *GC* and the *GA* are obtained by warping constant time-shift covariant classes using equation (15). However, in comparison to *GC* QFTRs, the *GA* satisfies an additional covariance property that is based on the scale covariance property of the affine class; thus, it yields new QTFRs that are useful in different type of applications. Applying the warping in equation (15) to the affine class QTFR formulation in equations (11) and (12), any *GA* QTFR can be written as

$$T_X^{(GA)}(t,f) = \frac{1}{\left|\xi(\frac{f}{f_r})\right|}\int_{-\infty}^{\infty}\int_{-\infty}^{\infty}\Gamma_T^{(GA)}\left(\frac{\xi(\frac{f_1}{f_r})}{\xi(\frac{f}{f_r})}, \frac{\xi(\frac{f_2}{f_r})}{\xi(\frac{f}{f_r})}\right)\sqrt{\left|\tau(f_1)\tau(f_2)\right|}$$

$$\cdot X(f_1)X^*(f_2)e^{j2\pi\frac{t}{\tau(f)}\left[\xi\left(\frac{f_1}{f_r}\right)-\xi\left(\frac{f_2}{f_r}\right)\right]}df_1\,df_2, \tag{27}$$

$$= \frac{1}{\left|\xi(\frac{f}{f_r})\right|}\int_{-\infty}^{\infty}\int_{-\infty}^{\infty}\Phi_T^{(GA)}\left(\frac{-b}{\xi(\frac{f}{f_r})}, \frac{\beta}{\xi(\frac{f}{f_r})}\right)V_X(b,\beta)e^{j2\pi\frac{t}{\tau(f)}\beta}\,db\,d\beta, \tag{28}$$

where $V_X(b,\beta)$ is defined in equation (19) and $\Phi_T^{(GA)}(b,\beta) = \Gamma_T^{(GA)}(-b+\frac{\beta}{2},\ -b-\frac{\beta}{2})$ is a two-dimensional kernel function that uniquely characterizes the *GA* QTFR $T^{(GA)}$. The kernels in equations (27) and (28) are identical in form to the corresponding affine class kernels in equations (11) and (12), i.e., $\Gamma_T^{(GA)}(b_1,b_2) = \Gamma_T^{(A)}(b_1,b_2)$ and $\Phi_T^{(GA)}(b,\beta) = \Phi_T^{(A)}(b,\beta)$.[36] Thus, if the kernel of an affine QTFR is known, then the corresponding generalized warped version of that affine QTFR uses the same kernel function. The *GA* provides a generalization of the affine class since, when $\xi(b)=b$, the *GA* QTFR formulation in equations (27) and (28) simplifies to the affine class QTFR formulation in equations (11) and (12), respectively.

Due to the warping, the constant time-shift covariance property in equation (1) of the affine class QTFRs is transformed to the generalized time-shift covariance property in equations (13) and (14) of the *GA* QTFRs. Similarly, the scale covariance property in equation (10) of the affine class QTFRs is transformed to the generalized warped scale covariance property defined as

$$T_{L_a^{(\xi)}X}^{(GA)}(t,f) = T_X^{(GA)}\left(at,\ \frac{\tau\left(f_r\, l(f,a)\right)}{\tau(f)},\ f_r\, l(f,a)\right), \tag{29}$$

where $l(f,a) = \xi^{-1}(\frac{1}{a}\xi(\frac{f}{f_r}))$. The covariance property in equation (29) follows since the scale operator C_a in the affine class maps to $W_\xi^{-1}C_aW_\xi = L_a^{(\xi)}$, which transforms the signal as

$$(L_a^{(\xi)}X)(f) = \sqrt{\frac{\left|\xi'(\frac{f}{f_r})\right|}{\left|a\xi'(l(f,a))\right|}}X(f_r l(f,a)). \tag{30}$$

The covariance property in equation (29) is not easy to understand, but simplifies to known covariance properties for the following functions: when $\xi(b) = \xi_\kappa(b) = sgn(b)|b|^\kappa$, equation (29) results in the scale covariance property in equation (10) since $W_{\xi_\kappa}^{-1}C_aW_{\xi_\kappa} = L_a^{(\xi_\kappa)} = C_{\xi_{1/\kappa}(a)}$. When $\xi(b) = \ln b$, equation (29) results in the power warping covariance property[34, 36] defined as

$$T_{W_{\xi_a}X}^{(GA)}(t,f) = T_X^{(GA)}\left(\frac{t}{f_r\tau_{\frac{1}{a}}(f)}, f_r\xi_{\frac{1}{a}}\left(\frac{f}{f_r}\right)\right),$$

since $W_{\ln}^{-1}C_aW_{\ln} = L_a^{(\ln)} = W_{\xi_a}$ $\left(\text{where } \xi_a(b) = sgn(b)|b|^a\right)$. Furthermore, when $\xi(b) = e^b$, equation (29) results in the frequency-shift covariance property in equation (2) since $W_{exp}^{-1}C_aW_{exp} = L_a^{(exp)} = M_{f_r \ln a}$ (see table 5).

Table 5. Examples of QTFR Classes from the Generalized Warped Affine Class with Associated Function ξ(b), Generalized Time Shift τ(f), and Covariance Operators Corresponding to Equations (13) – (14) and (29) – (30)

Characteristic Class Functions	**Examples of Generalized Warped Affine Class**			
	AffineClass	**Hyperbolically Warped Affine Class**	**κth Power Class**	**Exponential Class**
Function $\xi(b)$	b	$\ln b$	$\xi_\kappa(b)$	e^b
Generalized Time Shift $\tau(f)$	$\frac{1}{f_r}$	$\frac{1}{f}$	$\tau_\kappa(f)$	$\frac{1}{f_r}e^{\frac{f}{f_r}}$
Covariance Operator $D_c^{(\xi)}$ in Equation (14)	$S_{\frac{c}{f_r}}$	$H_c = D_c^{(\ln)}$	$D_c^{(\xi_\kappa)}$	$\varepsilon_c = D_c^{(\exp)}$
Covariance Property in Equation (13)	Constant Time-Shift	Hyperbolic Time-Shift	Power Time-shift	Exponential Time-shift
Covariance Operator $L_a^{(\xi)}$ in Equation (30)	C_a	W_{ζ_a}	$C_{\frac{\xi_1(a)}{\kappa}}$	$M_{f_r \ln a}$
Covariance Property in Equation (29)	Scale	Power Warping	Scale	Frequency-Shift

4.2.2 Generalized Warped Affine Class Members

GA QTFRs are specified by their kernel $\Phi_T^{(GA)}(b,\beta)$ in equation (28) and are obtained simply by warping known affine class QTFRs. One important member of the *GA* is the generalized warped Wigner distribution discussed in section 4.1.2 that is obtained by warping the Wigner distribution as in equation (22). Since the Wigner distribution is a member of the intersection between Cohen's class and the affine class, the generalized warped Wigner distribution in equation (22) is a member of the intersection between the *GC* and the *GA*. Another important member of the *GA* that may be used to remove cross terms in multicomponent signal analysis applications is the generalized warped version of the scalogram, which is the generalized warped version of the squared magnitude of the wavelet transform.[50]

4.2.3 Generalized Warped Affine Class Examples

The generalized warped affine power class and exponential class examples listed below are obtained by appropriately choosing the one-to-one, differentiable, and invertible function $\xi(b)$ in equations (27) or (28). Note that the classes are also summarized in table 5 with some additional examples.

1. **Power class:** When $\xi(b) = \xi_\kappa(b) = sgn(b)|b|^\kappa$ and $\tau(f) = \tau_\kappa(f) = \frac{\kappa}{f_r}\left|\frac{f}{f_r}\right|^{\kappa-1}$,

the corresponding *GA* class in equation (28) is the κth power class $\kappa \neq 0$.[36-40] Any member of the κth power class can be written as

$$T_X^{(P_\kappa)}(t,f) = \frac{1}{\left|\xi_\kappa'(\frac{f}{f_r})\right|}\int_{-\infty}^{\infty}\int_{-\infty}^{\infty}\Phi_T^{(P)}\left(\frac{-b}{\xi_\kappa(\frac{f}{f_r})}, \frac{\beta}{\xi_\kappa'(\frac{f}{f_r})}\right)V_X^{(P_\kappa)}(b,\beta)e^{j2\pi\frac{t}{\tau_\kappa(f)}\beta}\,db\,d\beta\,,$$

where $\Phi_T^{(P)}(b,\beta) = \Phi_T^{(GA)}(b,\beta)$ (equation (28)) is a two-dimensional kernel that uniquely characterizes the power QTFR $T^{(P_\kappa)}$, and $V_X^{(P_\kappa)}(b,\beta)$ is the signal product $V_X(b,\beta)$ in equation (28) when $\xi(b) = \xi_\kappa(b)$. Power class QTFRs satisfy two simplified covariance properties that correspond to the generalized time-shift covariance in equation (13) and the generalized warped scale covariance in equation (29) when $\xi(b) = \xi_\kappa(b)$. Thus, power class QTFRs satisfy the power time-shift covariance property defined as $T^{(P_\kappa)}_{D_c^{(\xi_\kappa)}X}(t,f) = T_X^{(P_\kappa)}(t - c\tau_\kappa(f), f)$, since $W_{\xi_\kappa}^{-1} S_{\frac{c}{f_r}} W_{\xi_\kappa} = D_c^{(\xi_\kappa)}$. Note that $D_c^{(\xi_\kappa)}$ is defined in equation (14) with $\xi(b) = \xi_\kappa(b)$, and W_{ξ_κ} is defined in equation (16) with $\xi(b) = \xi_\kappa(b)$. Power QTFRs also satisfy the scale covariance property in equation (10) since $W_{\xi_\kappa}^{-1} C_a W_{\xi_\kappa} = L_a^{(\xi_\kappa)} = C_{\xi_{\frac{1}{\kappa}}(a)}$. Thus, power QTFRs are useful for analyzing signals passing through systems with power time-frequency characteristics. An important member of the κth power class is the κth power Wigner distribution,[36, 37] which is the

generalized warped Wigner distribution in equation (22) when $\xi(b) = \xi_\kappa(b)$. The κth power Wigner distribution is defined as

$$WD_X^{(\kappa)}(t,f) = \left|\frac{f}{\kappa}\right| \int_{-\infty}^{\infty} X\left(f\xi_\kappa^{-1}\left(1+\frac{\beta}{2}\right)\right) X^*\left(f\xi_\kappa^{-1}\left(1-\frac{\beta}{2}\right)\right) e^{j2\pi\frac{tf}{\kappa}\beta} \frac{1}{\left|1-\frac{\beta^2}{4}\right|^{\frac{\kappa-1}{2\kappa}}} d\beta, \qquad (31)$$

and it reduces to the Wigner distribution when $\kappa = 1$. Another important member of the κth power class is the powergram, which is the squared magnitude of a power wavelet transform.[37]

2. **Exponential class:** When $\xi(b) = e^b$ and $\tau(f) = \frac{1}{f_r} e^{\frac{f}{f_r}}$, the corresponding *GA* class in equation (28) is the exponential class.[41, 42, 50] The generalized time-shift covariance property in equation (13) simplifies to the exponential time-shift covariance property defined as $T_{\varepsilon_c X}^{(GA)}(t,f) = T_X^{(GA)}(t - \frac{c}{f_r} e^{\frac{f}{f_r}}, f)$, since $W_{\exp}^{-1} S_{\frac{c}{f_r}} W_{\exp} = D_c^{(\exp)} = \varepsilon_c$. Here, $D_c^{(\exp)}$ and $W_{\exp}$ are defined in equations (14) and (16), respectively, with $\xi(b) = e^b$. Moreover, the generalized warped scale covariance property in equation (29) simplifies to the frequency-shift covariance in equation (2) since $W_{\exp}^{-1} C_a W_{\exp} = L_a^{(\exp)} = M_{f_r \ln a}$. Some important members of the exponential class include the exponential Wigner distribution and the exponogram.[42]

5. IMPLEMENTATION OF GENERALIZED TIME-SHIFT COVARIANT QTFRs, INCLUDING POWER CLASS QTFRs

The *GC* and *GA* QTFRs can be implemented directly using their formulation in equations (18) and (28), respectively. However, the direct implementation technique is computationally intensive, as it involves a two-dimensional integration. A less complicated technique is to implement the warping transformation in equation (15) because algorithms already exist to compute Cohen's class QTFRs and affine class QTFRs, and the only new algorithms needed are the ones to warp the analysis signal as in equation (16), and to transform the time-frequency axes as in equation (15). For example, the Altes Q-distribution in section 4.1.3 can be computed directly using equation (26) or indirectly as the hyperbolically warped version of the Wigner distribution in equation (5), i.e.,

$$AD_X(t,f) = WD_{W_{ln}X}\left(\frac{tf}{f_r},\ f_r \ln\frac{f}{f_r}\right), \text{where } (W_{ln}X)(f) = \sqrt{e^{\frac{f}{f_r}}}\, X\left(f_r e^{\frac{f}{f_r}}\right). \tag{32}$$

Note that equation (32) corresponds to the warping in equations (15) and (16) with $\xi(b) = \ln b$. Since simple and efficient algorithms exist to compute the Wigner distribution in equation (5), to compute the Altes Q-distribution, the signal must first be warped with the exponential mapping $X(f) \rightarrow (W_{\ln}X)(f)$, then the Wigner distribution of the warped signal must be computed, and finally the time and frequency axes must be transformed for the correct time-frequency localization using $(t,f) \rightarrow \left(\frac{tf}{f_r}, f_r \ln\frac{f}{f_r}\right)$.[27, 29] Similarly, any member of the hyperbolic class can be implemented in the same way simply by replacing the Wigner distribution in equation (32) with the corresponding member of Cohen's class.[34] Documented discrete implementation realization of the hyperbolic class using the warping approach, the power class QTFRs,[36, 37] and the exponential class QTFRs[41, 42] by appropriately warping the affine class QTFRs can be found in Canfield[59] and Praveenkumar.[60] An in-depth description of the three steps of the discrete

implementation of the power class QTFRs is provided in Hlawatsch.[39] The discrete implementation of the exponential class QTFRs was also realized, and the necessary computational steps were documented and can be found in Papandreou-Suppappola.[42]

As presented in section 4.2.3, any κth power QTFR $T_X^{(P_\kappa)}(t,f)$ can be obtained by warping a corresponding affine class QTFR $T_X^{(A)}(t,f)$ using equations (15) and (16) with $\xi(b) = \xi_\kappa(b) = sgn(b)|b|^\kappa$, i.e.,

$$T_X^{(P_\kappa)}(t,f) = T_{W_\kappa X}^{(A)}\left(\frac{t}{f_r\tau_\kappa(f)},\ f_r\xi_\kappa(\frac{f}{f_r})\right), \tag{33}$$

where the power warping operator is defined as

$$(W_\kappa X)(f) = \frac{1}{\sqrt{|\kappa|}}\left|\frac{f}{f_r}\right|^{\frac{1-\kappa}{2\kappa}} X\left(f_r\xi_{\frac{1}{\kappa}}(\frac{f}{f_r})\right). \tag{34}$$

The discrete implementation of power QTFRs is based on the warping relations in equations (33) and (34), which allow the use of existing efficient algorithms for computing affine class QTFRs.[61] This implementation technique is conceptually similar to the implementation technique used for hyperbolic class QTFRs[34] in Canfield[59] and Praveenkumar.[60] The first step consists of a power-law frequency warping of the signal $X(f)$ according to equation (34), the next step is a computation of the affine QTFR of the warped signal $T_{W_\kappa X}^{(A)}(t,f)$, and lastly a nonlinear time-frequency coordinate transform is performed according to equation (33), i.e.,

$$(t,f) \rightarrow \left(\frac{t}{f_r\tau_\kappa(f)}, f_r\xi_\kappa\left(\frac{f}{f_r}\right)\right).$$

For the discrete implementation of the first step, the discrete version of the signal's Fourier transform $X[l]\,(l = 0,1,\ldots,L-1)$ with frequency sample spacing Δf is first interpolated (upsampled) by factor u, yielding the Fourier transform samples $X'[l']\,(l' = 0,1,\ldots,uL-1)$. Next, discrete warped-frequency locations are computed according to equation (34), such that uniform sampling of the warped-frequency axis is achieved; these discrete warped-frequency locations are given by $f_m = f_r \xi_{\frac{1}{\kappa}}\left(\frac{m\Delta\upsilon}{f_r}\right)(m = 0,1,\ldots,M-1)$, where $\Delta\upsilon$ is the frequency sample spacing of the warped Fourier transform, computed such that $|f_{m+1} - f_m| \le \Delta f, \forall m$, and M is the number of warped Fourier transform samples required to represent the entire frequency domain. The Fourier transform value at each warped-frequency location f_m is obtained by linear interpolation of the closest neighbors in the upsampled Fourier transform $X'[l']$. This gives a discrete warped-frequency Fourier transform $Y[m]\,(m = 0,1,\ldots,M-1)$. In order to avoid time-aliasing effects in the subsequent computation of the affine QTFR, the warped-frequency Fourier transform $Y[m]$ is finally interpolated (upsampled) to bandlimit the Fourier transform to one quarter of the sampling rate, yielding $Y'[m']\,(m' = 0,1,\ldots,M'-1)$, where $M' = 2M$.

In the second step, a discrete-time, discrete-frequency version of the affine QTFR $T_{Y'}^{(A)}(t,f)$ [26, 61] is computed for the warped-frequency signal $Y'[m']$. The last step computes the warped time-frequency locations $(t_n,\ f_i) = \left(\frac{\frac{n}{f_r}}{f_r \tau_\kappa(f_i)},\ f_i\right)$, where $f_i = f_r \xi_\kappa\left(\frac{i\Delta f}{f_r}\right) \Big/ \left(\frac{\Delta\upsilon}{f_r}\right)(n,i = 0,1,\ldots,L-1)$, such that uniform two-dimensional sampling in the warped time-frequency domain is achieved, and subsequently calculates the corresponding sample values $T_{Y'}^{(A)}(t_n, f_i)$ using linear two-dimensional interpolation. Note that the κth power-warped Cohen's class in section 4.1.3 can be implemented using the same three steps above,

except that the affine class QTFR in the second step must be replaced with a Cohen's class QTFR. The MATLAB program for the implementation of the power Wigner distribution is given in section A.2 in the appendix. The power Wigner distribution in equation (31) is obtained by warping the affine Wigner distribution using equations (33) and (34).[36, 37]

6. TIME-FREQUENCY ANALYSIS OF SONAR CLICKS

As clicks are short-duration pulses (impulse like) in time and thus broadband in frequency, they are expected to have constant group delay characteristics. As a result, clicks may be analyzed by QTFRs that preserve constant group delay characteristics in the time-frequency plane. Thus, clicks may be well matched to Cohen's class of time-frequency shift covariant QTFRs, such as the Wigner distribution and the spectrogram presented in section 3.1.

As the sound records have long sample durations, the MATLAB function in section A.1 in the appendix allows small sections of the data to be read, starting at a sample offset. The MATLAB function in section A.3 in the appendix plots the data section in time and frequency, and also computes its Wigner distribution and spectrogram. This function is used to analyze a single click as the click duration is small, extending only over a small section of data samples. The Wigner distribution of the impulse $X(f) = \frac{1}{\sqrt{f_r}} e^{-j2\pi c \frac{f}{f_r}}$ is a Dirac delta function centered at the signal's constant group delay function $t = \frac{c}{f_r}$, i.e., $WD_X(t,f) = \frac{1}{f_r}\delta(t - \frac{c}{f_r})$. Note that this is a special case of the GWWD of a generalized impulse when $\xi(b) = b$ and $\tau(f) = \frac{1}{f_r}$ in equations (23) and (24). Thus, as the click shows similar time-frequency characteristics as an impulse, it is expected that the Wigner distribution of a single click will have a very short time duration, equivalent to the duration of a click, that extends over many frequencies due to its broadband nature. For example, the time domain signal is plotted in figure 2(a); for comparison, the Wigner distribution of a single click (shown in figure 1) of a white-sided dolphin from file 75001012.kay is shown in figure 2(b). Indeed, the Wigner distribution shows that the click has a short duration and is relatively broadband. Thus, the Wigner distribution provides good time-frequency resolution for single clicks. Note that although the data were filtered to remove low frequencies due to recording equipment or engine noise, the data is still noisy, and the Wigner distribution shows some interference terms. This interference is further removed using the spectrogram in equation (8) as shown in figure 2(c), but since the spectrogram uses a window to

smooth out the interference, it is not as localized as the Wigner distribution. Clicks can also be analyzed by other Cohen's class QTFRs, such as the pseudo-Wigner distribution and the smoothed pseudo-Wigner distribution using the MATLAB function given in section A.4 in the appendix. For comparison, this function also computes some hyperbolic QTFRs (section 4.1.3) such as the Altes Q-distribution and the pseudo-Altes Q-distribution, and some power QTFRs (section 4.2.3), such as the power Wigner distribution and the power pseudo-Wigner distribution. The hyperbolic QTFRs and the power QTFRs are not matched to signals with a constant group delay function,[56, 57] thus, they are not ideal for the analysis of clicks.

The smoothed versions of the Wigner distribution, such as the spectrogram or the pseudo-Wigner distribution, are important when a click train is analyzed (versus a single click), as they reduce the oscillatory cross terms that result in the Wigner distribution (equation (6)) that may impede analysis. Figure 3(a) shows a series of clicks (click trains) in time of a long-finned pilot whale from data file 75010001.kay. The Wigner distribution in figure 3(b) suffers from cross terms between any two-click terms and from the noise present in the data. For the sum of two impulses, $X(f) = \frac{1}{\sqrt{f_r}}(e^{-j2\pi c_1 \frac{f}{f_r}} + e^{-j2\pi c_2 \frac{f}{f_r}})$, the Wigner distribution results in the sum of two auto terms $\frac{1}{f_r}(\delta(t - \frac{c_1}{f_r}) + \delta(t - \frac{c_2}{f_r}))$ and in one cross term given by $\frac{2}{f_r}\cos\left(2\pi(c_1 - c_2)\frac{f}{f_r}\right)\delta\left(t - \frac{c_1 + c_2}{2f_r}\right)$. Thus, the cross term oscillates in the frequency direction and is centered at $t = \frac{c_1 + c_2}{2f_r}$ (equation (25) with $\xi(b) = b$)). Note that there are no cross terms oscillating in the time direction. The pseudo-Wigner distribution in figure 3(c) uses a short-duration Hanning window to smooth out cross terms in the frequency direction only. The pseudo-Wigner distribution is defined in equation (9) with $g(t) = \delta(t)$ and $H(f)$, which is a short-duration window for stronger smoothing in the frequency direction.[18] As the click train may be considered as the sum of the impulses, the Wigner distribution cross terms are centered at a constant group delay curve, and are found along the frequency direction. Thus, the pseudo-Wigner distribution in figure 3(c) has successfully reduced the cross terms with only some loss of time-frequency resolution, and it clearly shows the various clicks. There are about five click

trains present with about two to five clicks per click train; the click trains are about 0.5 ms apart, and the clicks in each click train are about 35 μs apart. On the other hand, the spectrogram does not allow separable time and frequency smoothing, and would, as a result, have more loss of time and frequency resolution.

In studying the nature of the click bursts present in the data files, table 6 compares the duration of the click burst, the start time of the click burst, the number of clicks per burst, and the instantaneous click rate (number of clicks per second in intervals of one-tenth of the duration of the click burst) for various click bursts. The click bursts usually lasted from 0.04 – 0.60 s, and the number of clicks per burst ranged from 37 – 892 clicks. The instantaneous click rate showed that in some cases, the number of clicks per second increased and then decreased, whereas in other cases, the number of clicks per second kept increasing or decreasing. Without any additional information on the mammal's behavior at the time of recording, it is difficult to determine the behavior of the instantaneous click rate. Another difficulty in obtaining the instantaneous click rate was that, if the duration of the click burst exceeded 0.6 s and was combined with closely spaced clicks, it was not easy to determine how many clicks were present. As analysis tools, the time signal was used as well as the spectrogram, but the spectrogram provided a faster implementation for longer sections of click bursts. Note, however, that as the duration of the click burst increased, it was difficult to differentiate the closely spaced, broadband clicks.

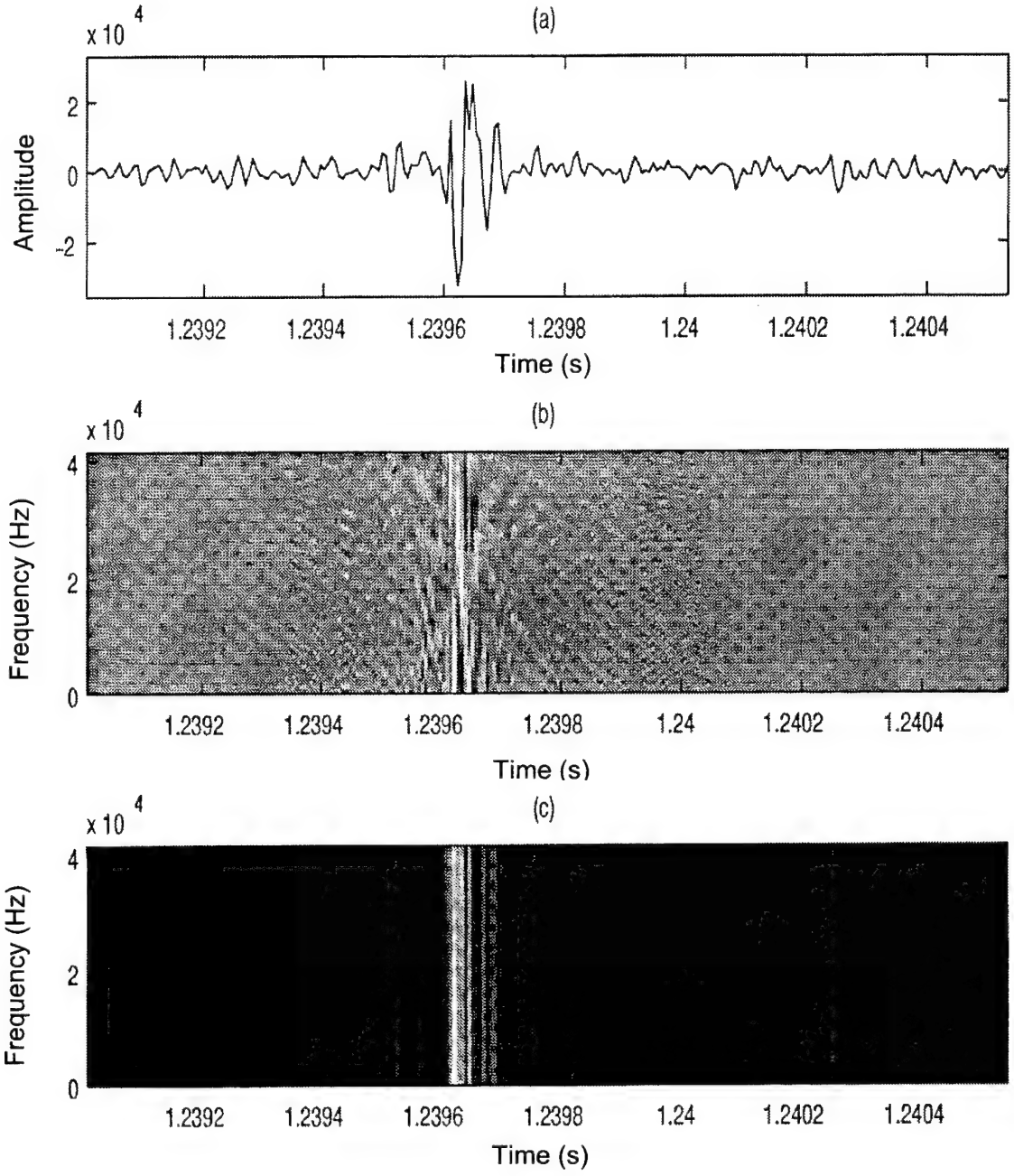

Figure 2. The Single Sonar Click of the White-Sided Dolphin from Data File 75001012.kay from Figure 1: (a) Signal in the Time Domain, (b) Wigner Distribution, and (c) Spectrogram of the Click

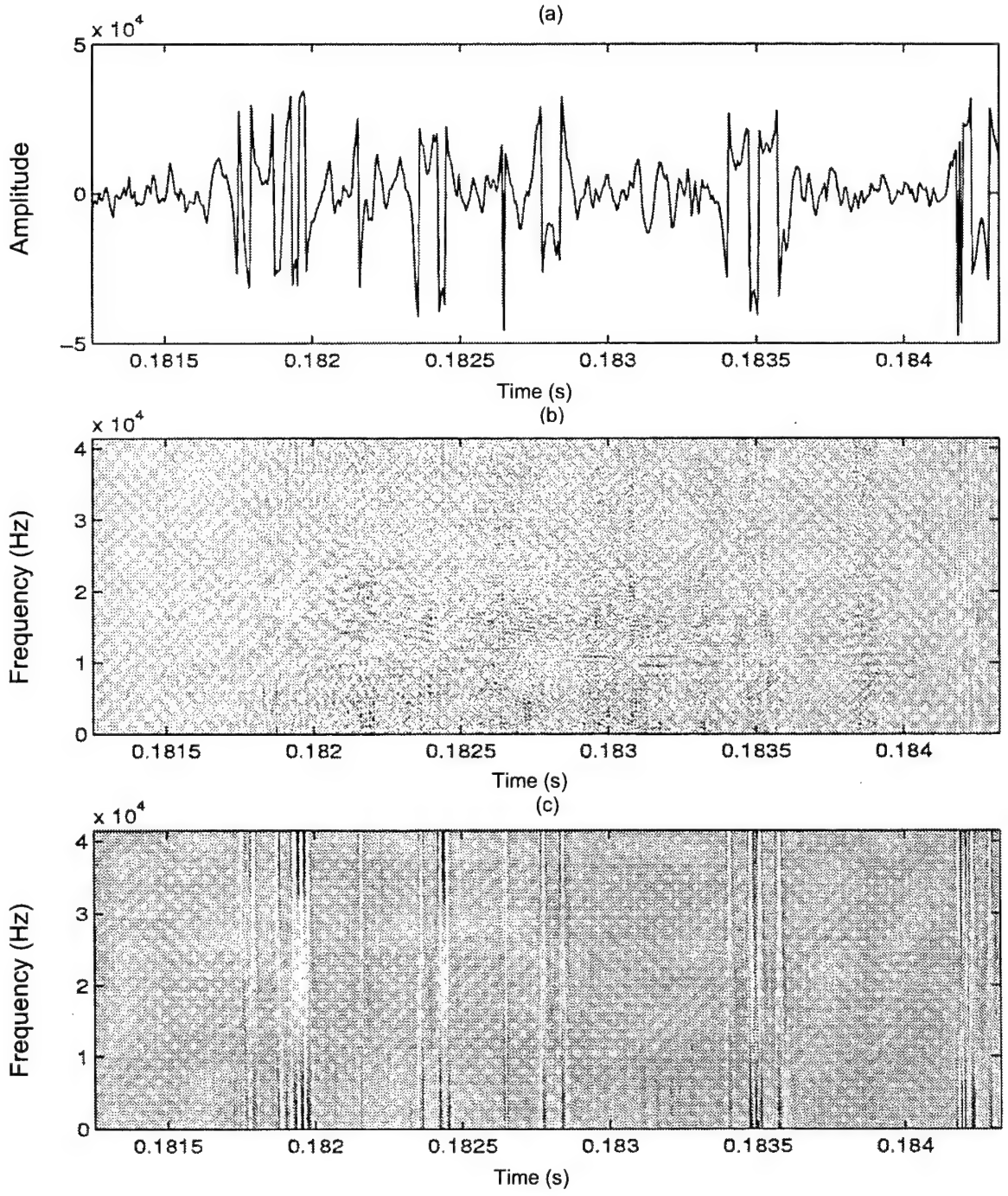

Figure 3. Click Trains of a Long-Finned Pilot Whale from the Data File 75010001.kay: (a) Signal in Time, (b) Wigner Distribution, (c) Pseudo-Wigner Distribution

Table 6. Comparison of Various Statistics of Marine Mammal Click Bursts

Mammal	File Number (.kay)	Duration (s)	Start Time (s)	Clicks/Burst	Instantaneous Click Rate ↑Clicks/s →Time(s)
White-Sided Dolphin	7500100l	0.403	0.881	268	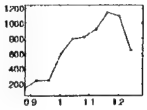
White-Sided Dolphin	7500101 m	0.520	0.298	373	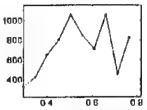
White-Sided Dolphin	7500100p	0.050	1.006	108	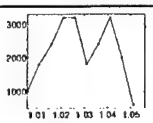
White-Sided Dolphin	7500100q	0.072	0.452	172	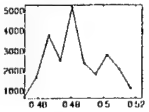
White-Sided Dolphin	7500100r	0.291	1.321	111	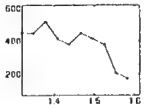
White-Sided Dolphin	75001012	0.360	0.521	159	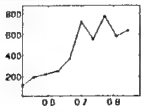
White-Sided Dolphin	75001019	0.232	0.481	229	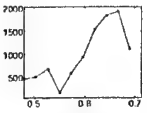
White-Sided Dolphin	7500101a	0.377	0.347	294	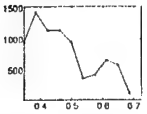
White-Sided Dolphin	7500101l	0.048	0.188	82	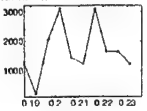
		0.044	0.303	106	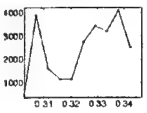
		0.055	0.505	109	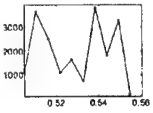

Table 6. Comparison of Various Statistics of Marine Mammal Click Bursts (Cont'd)

Mammal	File Number (.kay)	Duration (s)	Start Time (s)	Clicks/Burst	Instantaneous Click Rate ↑Clicks/s →Time(s)
White-Sided Dolphin	7500101m	0.145	0.293	37	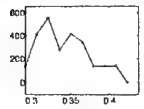
White-Sided Dolphin	7500101n	0.280	1.373	272	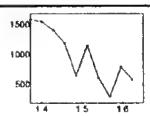
White-Sided Dolphin	7500101q	0.533	1.606	252	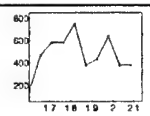
White-Sided Dolphin	7500101r	0.440	0.544	565	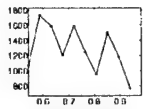
Long-Finned Pilot Whale	77026001	0.471	0.923	892	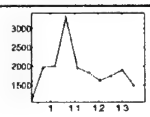
Spotted Dolphin	83006023	0.229	0.752	118	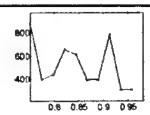
Spotted Dolphin	83006025	0.447	0.665	111	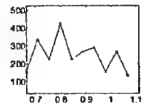
Spotted Dolphin	8300602b	0.376	0.925	142	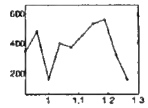
Spotted Dolphin	8300602m	0.602	1.116	98	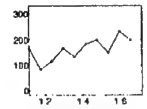
Spotted Dolphin	8300602x	0.232	1.284	505	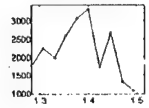

7. TIME-FREQUENCY ANALYSIS OF WHISTLES

Whistles are continuous, frequency-modulated, narrowband, nonstationary sounds whose time-frequency characteristics vary in duration, bandwidth, and shape depending on the marine mammal; i.e., their frequency content varies considerably and in different ways during the time duration of the sound. For example, it is reported[13] that the Atlantic pilot whale has seven categories of whistle time-frequency structures, as follows:

1. Level frequency (essentially no change in frequency throughout the entire duration of the whistle).
2. Falling frequency (decrease in frequency throughout the duration of the whistle).
3. Rising frequency (increase in frequency throughout the duration of the whistle).
4. Up-down frequency (frequency rise followed by frequency fall).
5. Down-up frequency (frequency fall followed by frequency rise).
6. Multiple humps frequency (frequency has at least two inflections).
7. Waver frequency (frequency has at least two inflections symmetrical about some mean).

Thus, for different mammals, the characteristic whistle structure may show a rise or fall in frequency or no change in frequency, or the structure may fall hyperbolically (as 1/frequency), or either change sinusoidally or as a function of some power. In many cases, the time-frequency structure may consist of a combination of various frequency modulation changes. Thus, the whistle's group delay characteristic changes from mammal to mammal. Due to the large variations in whistle structures, Cohen's class QTFRs may not yield the true time-frequency structure of all possible whistles, as these QTFRs are well matched only to constant or linear changes in group delay. Some whistles may be better matched to the generalized time-shift covariant QTFRs of section 4 that take into account the whistle's characteristic group delay structure (for example, a hyperbolic QTFR may be well matched to a whistle with a 1/frequency modulation characteristic). In the next section, various QTFRs are used to analyze the different types of whistles.

7.1 SPECTROGRAM ANALYSIS OF WHISTLES

The spectrogram of various whistles was computed to demonstrate the whistle variations in time-frequency structure using the built-in MATLAB function specgram.m. The spectrogram was used as it is computationally efficient for the large data records. The spotted-dolphin whistles in sound file 83006023.kay are shown in figure 4 to have a power and linear time-frequency characteristic structure, whereas the whistles of the spotted dolphins in sound file 9002709d.kay have sinusoidal time-frequency characteristics, as shown in figure 5. The long-finned pilot whale whistles often have hyperbolic time-frequency characteristics, as shown by the spectrogram of data file 7703500w.kay in figure 6. The spectrogram of the white-sided dolphin whistles from data file 75001016.kay, shown in figure 7, shows a linear/power fall in frequency. The data files may also contain several different types of whistles, as is the case with the striped dolphins from data file 7200700f.kay in figure 8; the frequency seems to be rising and falling in various ways during the sound duration. Most of the figures also contain broadband clicks and, although the figures show some characteristic time-frequency whistle structures for different marine mammals, other structures are also possible by the same mammal. For analysis purposes, the data have been preprocessed to remove low frequencies due to recording equipment or engine noise and have been decimated to reduce the number of samples.

In order to quantify the data, table 7 was compiled with various statistics of the marine mammal's whistles for comparison purposes. The table includes the type of marine mammal producing the whistle, the file from which the data was obtained, and the duration, start time (from the beginning of the file), bandwidth, lowest frequency, and initial frequency of the whistle, as well as a plot of the whistle's idealized time-frequency structure. The spectrogram was used as an analysis tool because of its speed and because it provides sufficient means to obtain these types of measurements. The results of the analysis closely agree with previously published results,[11, 13] and the following characterizations can be derived from the data:

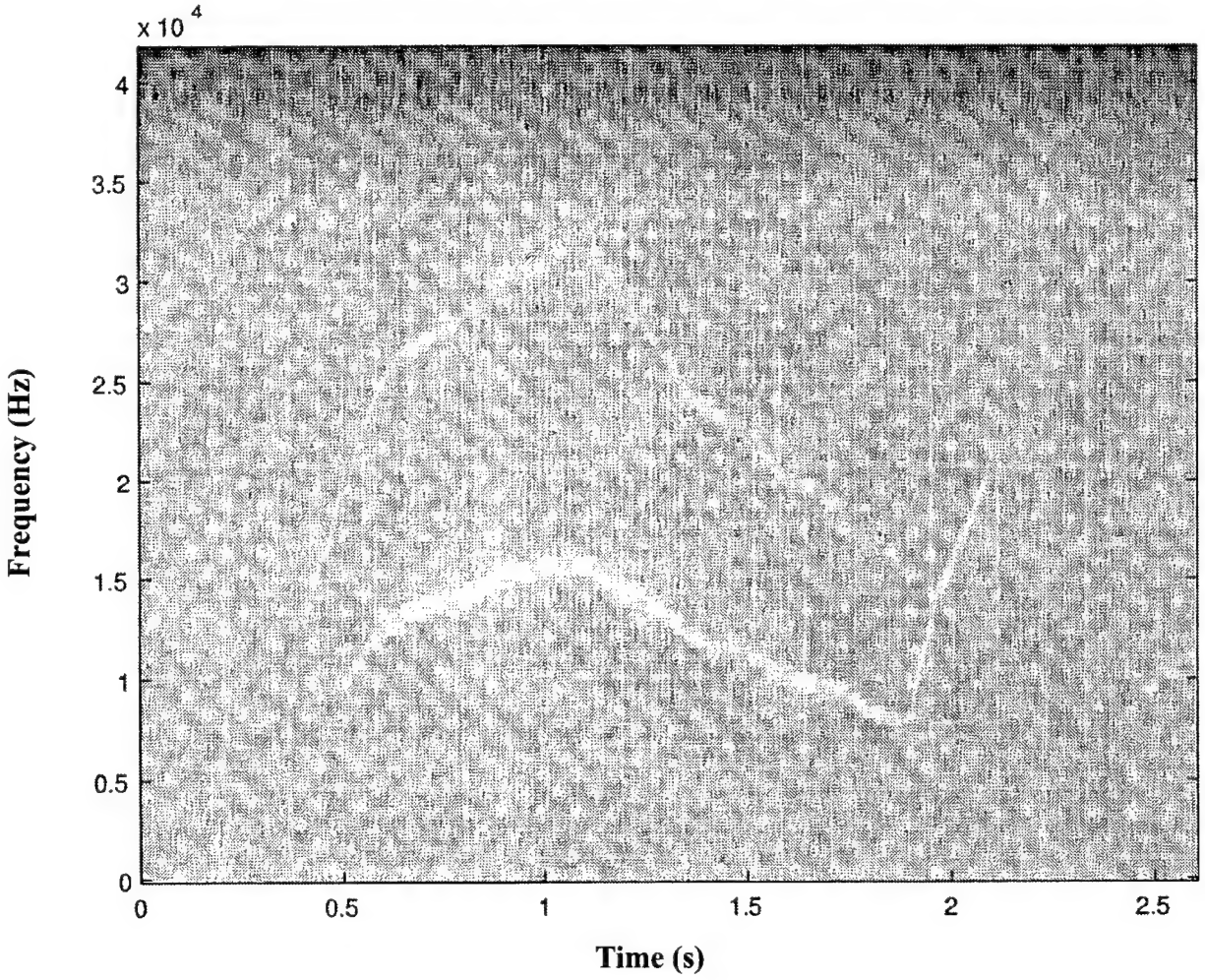

Figure 4. Spectrogram of Spotted-Dolphin Whistles from Data File 83006023.kay Demonstrating Power and Linear (Rise and Fall) Time-Frequency Characteristics

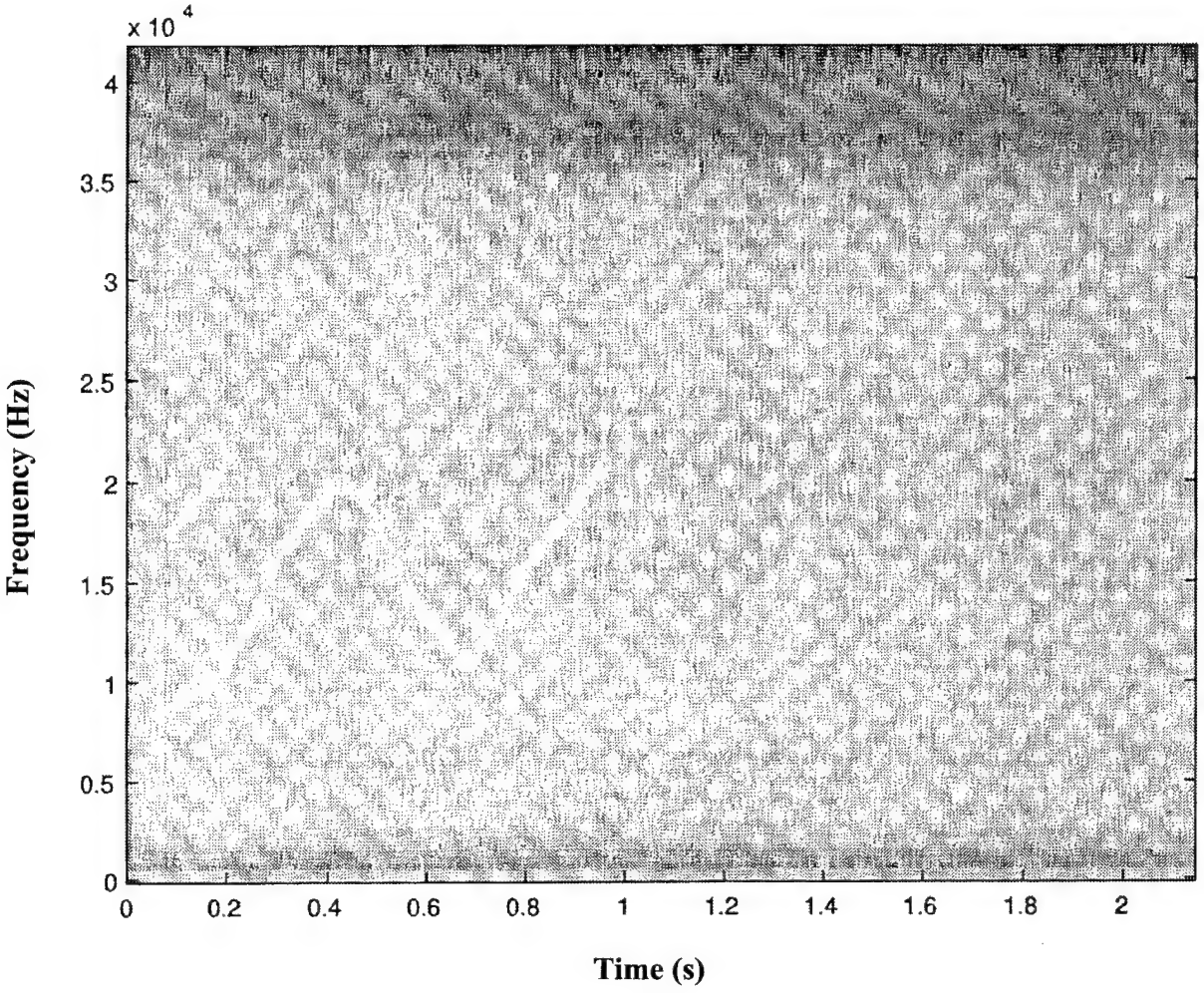

Figure 5. Spectrogram of Spotted-Dolphin Whistles from Data File 9002709d.kay Demonstrating Sinusoidal (Rise, Fall, and Rise) Time-Frequency Characteristics (Sound file also contains humpback and sperm whales.)

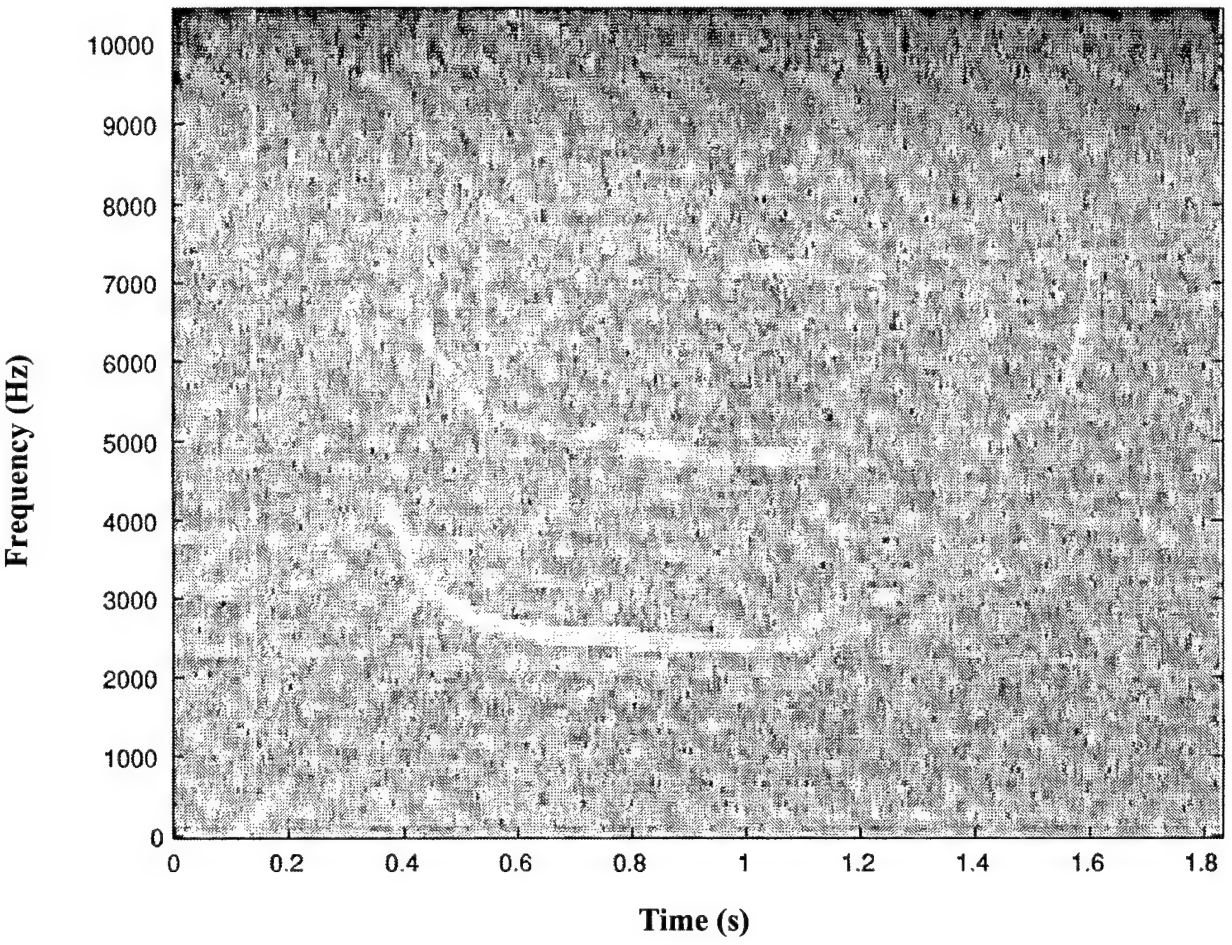

Figure 6. Spectrogram of Long-Finned Pilot Whale Whistles from Data File 7703500w.kay Demonstrating Hyperbolic Time-Frequency Characteristics (Sound file also contains sperm whales.)

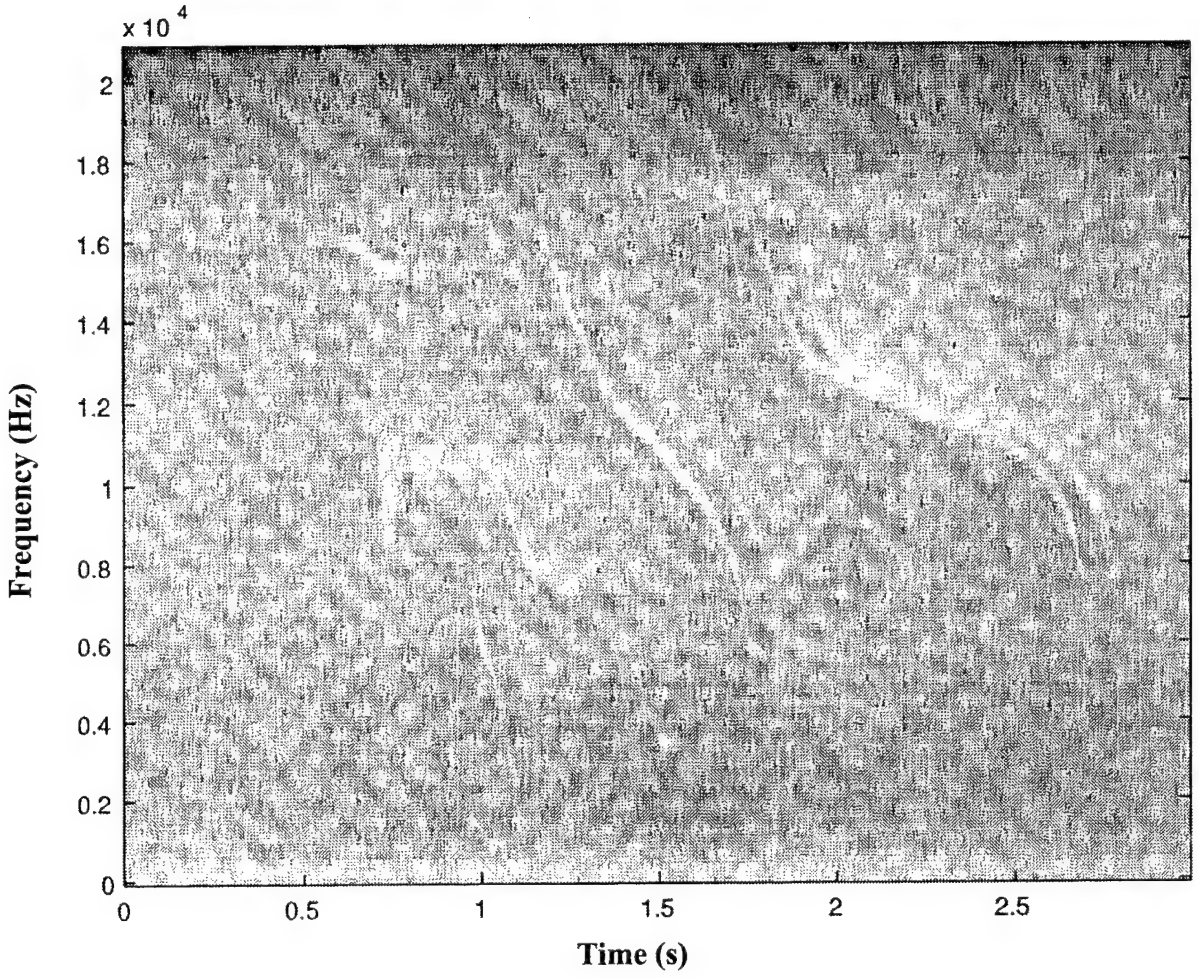

Figure 7. Spectrogram of White-Sided Dolphin Whistles from Data File75001016.kay Demonstrating Linear Fall and Power Time-Frequency Characteristics (Sound file also contains finback whales.)

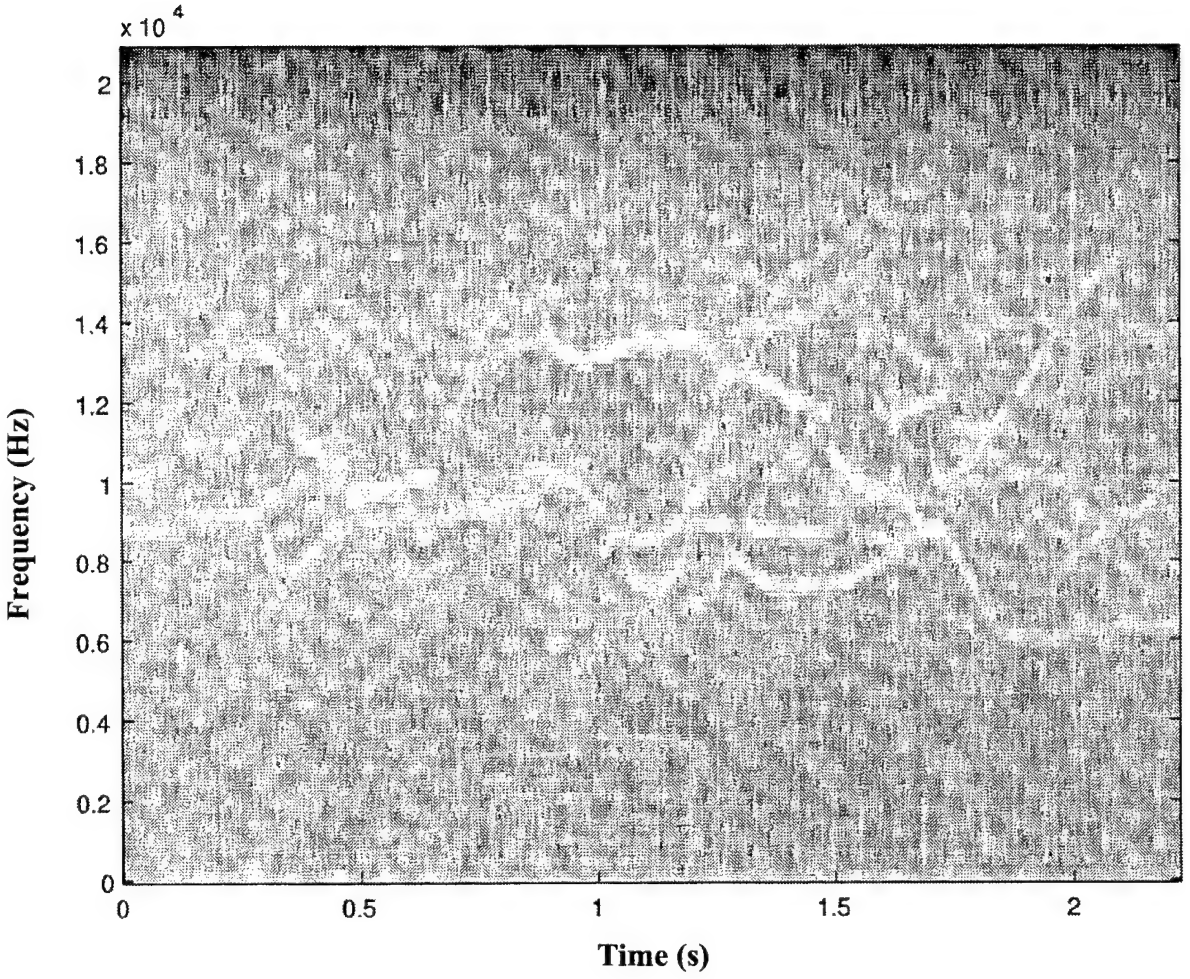

Figure 8. Spectrogram of Striped Dolphin Whistles from Data File 7200700f.kay Demonstrating Various Types of Time-Frequency Characteristics (Sound file also contains sperm whales.)

Table 7. Comparison of Various Statistics of Marine Mammal Whistles

Mammal	File Number (.kay)	Duration (s)	Start Time (s)	Bandwidth (kHz)	Lowest Frequency (kHz)	Initial Frequency (kHz)	Time-Frequency Structure ↑frequency (kHz)→ time (s)
Long-Finned Pilot Whale	7501000f	0.57 0.83 0.57	0.05 0.5 1.5	3.3 3.0 1.91	4.7 4.4 4.4	8.0 4.4 6.3	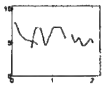
Long-Finned Pilot Whale	75010010	1.3 1.46	0.48 0.45	8.9 4.7	9.7 3.8	9.7 4.2	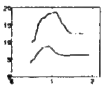
Long-Finned Pilot Whale	75011005	0.63 0.7 0.56	0.97 0.12 0.79	2.4 5.7 5.2	4.5 3.9 6.1	6.6 3.9 6.1	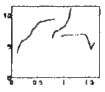
Long-Finned Pilot Whale	75011006	1.04 1.04 0.74 0.43	0.53 0.98 1.2 0.1	5.4 4.6 3.7 4.6	4.3 4.7 3.7 9.0	4.3 4.7 3.7 11.8	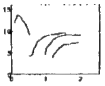
Long-Finned Pilot Whale	75011007	0.87 0.52 0.41 0.74	0.04 0.11 1.17 1.5	2.8 2.4 3.4 5.8	6.5 5.1 5.2 8.7	6.5 5.1 6.2 12.1	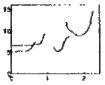
Long-Finned Pilot Whale	7501100b	0.48 0.56	1.33 1.67	4.0 3.4	5.6 5.1	7.5 6.4	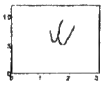
Long-Finned Pilot Whale	75012001	0.52 0.39 0.28 0.97	0.31 0.85 1.33 1.3	3.0 1.6 1.4 2.4	4.4 5.4 4.4 5.9	6.0 6.3 4.9 8.3	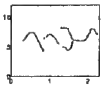
Long-Finned Pilot Whale	7501203q	0.57 0.3 0.5 0.48	0.09 0.92 1.43 2.2	2.4 2.0 2.6 1.4	7.1 6.4 6.4 7.2	7.1 7.1 7.5 7.2	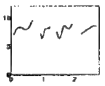
Long-Finned Pilot Whale	7501204h	0.67	1.44	3.7	3.2	3.4	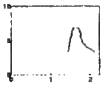

Table 7. Comparison of Various Statistics of Marine Mammal Whistles (Cont'd)

Mammal	File Number (.kay)	Duration (s)	Start Time (s)	Bandwidth (kHz)	Lowest Frequency (kHz)	Initial Frequency (kHz)	Time-Frequency Structure ↑frequency (kHz)→ time (s)
Long-Finned Pilot Whale	7703500a	0.9	0.34	2.0	3.1	3.2	
		0.34	0.25	3.2	4.8	4.8	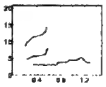
		0.36	0.21	5.4	8.9	8.9	
Long-Finned Pilot Whale	7703500b	0.64	0.11	3.3	1.7	5.0	
		0.39	0.85	1.8	1.9	3.7	
		0.31	1.22	3.0	2.4	5.5	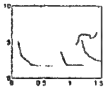
		0.36	1.11	1.7	4.7	4.7	
Long-Finned Pilot Whale	7703500c	0.57	0.62	4.6	2.9	2.9	
		0.79	0.61	4.4	2.3	6.7	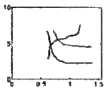
		0.66	0.71	2.3	4.5	6.8	
Long-Finned Pilot Whale	7703500e	0.99	0.02	0.73	1.7	2.4	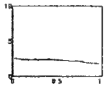
Long-Finned Pilot Whale	7703500g	0.25	0.02	0.03	3.1	3.1	
		0.45	0.2	4.5	2.4	6.9	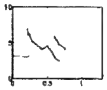
		0.17	0.6	1.8	4.1	5.9	
Long-Finned Pilot Whale	7703500n	0.38	0.18	3.8	4.4	4.4	
		0.36	0.18	5.1	9.5	9.5	
		0.56	0.84	5.4	2.0	7.6	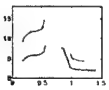
		0.23	0.98	1.7	4.5	6.1	
Long-Finned Pilot Whale	7703500r	0.5	0.23	6.2	2.1	8.2	
		0.71	0.37	1.3	3.2	4.4	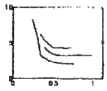
		0.38	0.34	2.0	4.3	6.2	
Long-Finned Pilot Whale	7703500u	0.6	0.2	7.3	2.1	9.3	
		0.43	0.3	2.5	4.2	6.6	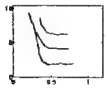
		0.39	0.34	2.2	6.4	8.5	
Long-Finned Pilot Whale	7703500w	0.91	0.29	4.6	2.4	6.9	
		0.69	0.41	2.8	4.7	7.5	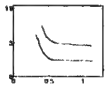
Long-Finned Pilot Whale	7703500x	0.55	0.65	4.2	2.2	6.4	
		1.16	0.17	3.2	4.5	7.6	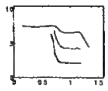
		0.5	0.7	2.6	4.3	6.9	

Table 7. Comparison of Various Statistics of Marine Mammal Whistles (Cont'd)

Mammal	File Number (.kay)	Duration (s)	Start Time (s)	Bandwidth (kHz)	Lowest Frequency (kHz)	Initial Frequency (kHz)	Time-Frequency Structure ↑frequency (kHz)→ time (s)
Long-Finned Pilot Whale	77035010	0.75 0.51	0.08 0.18	0.3 2.1	1.8 3.2	2.0 4.6	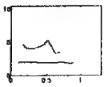
Long-Finned Pilot Whale	77035011	0.43 0.70	0.51 0.57	1.9 1.8	1.9 3.4	3.8 5.3	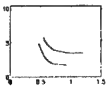
Long-Finned Pilot Whale	77035013	0.42 0.37	0.57 0.64	2.2 1.3	1.8 3.5	4.0 4.5	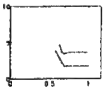
Long-Finned Pilot Whale	77035015	0.81 0.72	0.63 0.72	2.5 2.0	1.8 3.7	4.1 5.7	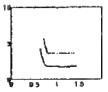
Long-Finned Pilot Whale	7703501a	1.48 0.65	0.21 1.53	1.6 1.1	2.6 3.7	2.6 4.7	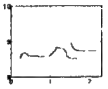
Long-Finned Pilot Whale	7703501e	1.18 0.36	0.02 0.32	9.7 7.2	1.8 4.0	4.4 5.5	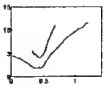
Long-Finned Pilot Whale	7703501g	1.55 0.76 0.63	0.08 0.21 0.89	4.8 1.4 3.4	3.2 2.4 5.3	3.2 3.8 8.7	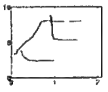
Long-Finned Pilot Whale	7703501w	0.58 0.51 0.41	0.4 0.43 0.76	1.5 2.3 1.3	4.2 1.4 2.6	5.0 3.4 3.9	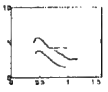
Long-Finned Pilot Whale	77035024	1.24 0.24 0.51	0.16 0.06 0.39	1.4 1.1 0.8	2.4 3.9 6.7	2.3 3.9 7.5	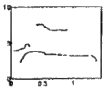
Long-Finned Pilot Whale	7703502c	1.1	0.32	3.5	1.7	1.7	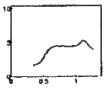
Long-Finned Pilot Whale	7703502d	1.04 0.68	0.29 0.74	1.5 2.7	2.3 2.1	4.0 2.1	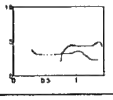

Table 7. Comparison of Various Statistics of Marine Mammal Whistles (Cont'd)

Mammal	File Number (.kay)	Duration (s)	Start Time (s)	Bandwidth (kHz)	Lowest Frequency (kHz)	Initial Frequency (kHz)	Time-Frequency Structure ↑frequency (kHz) → time (s)
White-Sided Dolphin	7500100z	1.0 0.8	0.08 1.9	6.1 9.0	8.1 7.0	14.1 16.0	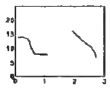
White-Sided Dolphin	75001013	0.26	0.29	3.5	7.6	10.6	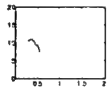
White-Sided Dolphin	75001014	0.50	0.49	5.0	9.3	14.3	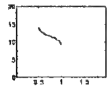
White-Sided Dolphin	75001015	1.11	1.09	8.6	8.9	17.5	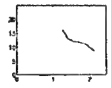
White-Sided Dolphin	75001016	0.7 0.9	1.09 1.8	10.8 7.8	5.7 8.0	16.5 15.8	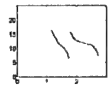
White-Sided Dolphin	75001017	0.76	0.63	5.4	8.9	14.3	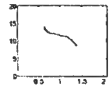
White-Sided Dolphin	75001019	0.72	0.63	6.0	8.8	14.6	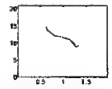
White-Sided Dolphin	7500101a	0.40	0.34	4.7	6.1	10.9	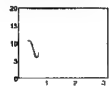
White-Sided Dolphin	7500101b	0.26 0.32 0.52	0.04 0.86 1.2	7.5 4.3 3.0	4.8 7.4 19.4	11.8 11.4 20.5	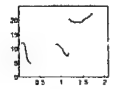
White-Sided Dolphin	7500101d	0.81	0.24	7.2	8.9	16.1	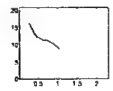
White-Sided Dolphin	7500101f	0.53	0.06	7.6	12.7	19.9	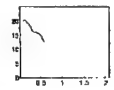
White-Sided Dolphin	7500101h	0.35 0.41	0.02 1.39	2.4 6.3	8.0 7.3	10.6 13.6	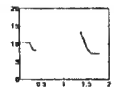

Table 7. Comparison of Various Statistics of Marine Mammal Whistles (Cont'd)

Mammal	File Number (.kay)	Duration (s)	Start Time (s)	Bandwidth (kHz)	Lowest Frequency (kHz)	Initial Frequency (kHz)	Time-Frequency Structure ↑frequency (kHz) → time (s)
White-Sided Dolphin	7500101j	0.59	0.70	2.9	9.6	12.5	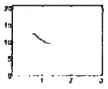
White-Sided Dolphin	7500101n	0.66	1.02	2.6	7.4	10.1	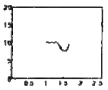
White-Sided Dolphin	7500101q	0.63	1.27	6.7	14.4	17.8	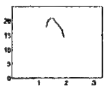
White-Sided Dolphin	7500101r	0.71	0.19	5.4	8.9	12.2	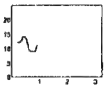
White-Sided Dolphin	75001027	0.59	0.50	6.6	8.8	15.7	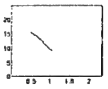
White-Sided Dolphin	75001028	1.0	0.62	10.1	12.2	12.2	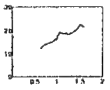
White-Sided Dolphin	7500102a	0.60	0.30	5.9	8.5	14.3	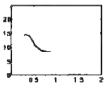
White-Sided Dolphin	7500102b	0.81	0.12	7.6	7.8	15.4	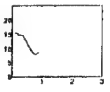
White-Sided Dolphin	7500102f	0.27	0.99	7.6	5.1	12.7	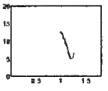
White-Sided Dolphin	7500102g	0.91 0.50 0.22	0.33 1.23 1.73	10.5 10.8 5.4	6.5 10.4 15.5	9.4 21.3 21.0	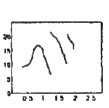
White-Sided Dolphin	7500102i	1.40	0.04	15.3	8.4	22.7	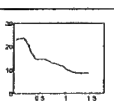
White-Sided Dolphin	7500102m	0.47 0.36 0.38	0.12 0.71 1.28	11.2 4.1 10.7	6.5 16.0 7.1	16.2 18.7 17.7	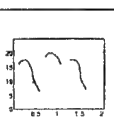
White-Sided Dolphin	7500102o	0.50	0.14	12.2	6.4	16.8	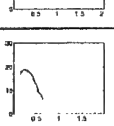

Table 7. Comparison of Various Statistics of Marine Mammal Whistles (Cont'd)

Mammal	File Number (.kay)	Duration (s)	Start Time (s)	Bandwidth (kHz)	Lowest Frequency (kHz)	Initial Frequency (kHz)	Time-Frequency Structure ↑frequency (kHz)→ time (s)
White-Sided Dolphin	7500102r	0.95	0.33	7.5	8.0	13.0	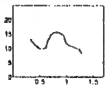
White-Sided Dolphin	7500102s	0.85 0.44 1.25	0.13 1.01 1.71	10.5 10.8 14.2	9.2 7.0 7.7	14.1 15.5 19.9	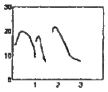
White-Sided Dolphin	7500102v	0.93	0.25	8.9	10.1	13.9	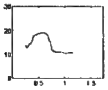
White-Sided Dolphin	7500102w	0.14 0.23	0.12 0.91	8.5 9.2	7.1 6.0	15.5 15.2	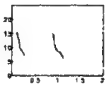
White-Sided Dolphin	7500102x	0.77 0.90	0.38 0.39	13.3 7.0	17.0 7.6	27.1 13.3	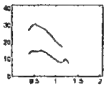
White-Sided Dolphin	7500103d	0.39 0.23 0.55	0.38 1.08 1.94	4.6 3.2 10.0	8.1 11.4 7.7	12.5 14.6 17.7	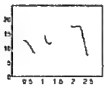
White-Sided Dolphin	7500103e	0.46 0.48	0.35 1.78	10.7 5.8	7.1 7.6	17.1 12.0	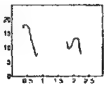
White-Sided Dolphin	7500103g	0.35 0.43 0.70	0.84 1.24 1.77	5.0 9.8 3.9	10.1 7.3 10.5	15.0 14.4 14.3	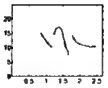
White-Sided Dolphin	75001031	0.45 0.46	0.32 0.73	2.3 3.3	12.3 7.4	14.7 10.7	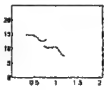
White-Sided Dolphin	7500103p	0.21 0.80	0.05 0.26	3.5 5.6	17.7 8.2	21.0 13.7	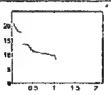
White-Sided Dolphin	7500103w	0.47 0.24 0.27	0.14 1.45 1.70	2.6 2.9 4.4	8.0 12.4 5.8	10.7 15.3 10.3	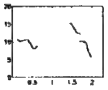
White-Sided Dolphin	75001041	0.60 0.80 0.60	0.13 1.14 1.78	4.6 6.2 4.9	9.1 7.1 8.6	14.0 13.4 13.4	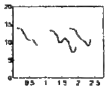

Table 7. Comparison of Various Statistics of Marine Mammal Whistles (Cont'd)

Mammal	File Number (.kay)	Duration (s)	Start Time (s)	Bandwidth (kHz)	Lowest Frequency (kHz)	Initial Frequency (kHz)	Time-Frequency Structure ↑frequency (kHz) → time (s)
Spotted Dolphin	8300601q	1.03 1.14	0.43 1.0	14.5 5.2	7.3 6.4	7.3 8.9	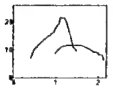
Spotted Dolphin	83006023	1.38	0.49	8.0	7.5	9.2	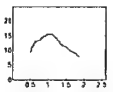
Spotted Dolphin	83006025	0.89	0.28	6.3	9.1	9.1	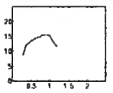
Spotted Dolphin	83006027	0.96	0.19	7.4	7.9	7.9	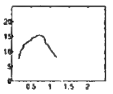
Spotted Dolphin	8300602b	0.96 1.39 0.7	0.49 1.05 1.35	7.4 17.3 6.9	8.2 6.5 8.6	8.2 8.9 11.1	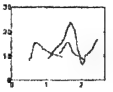
Spotted Dolphin	8300602i	1.37 2.17	0.18 0.61	11.2 19.2	10.5 4.8	15.7 4.8	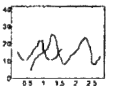
Spotted Dolphin	8300602m	2.46 1.49 0.72	0.41 0.97 2.23	22.5 9.6 9.1	8.0 5.6 6.9	8.0 8.1 11.0	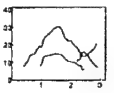
Spotted Dolphin	8300602t	1.72	0.15	8.8	6.9	6.9	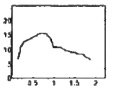
Spotted Dolphin	8300602x	1.05 1.12 1.03	0.38 0.75 1.45	9.4 7.8 14.0	7.7 7.6 10.1	7.9 7.6 12.4	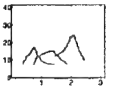
Spotted Dolphin	83006031	1.24	0.75	8.1	7.5	9.3	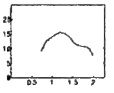

Table 7. Comparison of Various Statistics of Marine Mammal Whistles (Cont'd)

Mammal	File Number (.kay)	Duration (s)	Start Time (s)	Bandwidth (kHz)	Lowest Frequency (kHz)	Initial Frequency (kHz)	Time-Frequency Structure ↑frequency (kHz) → time (s)
Spotted Dolphin	83006032	1.09	0.06	6.4	8.6	8.6	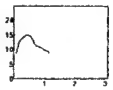
Spotted Dolphin	83006033	1.57	0.37	7.1	8.1	8.6	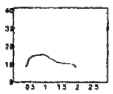
Spotted Dolphin	8300603c	1.04	1.57	11.7	5.1	5.1	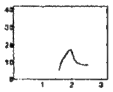
Spotted Dolphin	8300603s	0.82	0.66	9.0	7.2	7.2	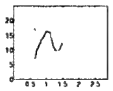
Spotted Dolphin	8300603u	1.21	0.53	9.5	7.1	7.1	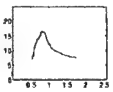
Spotted Dolphin	83006047	1.43	0.36	10.6	5.3	5.3	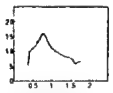
Spotted Dolphin	83035024	1.17	0.75	12.8	7.3	7.3	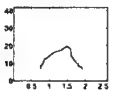
Spotted Dolphin	90027091	0.69 0.36	0.23 0.72	13.4 9.2	10.7 8.7	10.7 8.5	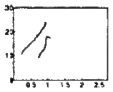
Spotted Dolphin	90027092	0.52	0.07	5.9	11.3	11.2	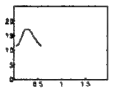
Spotted Dolphin	9002709d	0.84	0.12	12.2	9.6	9.6	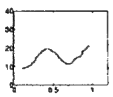

Table 7. Comparison of Various Statistics of Marine Mammal Whistles (Cont'd)

Mammal	File Number (.kay)	Duration (s)	Start Time (s)	Bandwidth (kHz)	Lowest Frequency (kHz)	Initial Frequency (kHz)	Time-Frequency Structure ↑frequency (kHz)→ time (s)
Striped Dolphin	72007003	0.94	0.45	7.5	7.6	7.6	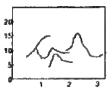
		1.15	0.85	3.4	7.3	10.7	
		0.84	1.28	4.2	4.3	4.3	
		1.32	1.88	8.2	7.6	9.9	
Striped Dolphin	72007004	0.99	0.04	9.7	6.3	6.3	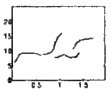
		0.52	0.89	1.6	7.6	7.6	
		0.43	1.28	3.7	10.6	10.6	
Striped Dolphin	72007005	0.43	0.11	4.9	7.3	7.3	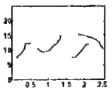
		0.66	0.69	5.6	9.3	10.6	
		0.43	1.69	4.8	7.4	7.6	
		0.7	1.83	4.8	10.6	15.4	
Striped Dolphin	72007006	1.48	0.03	9.0	8.5	13.6	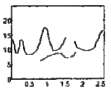
		1.04	0.78	3.1	6.3	6.3	
		0.77	1.79	7.2	9.7	12.7	
Striped Dolphin	72007007	0.49	0.02	5.1	8.9	8.9	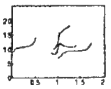
		0.36	0.90	8.2	9.9	9.9	
		0.53	0.87	4.0	8.0	8.5	
		0.73	1.01	5.4	6.8	6.8	
Striped Dolphin	7200700a	1.65	0.03	9.4	9.8	9.8	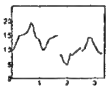
		0.72	1.75	6.0	4.7	8.2	
		0.69	2.55	5.4	8.6	9.6	
Striped Dolphin	7200700b	1.09	0.03	4.6	5.9	7.3	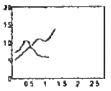
		1.22	0.08	8.5	5.2	5.2	
Striped Dolphin	7200700c	1.10	0.02	7.9	4.9	9.4	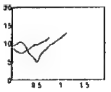
		0.73	0.04	4.2	7.3	8.6	
Striped Dolphin	7200700e	0.42	0.11	9.0	7.9	16.3	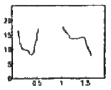
		0.59	1.03	11.0	7.5	18.5	
Striped Dolphin	7200700f	0.71	0.07	4.3	9.4	9.7	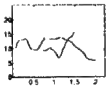
		0.73	0.74	9.0	6.8	9.3	
		1.10	0.89	8.2	5.5	13.3	

Table 7. Comparison of Various Statistics of Marine Mammal Whistles (Cont'd)

Mammal	File Number (.kay)	Duration (s)	Start Time (s)	Bandwidth (kHz)	Lowest Frequency (kHz)	Initial Frequency (kHz)	Time-Frequency Structure ↑frequency (kHz) → time (s)
Striped Dolphin	7200700g	0.76	0.10	10.1	10.4	12.0	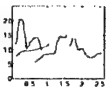
		0.93	0.12	4.4	7.7	7.7	
		0.93	0.64	9.3	5.8	5.8	
		0.88	1.66	6.5	7.3	11.6	
Striped Dolphin	7200700h	0.81	0.05	3.5	5.0	8.5	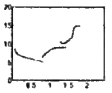
		0.62	0.81	2.7	6.3	6.3	
		0.49	1.30	4.9	10.1	10.7	
Striped Dolphin	7200700k	0.99	0.56	10.3	8.9	11.4	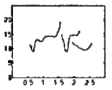
		0.59	1.59	7.1	9.0	14.8	
		0.63	1.93	2.7	9.4	12.2	
Striped Dolphin	7200700m	1.04	0.91	5.4	5.7	11.1	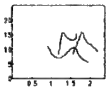
		0.48	1.18	7.5	8.4	8.4	
		0.63	1.56	7.7	8.3	8.3	
Striped Dolphin	7200700o	1.11	0.69	7.3	5.7	12.8	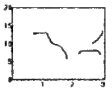
		0.70	2.22	1.2	6.8	7.3	
		0.35	2.66	3.5	10.3	10.3	
Striped Dolphin	7200700q	0.94	0.03	9.4	11.2	13.2	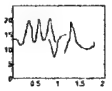
		0.38	0.80	8.1	7.1	13.7	
		0.67	1.15	10.9	8.8	8.8	
Striped Dolphin	7200700t	0.93	0.15	8.7	7.0	15.1	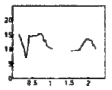
		0.66	1.55	4.2	9.3	9.3	
Striped Dolphin	7200700v	0.90	0.03	5.4	8.1	12.7	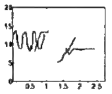
		0.41	0.64	5.4	8.1	8.1	
		0.55	1.32	6.5	5.2	5.2	
		0.86	1.57	1.7	7.3	8.9	
Striped Dolphin	72007027	0.53	0.60	7.3	9.2	16.7	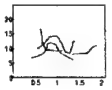
		0.84	0.55	5.6	8.5	9.9	
		0.93	0.42	6.0	6.2	6.8	
		0.56	1.33	3.0	8.0	8.0	
Striped Dolphin	7200702b	1.20	0.02	5.7	8.5	8.4	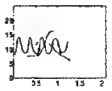
		0.62	0.30	9.1	7.5	7.5	
		0.50	0.80	5.9	6.1	12.0	

- Long-finned pilot whales are characterized by low-frequency-range whistles. The mean initial frequency is 5.7 kHz, the mean minimum frequency is 4.1 kHz, and the mean bandwidth is 3.1 kHz. Rhythmically repeated individual whistles were often noted. Many of the whistles have hyperbolic time-frequency characteristics; however, other time-frequency structures were also observed.

- White-sided dolphins are characterized by high-frequency-range whistles. The mean initial frequency is 15 kHz, the mean minimum frequency is 9.1 kHz, and the mean bandwidth is 6.9 kHz. The whistles often seem to repeat rhythmically. Similar to the whistle of the long-finned pilot whale, this whistle does not have the stereotypical sinusoidal frequency modulation. The whistles appear to fall in frequency in a somewhat linear fashion.

- Spotted-dolphin whistles are characterized by high-frequency-range whistles. The mean initial frequency is 8.7 kHz, the mean minimum frequency is 7.8 kHz, and the mean bandwidth is 10.4 kHz. The whistles appear to have power time-frequency characteristics.

- Striped dolphins are also characterized by high-frequency-range whistles. The mean initial frequency is 9.9 kHz, the mean minimum frequency is 7.7 kHz, and the mean bandwidth is 6.2 kHz. The whistles appear to have the stereotypical sinusoidal frequency modulation and have both rising and falling time-frequency components.

Thus, from the data analyzed, the long-finned pilot whale whistles start at a lower frequency and have narrower bandwidths than the white-sided, spotted, and striped dolphins. Although the time-frequency structure of the whistle varied greatly, it is noted that the observed long-finned pilot whale whistles have a hyperbolic or exponential structure; however, other studies show that the long-finned pilot whales do not have a characteristically exclusive whistle type.[14]

The last column in table 7 provides a convenient and intuitive tool for interpreting the time-frequency characteristics of the whistles. It also provides some preliminary information on the group delay structure of the whistles so that the generalized time shift of the generalized warped QTFR can be chosen to match the signal's group delay for better analysis results. The time-frequency curves in the last column of table 7 were obtained by selecting time-frequency points from the spectrogram analysis of the whistles, and then by using cubic spline interpolation to fit the selected points.

Additional deductions were also made from table 7 and are summarized in table 8 for long-finned pilot whales, in table 9 for white-sided dolphins, in table 10 for spotted dolphins, and in table 11 for striped dolphins. The tables show the mean value and the standard deviation of the initial frequency, the minimum frequency, the bandwidth, and the duration of the whistles of each marine mammal. Below each table, histograms of the various statistics are also given to show the distribution of each of the whistle characteristics. Based on the computed mean and standard deviation, the corresponding Gaussian distribution was also computed and superimposed on the histogram. Although the distribution of the whistle characteristic is not clearly Gaussian, the superposition helps to show the mean value of the whistle characteristic. For example, the initial frequency of the white-sided dolphin in table 9 has a mean value of 15.04 kHz and a standard deviation of 3.44 kHz. The corresponding histogram for the initial frequency in table 9 shows that the distribution of the initial frequencies is close to a Gaussian distribution with the given mean and standard deviation.

Table 8. Whistle Statistics for Long-Finned Pilot Whales
(Statistical sample size is 80 data sets.)

Statistic	Initial Frequency (kHz)	Minimum Frequency (kHz)	Bandwidth (kHz)	Duration (sec)
Mean	5.66	4.13	3.11	0.64
Standard Deviation	2.16	1.96	1.86	0.30

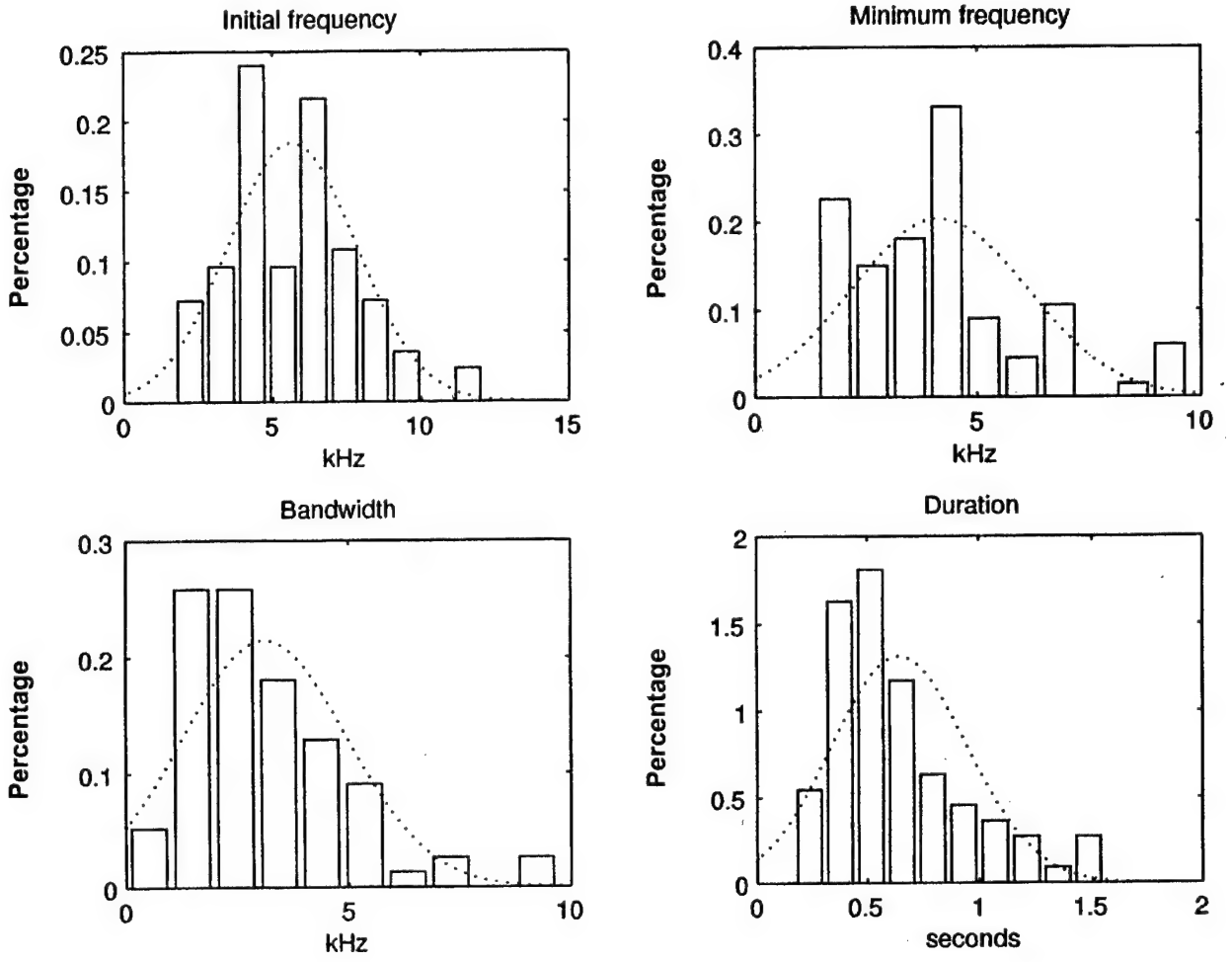

Table 9. Whistle Statistics for White-Sided Dolphins
(Statistical sample size is 61 data sets.)

Statistic	Initial Frequency (kHz)	Minimum Frequency (kHz)	Bandwidth (kHz)	Duration (sec)
Mean	15.04	9.06	6.95	0.59
Standard Deviation	3.44	3.09	3.18	0.27

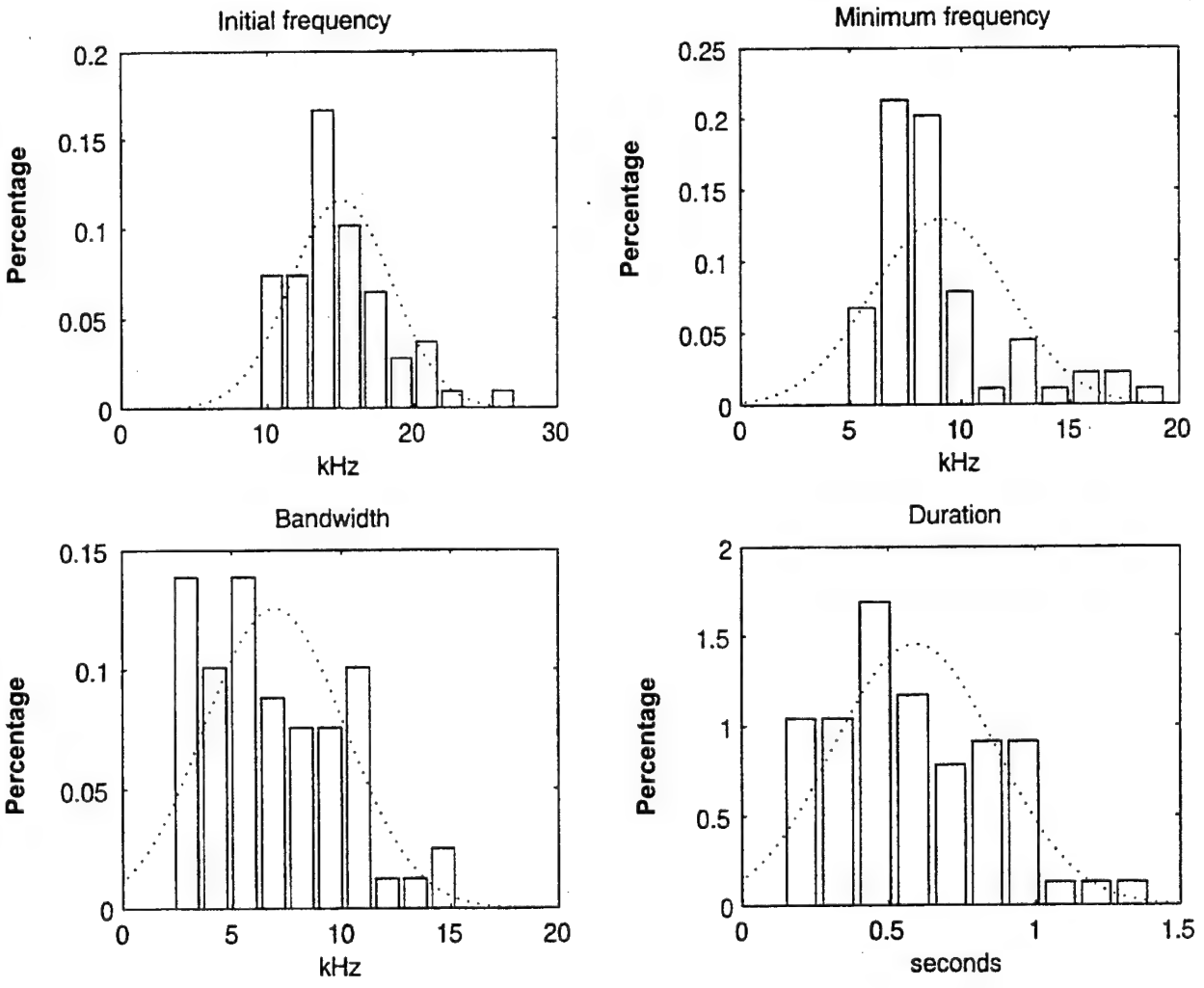

Table 10. Whistle Statistics for Spotted Dolphins
(Statistical sample size is 29 data sets.)

Statistic	Initial Frequency (kHz)	Minimum Frequency (kHz)	Bandwidth (kHz)	Duration (sec)
Mean	8.67	7.80	10.36	1.16
Standard Deviation	2.24	1.63	4.10	0.45

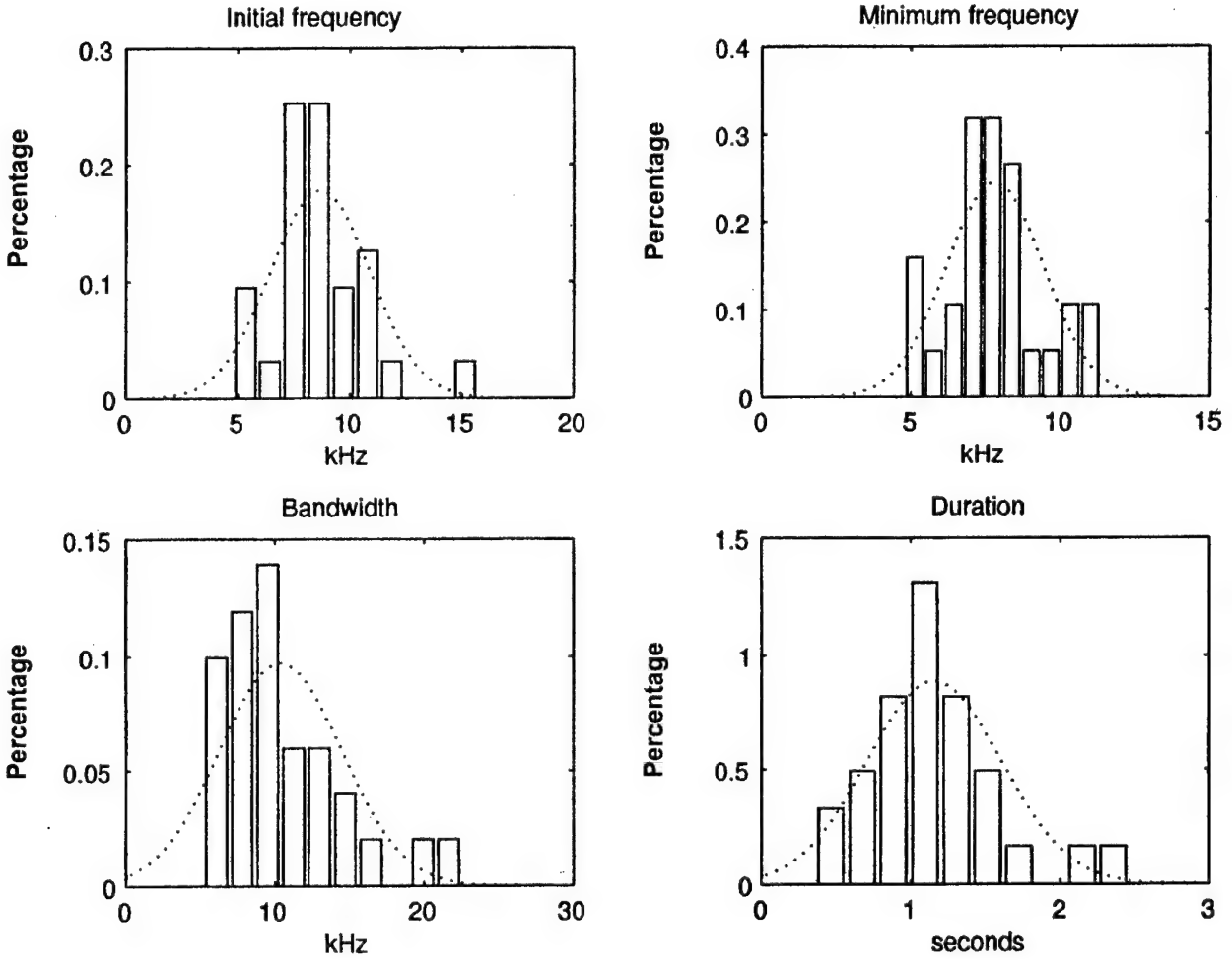

Table 11. Whistle Statistics for Striped Dolphins
(Statistical sample size is 62 data sets.)

Statistic	Initial Frequency (kHz)	Minimum Frequency (kHz)	Bandwidth (kHz)	Duration (sec)
Mean	9.98	7.72	6.21	0.77
Standard Deviation	3.04	1.66	2.46	0.28

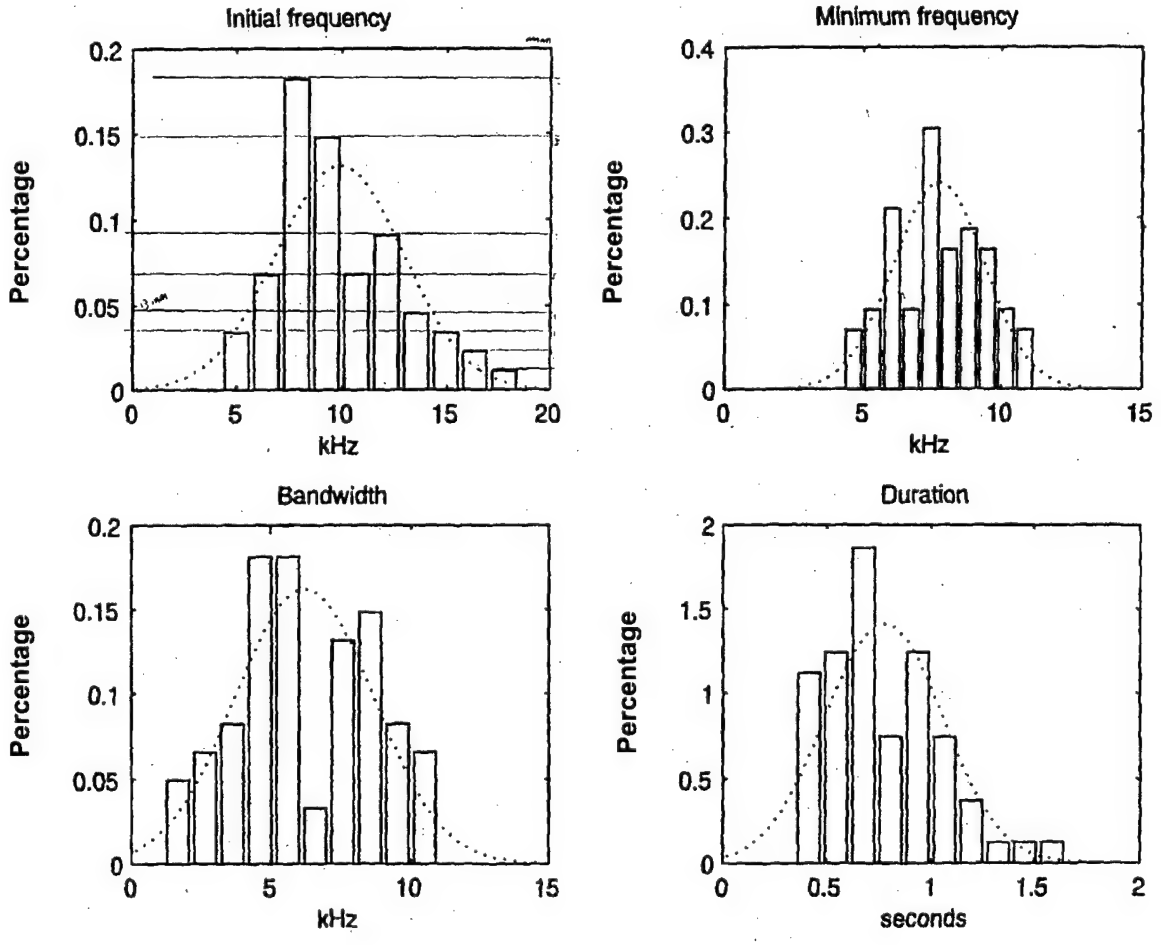

For some of the data files, the spectrogram analysis of whistles yielded various higher harmonics as well as the first harmonic (belonging to the actual whistle). This phenomenon usually occurred in files consisting of spotted dolphin whistles, together with clicks and pulsed clicks. In particular, the whistle harmonics appear to occur in the region of the pulsed clicks. For example, figure 9 shows the spectrogram of data file 8300603c.kay; although the data information that came with the file states that one whistle is present, other harmonics are clearly present. It is important to investigate whether the harmonics effect was due to the analysis tool or whether it was either a biological effect or a recording artifact. Watkins[16] states that, depending on the spectrogram window, the interpretation of spectrogram analysis composed of pulsed trains (such as pulsed clicks) could be confusing. This is because as the pulse rate increases (that is, as the number of clicks per second increases), harmonics result at multiple increments of the pulse rate if the window used is not shorter than the time duration between clicks. The harmonics at the various frequencies now appear more like whistles, since their frequencies change as the pulse rate changes. In our case, however, the spectrogram window length and the pulse rate were such that a harmonic effect should not have been observed in the data. In addition, figure 9 shows that the pulsed clicks are still present. This indicates that the harmonics are actually part of the whistles, not the clicks. Further analysis using the time signal and the Wigner distribution (that have no windowing effect) show that the harmonics are still present; the higher harmonics, therefore, may be part of the sounds that the mammals produce, and the higher harmonic (higher frequencies) indicates a decrease in harmonic energy. Another possibility is that the harmonics are the result of the recording. In either case, it is important to know that the harmonics are present at the higher frequencies, even if their energy decreases.

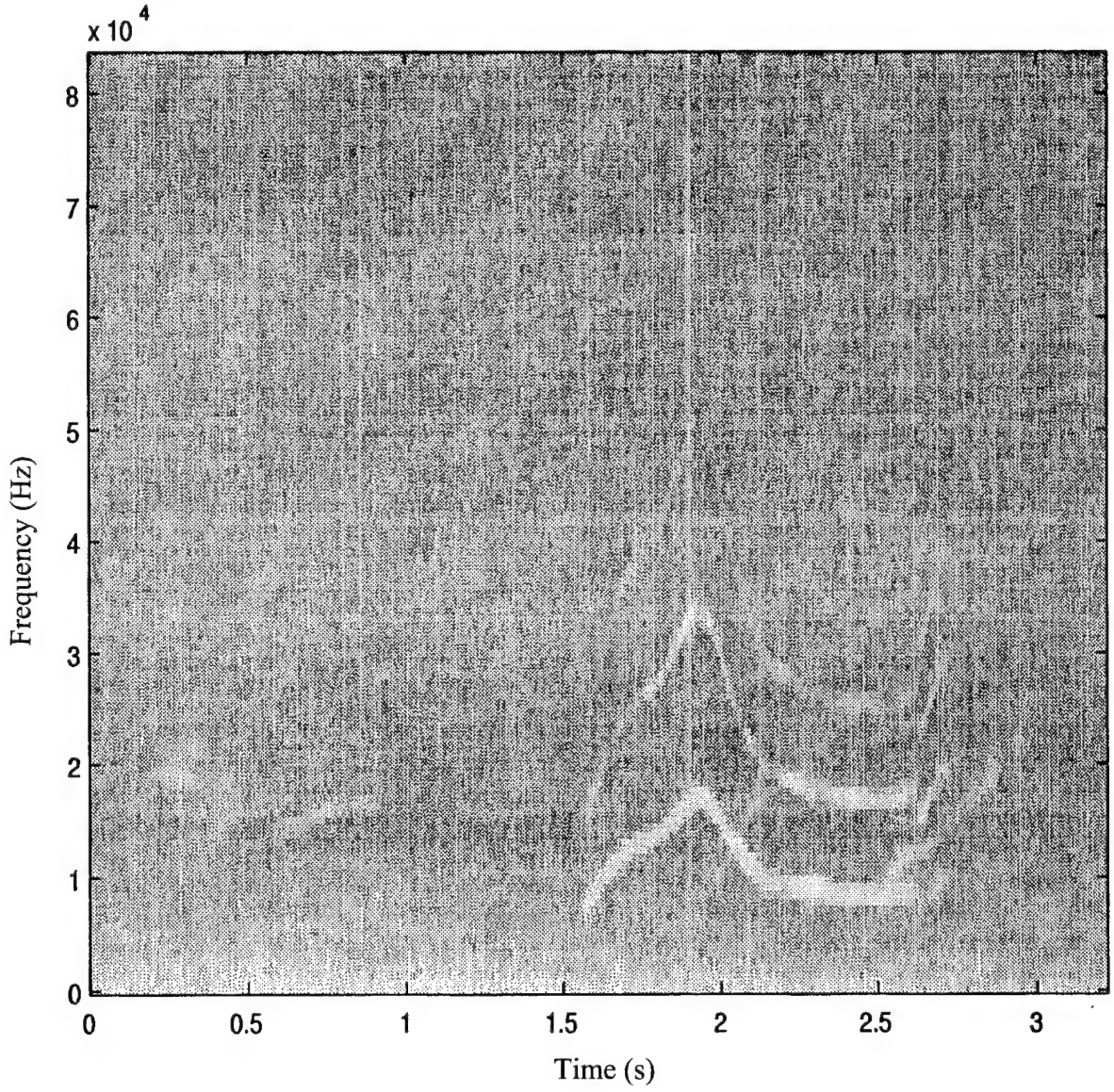

Figure 9. Spectrogram of a Spotted-Dolphin Whistle from Data file 8300603c.kay (Note the four whistle harmonics between 1.5 s and 2.7 s.)

7.2 OTHER COHEN'S CLASS QTFRs ANALYSIS OF WHISTLES

7.2.1 Wigner Distribution

The whistles extend over a large number of samples in the data, as shown by the fact that the data sampling rate is 166.66 kHz, and the mean values of the duration of the various whistles, as shown in tables 8 through 11, range from 0.59 s to 1.16 s. Thus, most whistles extend over a sample duration of 98,000 to 193,000 data samples. As a result, the QTFR implementation algorithms must be able to handle large data files. The spectrogram is computed efficiently using a built-in MATLAB function; however, the current implementation of the Wigner distribution using MATLAB can only be used to analyze small blocks of data (block lengths of 1024 samples). Since the sampling rate of the data (166.666 kHz) is at least four times the bandwidth of the analog data, and not much information is present above 20 kHz other than the broadband clicks, decimation was used to decrease the number of data samples as it allows Wigner distributions of larger sections of data in time to be computed. An algorithm was also devised to compute the Wigner distribution of small records, and then to piece the resulting Wigner distributions into one large time-frequency representation. This increases the resulting block section that can be analyzed to 12,800 samples. Note, however, that the resulting representation is not equivalent to the true Wigner distribution of the entire data section, as the representation does not include the cross terms between any two data blocks. The MATLAB function for this representation is given in section A.5 in the appendix. This function also demonstrates the use of decimation to reduce the data samples.

7.2.2 Smoothed Pseudo-Wigner Distribution

Most of the MATLAB algorithms presently available to compute various QTFRs, as shown in section A.4 in the appendix, can only process short signals in an off-line fashion. However, the mammal sounds from the SOUND database are long signals with a sampling rate of 166,666 samples per second. For example, a dolphin whistle of only 2 s is considered a long signal, as it consists of 333,332 samples. Thus, to analyze long segments of data, new methods of computing QTFRs are needed for real-time, on-line operations.

7.2.2.1 Direct Method and Short-Time Technique. Two methods for computing the smoothed pseudo-Wigner distribution of long data sets are discussed below.

1. **Direct Method**. The smoothed pseudo-Wigner distribution is a smoothed version of the Wigner distribution that can be used to remove cross terms when multicomponent or complicated monocomponent signals are analyzed. As defined in equation (9), the SPWD uses a time-smoothing window $g(t)$ and a frequency-smoothing window $H(f)$ that independently control the smoothing in the time and frequency directions. The current MATLAB program computes the SPWD indirectly by first multiplying the signal's narrowband ambiguity function $AF_X(\tau, \nu)$ with the function $G(\nu)h(\tau)$ then the two-dimensional Fourier transform of the product is taken. That is,

$$SPWD_X(t, f) = \int_{-\infty}^{\infty} \int_{-\infty}^{\infty} G(\nu)h(\tau)AF_X(\tau, \nu)e^{j2\pi(\nu - ft)}\, d\tau\, d\nu, \tag{35}$$

where the ambiguity function is the two-dimensional Fourier transform of the Wigner distribution in equation (5), $AF_X(\tau,\nu) = \int_{-\infty}^{\infty} \int_{-\infty}^{\infty} WD_X(t, f)e^{-j2\pi(\nu - ft)}\, dtdf$; $G(\nu)$ is the Fourier transform of $g(\tau)$ and $h(\tau)$ and is the inverse Fourier transform of H (f) in equation (9). This indirect method requires the whole data segment (off-line) in order to compute the ambiguity function, and can only process short signals as the result is saved as an N × N matrix, where N is the number of signal samples. In order to enable an on-line computation of the SPWD, a program was written that computes the SPWD using a more direct method. In particular, the local autocorrelation function $x\left(t+\frac{\tau}{2}\right)x^*\left(t-\frac{\tau}{2}\right)$ of the signal $x(t)$ is first computed and then convolved with the time-smoothing window $g(\tau)$ of length N_g. Since the length of the window is considerably smaller than the length of the data, i.e., $N_g << N$, only a small section of the local autocorrelation function needs to be computed. In addition, the local autocorrelation function can be updated so that the previous value can be used to compute the next value. The result of the convolution then gets multiplied with the squared magnitude of the frequency-smoothing window $h(t)$ of even length N_h and the Fourier transform of the product is obtained.

Thus, although the SPWD is a smoothed version of the Wigner distribution as shown in equation (9), it can also be computed as

$$SPWD_X(t,f) = \int_{-\infty}^{\infty}\left[h\left(\frac{\tau}{2}\right)h^*\left(-\frac{\tau}{2}\right)\left(\int_{-\infty}^{\infty}x\left(\hat{t}+\frac{\tau}{2}\right)x^*\left(\hat{t}-\frac{\tau}{2}\right)g(t-\hat{t})d\hat{t}\right)\right]e^{-j2\pi\tau f}d\tau, \qquad (36)$$

where $h(t)$ is the inverse Fourier transform of $H(f)$ in equation (9). At the end of the computation, the SPWD is stored in an $N_h \times N$ matrix. As a result, since not all the data is used at once to produce each time-slice of the SPWD, the computation is performed on-line and is not computationally intensive. In addition, it allows for larger sections of the data to be analyzed. The MATLAB function for this algorithm is given in section A.6 in the appendix. Figures 10 and 11 show two examples of using the SPWD in equation (36) to analyze large sections of the mammal sounds. Figure 10 shows the SPWD of a long-finned pilot whale whistle for a data segment of 14,815 samples (corresponding to 0.8 s, where the data was decimated by a factor of 9 to reduce the total number of samples without aliasing). The hyperbolic time-frequency signature of the whistle is clearly shown by the SPWD, without suffering from any inner cross terms. Here, a Blackman time-smoothing window of length $N_g = 114$ and a Hamming frequency-smoothing window of length $N_h = 200$ were used. The resulting SPWD was a $100 \times 14{,}815$ matrix, since only the positive frequencies were obtained as the analysis signal is real. Similarly, figure 11 shows the SPWD of a spotted-dolphin whistle for a data segment of 37,500 samples (corresponding to 0.45 s, where the data was decimated by a factor of 2).

2. **Short-Time Technique**. Any member of Cohen's class in section 3.1 can be obtained as in equation (7). Another way of obtaining Cohen's class QTFRs $T_X^{(C)}(t,f)$ is by first computing the ambiguity function $AF_X(\tau,\nu)$ of the data and multiplying the ambiguity function with a two-dimensional kernel $\Psi_T^{(C)}(\tau,\nu)$ that completely characterizes the chosen QTFR; then the two-dimensional Fourier transform of the product is taken; i.e,

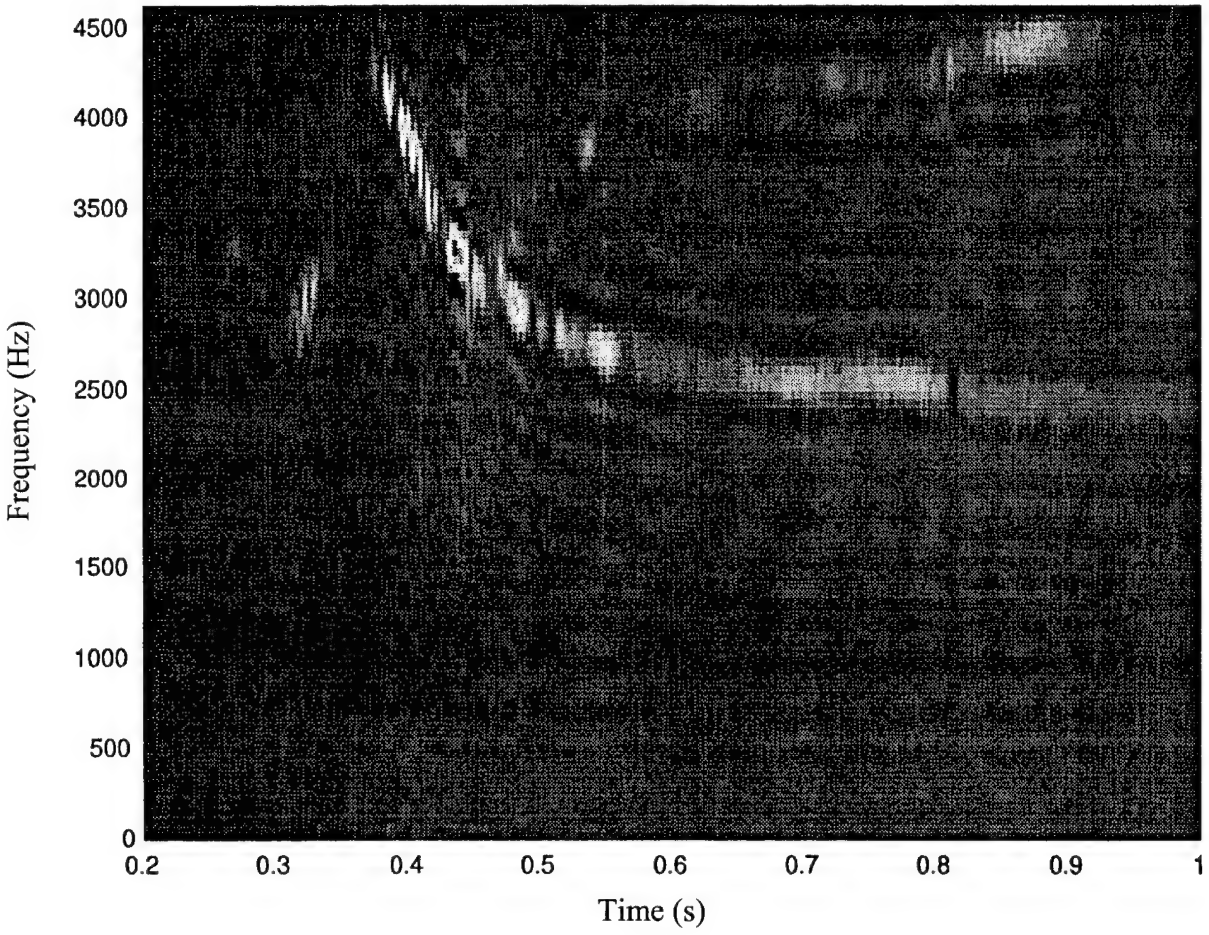

Figure 10. Direct SPWD of a Long-Finned Pilot Whale Whistle from Data File 7703500w.kay (Image shows the whistle's hyperbolic modulation in frequency.)

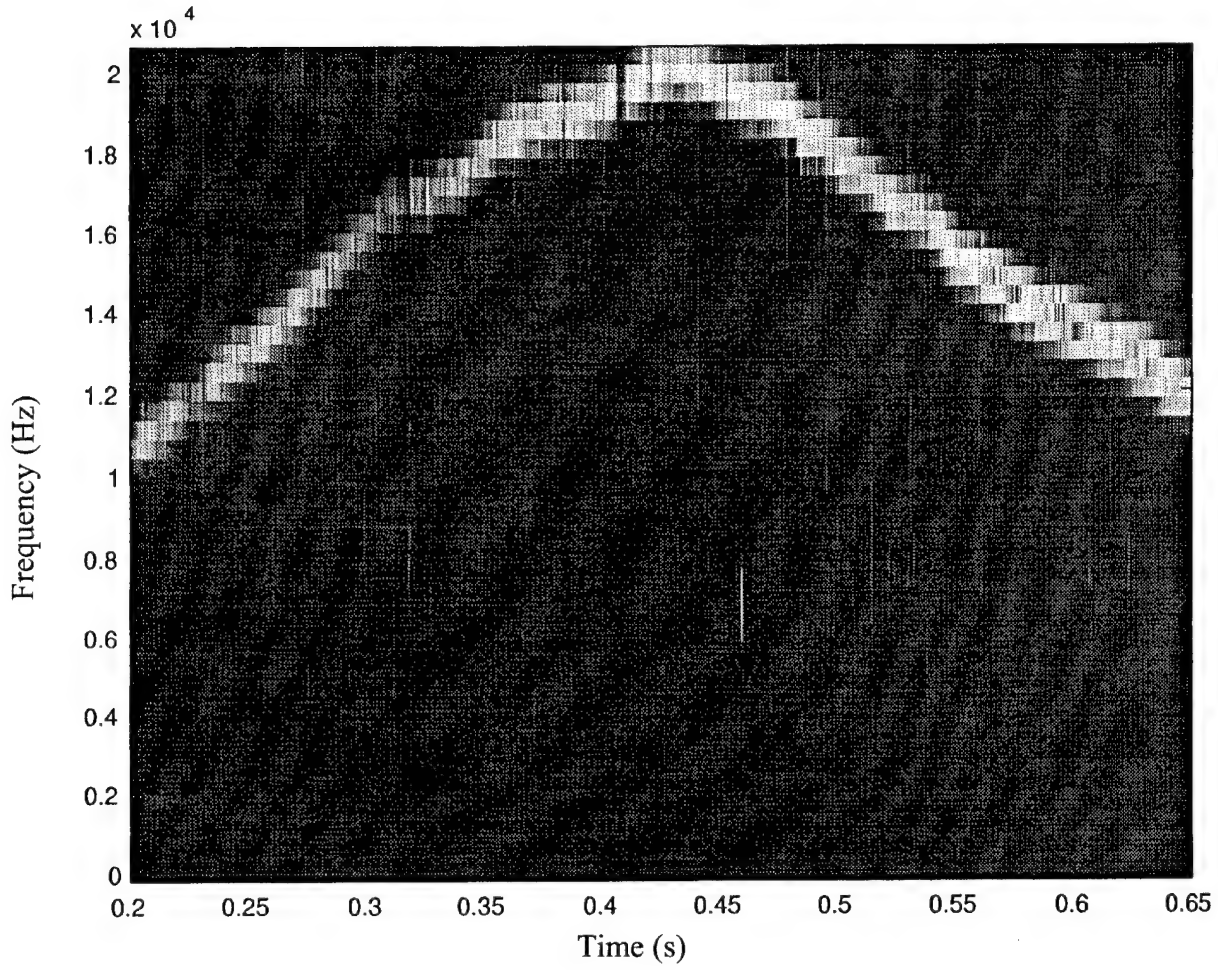

Figure 11. Direct SPWD of a Spotted-Dolphin Whistle from Data File 9002709d.kay (Image shows the whistle's power modulation in frequency.)

$$T_X^{(C)}(t,f) = \int_{-\infty}^{\infty}\int_{-\infty}^{\infty}\Psi_T^{(C)}(\tau,\nu)\, AF_X(\tau,\nu)e^{j2\pi(\nu-ft)}d\tau\, d\nu, \tag{37}$$

where the kernel $\Psi_T^{(C)}(\tau,\nu)$ is the two-dimensional Fourier transform of the kernel in $\Psi_T^{(C)}(t,f)$ (equation (7)). Note that this method requires all the data to be present in an off-line fashion. Also, due to the computational complexity, only short signals can be processed. If the signal has length N samples, then the resulting QTFR has dimensions $N \times N$. However, if N is large, the method is computationally intensive due to memory constraints. The short-time technique,[62] on the other hand, yields a real-time, on-line operation, as it does not require the whole signal to be present in memory. In particular, the technique sections the data by windowing it using a rectangular window centered at time t. The short-time ambiguity function is then computed by computing the ambiguity function of each windowed section. The two-dimensional Fourier transform of the product of the short-time ambiguity function with the kernel is obtained, but only the time-slice at time t is kept. Thus, there is no need to compute the other time slices, resulting in memory conservation and a reduction in computational time. If the signal has length N samples (for N large) and a window of length N_w is used, then the resulting QTFR has dimensions $N_w/2 \times N/N_w$. The dimensions are much smaller than $N \times N$, which would result from an off-line operation; thus, memory is saved, allowing for a more efficient computational method. Note that the sections may be overlapped for better resolution in the time-frequency plane.

Although the short-time technique can be used with any Cohen's class QTFR, it is demonstrated here for the smoothed pseudo-Wigner distribution (note that the kernel of the SPWD in equation (37) is $\Psi_{SPWD}^{(C)}(\tau,\nu) = G(\nu)h(\tau)$, as shown in equation (35)). The short-time SPWD method resulted in the successful analysis of many long-duration records of mammal sounds. For example, in figure 12 the sounds of spotted dolphins, including both clicks and a whistle, are analyzed using the short-time SPWD. The whole data segment of $N = 436{,}160$ samples (corresponding to 2.6 s) was successfully analyzed and the resulting SPWD had dimensions $128 \times 1{,}703$, since a window of length $N_w = 256$ was used. The short-time SPWD clearly shows the various broadband clicks as well as the narrowband whistle (with a

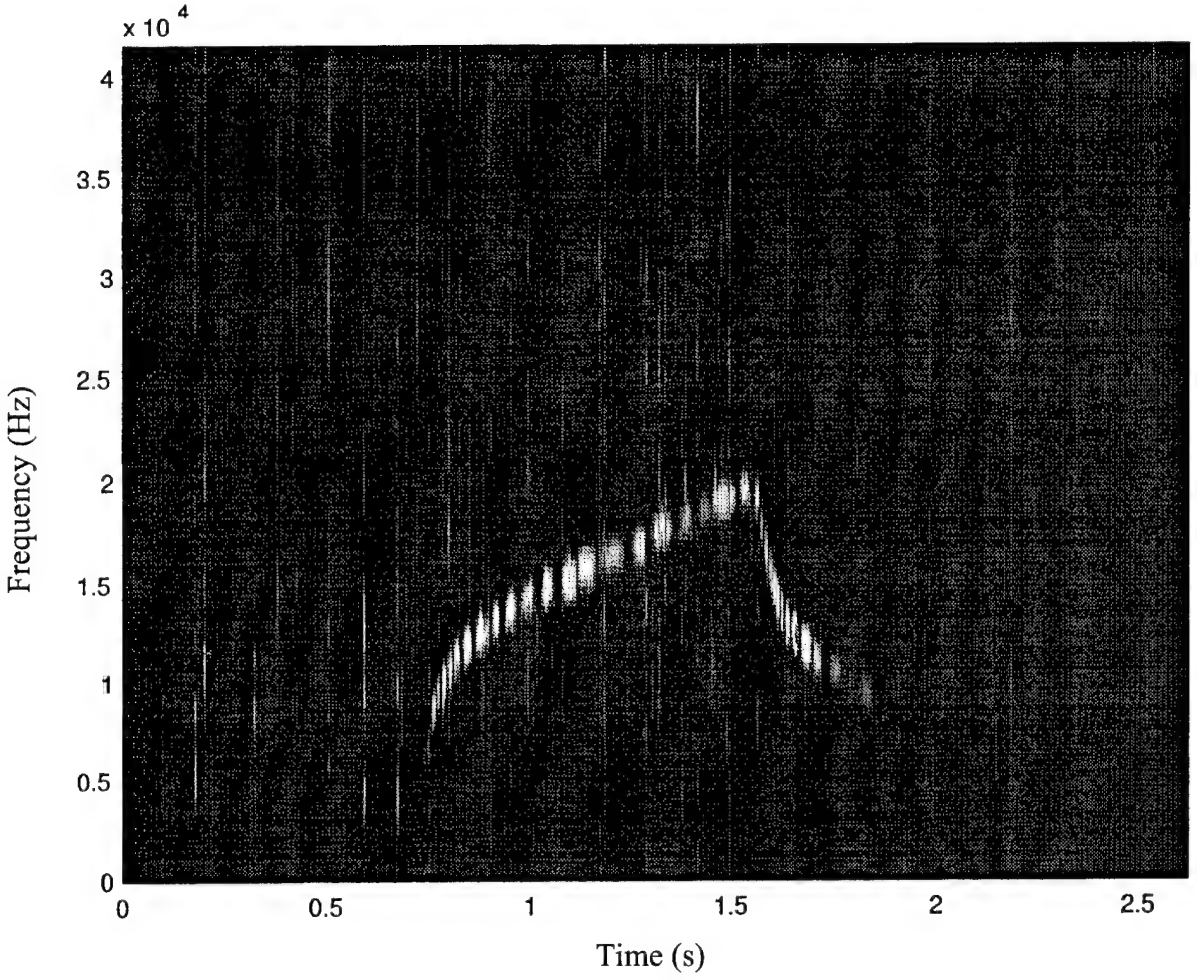

Figure 12. Short-Time SPWD of a Spotted Dolphin Whistle from Data File 83035024.kay

bandwidth of 12 kHz and a duration of 1.1 s). The MATLAB function used to compute the short-time SPWD is given in section A.7 in the appendix. Note that the direct computation of the SPWD as discussed above requires more memory; therefore, it cannot handle data sets as large as the short-time SPWD.

7.3 HYPERBOLIC CLASS QTFRs ANALYSIS OF WHISTLES

Many whistles have a hyperbolic time-frequency characteristic structure (table 7). This hyperbolic structure often occurs at lower frequencies with long-finned pilot whale whistles, since the whistles of these marine mammals are emitted at lower frequencies than the other marine mammals in the data. These hyperbolic whistles start at high frequencies and diminish in frequency in a $1/f$ fashion during the duration of the whistle. Thus, the hyperbolic class QTFRs presented in section 4.1.3 would be well matched to analyze the hyperbolic whistles, as the whistle's group delay characteristics are matched to the time shift $\tau(f) = 1/f$ preserved by hyperbolic QTFRs.[56, 57]

The implementation of hyperbolic QTFRs[59, 60] is similar to the implementation of power QTFRs in section 5, as it is based on the warping approach. Any member of the hyperbolic class can be obtained by warping the corresponding member of Cohen's class using the warping relation in equation (15) with $\xi(b) = \ln b$.[34] For example, as demonstrated in equation (32), the hyperbolic class Altes Q-distribution in equation (26) can be obtained by warping the Cohen's class Wigner distribution in equation (5). Specifically, the Altes Q-distribution of a signal is obtained by first warping the analysis signal in the frequency domain using an exponential frequency axis transformation, then by computing the Wigner distribution of the warped signal, and lastly by transforming the time and frequency axes for correct time-frequency localization.[27, 28, 34] To demonstrate the advantage of hyperbolic class QTFRs over Cohen's class QTFRs when analyzing signals with $t = 1/f$ time-frequency characteristics, figure 13 analyzes the sum of two hyperbolic impulses defined as $X(f) = \frac{1}{\sqrt{f}}\left(e^{-j2\pi 3 \ln\left(\frac{f}{f_r}\right)} + e^{-j2\pi 7 \ln\left(\frac{f}{f_r}\right)} \right)$, $f > 0$. Note that a hyperbolic impulse is defined in equation (23) with $\tilde{\xi}(b) = \ln(b)$.

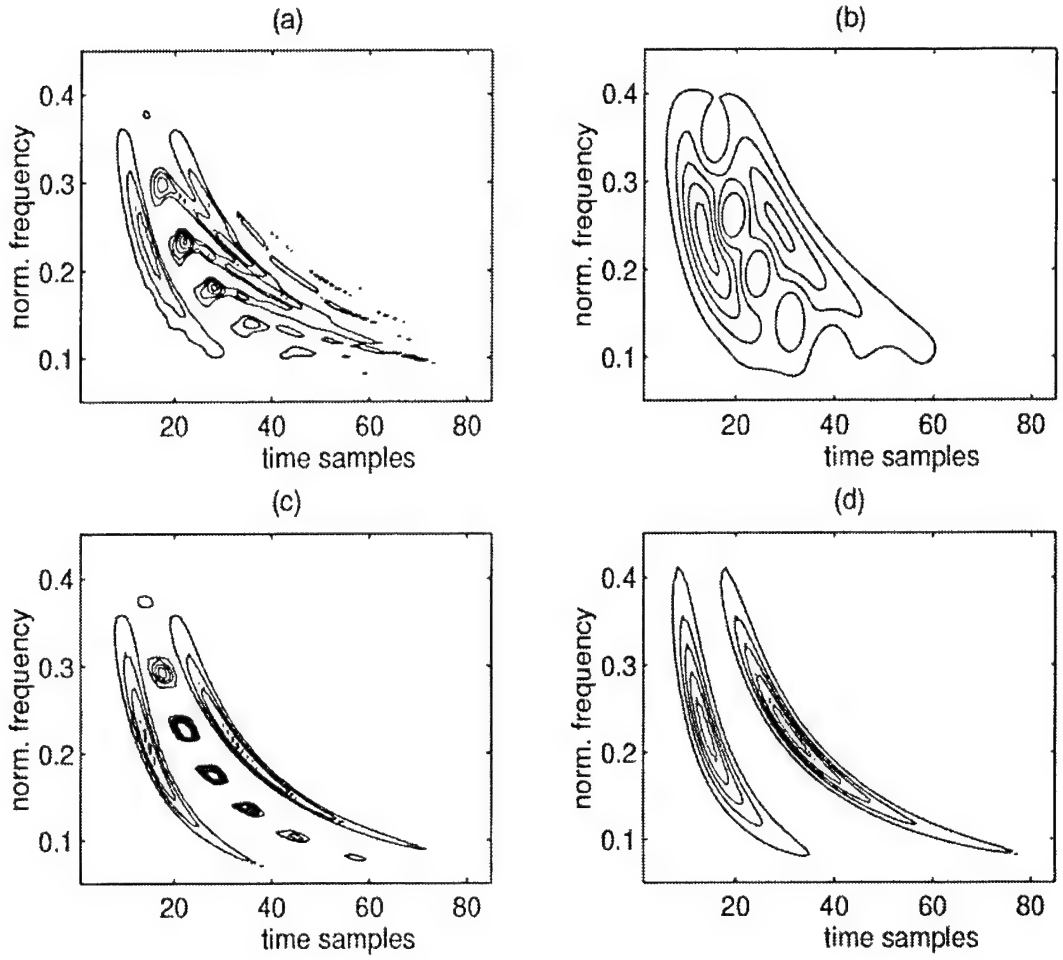

Figure 13. Time-Frequency Analysis of the Sum of Two Hyperbolic Impulses: (a) Wigner Distribution, (b) Smoothed Pseudo-Wigner Distribution, (c) Altes Q-Distribution, and (d) Smoothed Pseudo-Altes Q-Distribution

Hyperbolic QTFRs are well matched to signals similar to hyperbolic impulses with hyperbolic group delay structure. Thus, the Altes Q-distribution (equation (32)) in figure 13(c) has good time-frequency concentration along the two hyperbolae $t = 3/f$ and $t = 7/f$. However, it also results in a cross term along the mean hyperbola[35] $t = 5/f$, as shown in equation (25) with $\xi(b) = \ln b$; i.e., the Altes Q-distribution is the sum of two auto terms and one cross term given by

$$AD_x(t,f) = \frac{1}{f}\delta\left(t - \frac{3}{f}\right) + \frac{1}{f}\delta\left(t - \frac{7}{f}\right) + \frac{2}{f}cos\left(2\pi 4 ln\frac{f}{f_r}\right)\delta\left(t - \frac{5}{f}\right). \qquad (38)$$

The smoothed pseudo-Altes Q-distribution can be obtained by hyperbolically warping the smoothed pseudo-Wigner distribution as in equation (32). As is shown in figure 13(d), the smoothed pseudo-Altes Q-distribution removes the cross term in equation (38) with only some loss of time-frequency resolution. Cohen's class QTFRs, such as the Wigner distribution in figure 13(a) and the smoothed pseudo-Wigner distribution in figure 13(b), are not well-matched to hyperbolic impulses. The Wigner distribution results in complicated cross terms between the two signal components as well as inner interference terms. In comparison to the smoothed pseudo-Altes Q-distribution in figure 13(d), the smoothed pseudo-Wigner distribution in figure 13(b) has a larger loss of time-frequency resolution and is not as successful at removing all of the cross terms.

The implementation technique for hyperbolic QTFRs that is based on the warping approach depends on the implementation technique for Cohen's class QTFRs, together with a signal mapping implementation and an axes transformation. Thus, since most of the algorithms for Cohen's class QTFRs only can efficiently analyze small blocks of data, similar problems exist for hyperbolic QTFRs. Hyperbolic QTFRs are more computationally involved since, for a signal of length N samples, the corresponding warped signal is $4 \times N$ samples; therefore, a Cohen's class QTFR has to be computed for a signal that is four times longer than the initial signal.[59] Thus, in order to be able to analyze the long-duration hyperbolic whistles, the short-time technique was applied to hyperbolic QTFRs such as the Altes Q-distribution and its smoothed versions.

Using the short-time technique for hyperbolic QTFRs, the long data was first divided into short sections. A hyperbolic QTFR of each time section was computed using the warping approach, but only the center time slice corresponding to the center of the window used to section the data was saved. The hyperbolic QTFR was computed first by hyperbolically warping the signal, computing the corresponding Cohen's class QTFR of the warped signal, and then transforming the time and frequency axes for correct time-frequency localization. Similar to Cohen's class QTFRs, memory was saved with the resulting short-time QTFR having dimensions of $N_w/2 \times N/N_w$ (where N is the signal length and N_w is the length of the

sectioning window); the dimensions are much smaller than if computed directly (with dimensions $N \times N$). Since implementation of the hyperbolic QTFRs involves computation of Cohen's class QTFRs as part of the computation, hyperbolic QTFRs are more computationally intensive. As a result, although the analysis of long data with hyperbolic QTFRs was possible, it took 8 – 12 hours to compute. Since the computation time is not practical, it was evident that the algorithm required improvements to speed up processing; additional steps were taken to reduce the computation by eliminating unnecessary processing in the algorithm.

The existing code for hyperbolic QTFRs was used originally to ensure that the short-time implementation was possible. However, these algorithms compute entire representations. The short-time technique, on the other hand, uses only the center time slice of each hyperbolic analysis of the filtered data. Thus, the computation of all the time slices was unnecessary. Each step of the algorithm was analyzed to determine which processing was redundant or unneeded. Overall, the computation time was reduced by approximately 80% (or a speedup of 5.7); the resulting MATLAB algorithm to compute the short-time smoothed pseudo-Altes Q-distribution (SPAD) is given in section A.8 in the appendix.

The short-time technique was used with the SPAD to analyze the whistles of long-finned pilot whales, as these marine mammals emitted whistles with a hyperbolic time-frequency structure in many data files. For example, figure 14 analyzes the whistles of a long-finned pilot whale using a short-time SPAD. The whole data segment of $N = 32{,}984$ samples was analyzed (the data was decimated nine times and it corresponds to 1.78 s), and the resulting SPAD had dimensions 64×257. The short-time SPAD clearly shows three hyperbolic whistles with $1/f$ characteristic time-frequency structure. For example, the first hyperbolic whistle lasts for 0.43 s starting at 0.51 s. It has a bandwidth of 1.9 kHz starting with an upper frequency of 3.8 kHz and ending at a lower frequency of 1.9 kHz. The computation required 8.65 hours with the original short-time programming; after the changes were made to increase the computational speed, the same results were obtained in 1.52 hours.

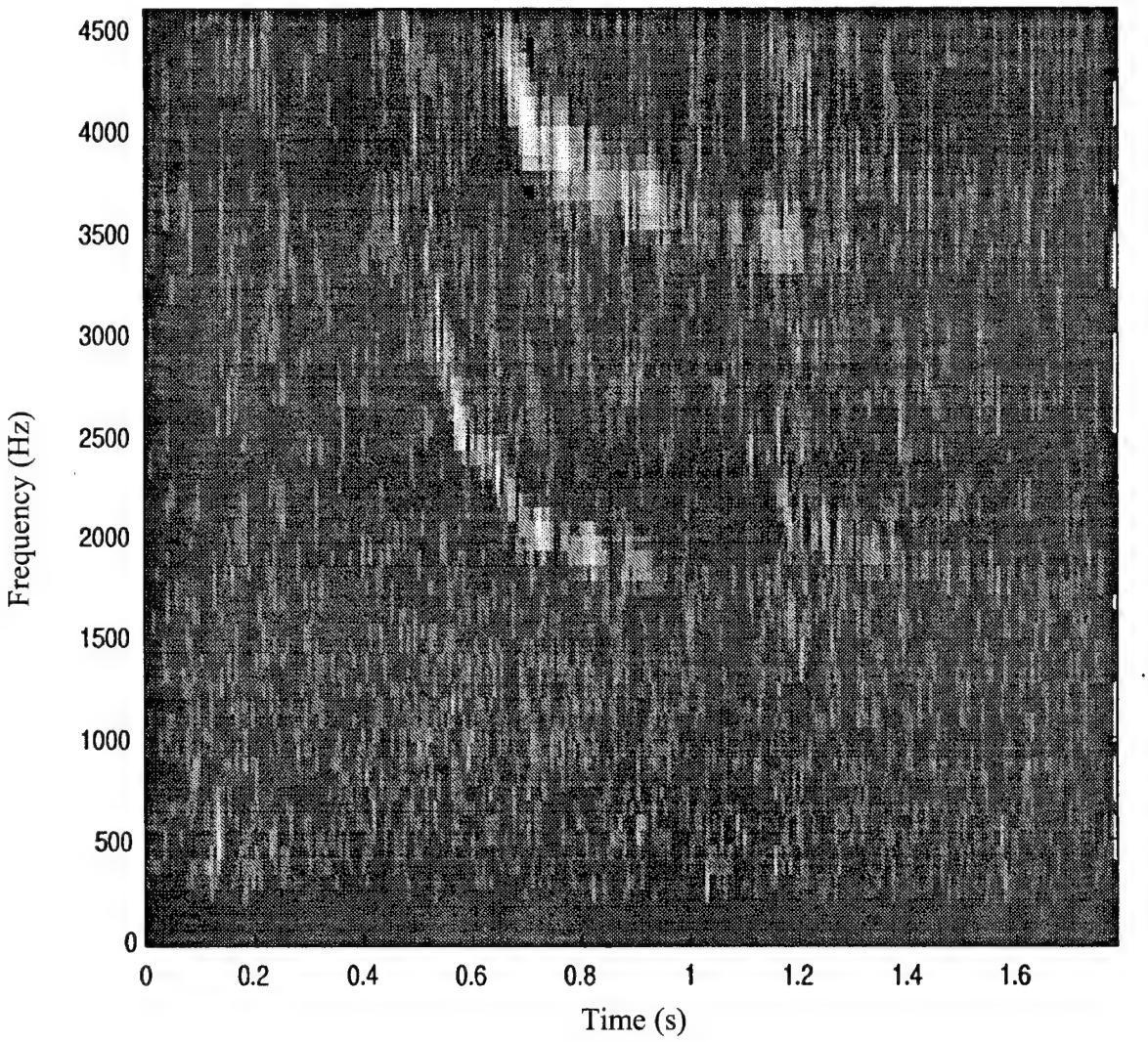

Figure 14. Short-Time SPAD of Long-Finned Pilot Whale Whistles from Data File 77035011.kay (Note that the hyperbolic time-frequency structure of the whistles is matched to the hyperbolic QTFR.)

7.4 POWER CLASS QTFRs ANALYSIS OF WHISTLES

Many marine mammals from the SOUND database emit whistles with a characteristic power time-frequency structure, i.e., the whistle's frequency content changes in a power fashion $t = f^{\kappa-1}$ during the duration of the whistle. For example, initial analysis of some of the whistles of spotted dolphins show components with power function time-frequency characteristics. These types of signals would be best analyzed using power class QTFRs with variable power parameter κ, as presented in section 4.2.3. The power QTFR would be a good analysis tool provided that the time shift $\tau(f) = \frac{\kappa}{f_r}\left|\frac{f}{f_r}\right|^{\kappa-1}$ preserved by the power QTFR is closely matched to the signal's power group delay function.

In section 5.1, the discrete implementation of power class QTFRs was presented based on the fact that any power class QTFR can be obtained by warping the corresponding affine class QTFR as shown in equation (33).[39] The example in figure 15 demonstrates the advantage of using power class QTFRs over affine class QTFRs when analyzing signals with $t = f^{\kappa-1}$ group delay time-frequency characteristics. Figures 15(a) and 15(b) show the results obtained with the power Wigner distribution (power warped version as in equation (33) of the Wigner distribution) and a smoothed pseudo-power Wigner distribution (power warped version as in equation (33) of the affine smoothed pseudo-Wigner distribution) with a very short window, and both with $\kappa = 3$ for a two-component signal consisting of two power impulses, windowed in the frequency domain, with $\kappa = 3$. The κth power impulse is defined in the frequency domain as $I_c^{(\kappa)}(f) = \sqrt{\left|\frac{\kappa}{f_r}\left(\frac{f}{f_r}\right)^{\kappa}\right|}\, e^{-j2\pi c\left(\frac{f}{f_r}\right)^{\kappa}}$, $f > 0$. Note that the power impulse is the generalized impulse in equation (23) with $\tilde{\xi}(b) = \xi_\kappa(b)$, and the power parameter κ of the two power QTFRs is matched to that of the power impulses. The power Wigner distribution has very good time-frequency concentration, but it also results in a cross term as in equation (25) with $\xi(b) = \xi_\kappa(b) = sgn(b)|b|^{\kappa}$. This cross term is effectively suppressed in the smoothed pseudo-power Wigner distribution with minimal loss of time-frequency concentration.

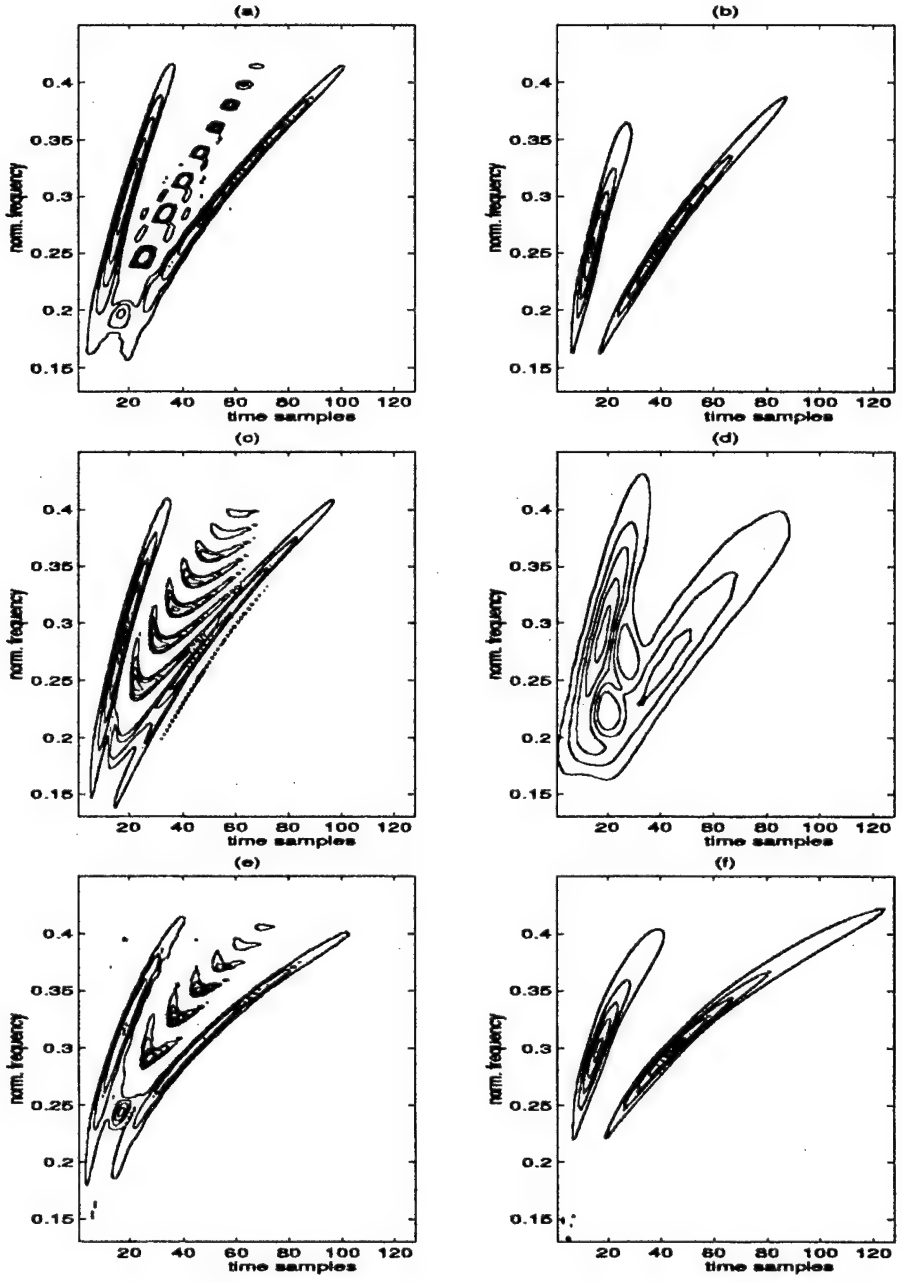

Figure 15. Power Class Analysis of Two Power Impulses: (a) Power Wigner Distribution with $\kappa = 3$*, (b) Smoothed Pseudo-Power Wigner Distribution with* $\kappa = 3$*, (c) Wigner Distribution, (d) Affine Smoothed Pseudo-Wigner Distribution of a Two-Component Signal Consisting of Two Windowed Power Impulses with* $\kappa = 3$*, (e) Power Wigner Distribution with* $\kappa = 3$*, and (f) Smoothed Pseudo-Power Wigner Distribution with* $\kappa = 3$ *of a Two-Component Signal Consisting of Two Windowed Power Impulses with* $\kappa = 4$ *(Duration of signals is 128 samples.)*

Figures 15(c) and 15(d) show the results obtained with the Wigner distribution and an affine smoothed pseudo-Wigner distribution, both members of the affine class. The Wigner distribution in figure 15(c) is not matched to the power impulses as evidenced by complicated cross terms. The affine smoothed pseudo-Wigner distribution in figure 15(d) does not remove all the cross terms and has a larger loss of time-frequency concentration than the smoothed pseudo power-Wigner distribution in figure 15(b). The results of the two power QTFRs with $\kappa = 3$ in figures 15(a) and 15(b) are better than those of the corresponding two affine class QTFRs in figures 15(c) and 15(d) because the former are optimally matched to the power-law group delays of the two power impulse signal components. In order to demonstrate the effect of a slightly mismatched power parameter κ, figures 15(e) and 15(f) show the results obtained when analyzing two power impulses with $\kappa = 4$ (instead of $\kappa = 3$) using the power Wigner distribution and a smoothed pseudo-power Wigner distribution with $\kappa = 3$. The power QTFRs with $\kappa = 3$ used in figures 15(e) and 15(f) are the same as those used in figures 15(a) and 15(b), respectively, but the two power impulses now have power parameter $\kappa = 4$ instead of $\kappa = 3$; thus, the power parameters of the signal and the power QTFRs are different. The results are better than those of the Wigner distribution and the affine smoothed pseudo-Wigner distribution in figures 15(c) and 15(d) due to the fact that the power parameter mismatch in figures 15(e) and 15(f) is smaller than that in figures 15(c) and 15(d).[39, 56, 57]

The power class as defined in section 4.2.3 is obtained by warping the affine class. The power time-shift covariance property in the power class is useful in analyzing signals whose group delay is matched to the power time shift. The power class QTFRs also satisfy the scale covariance property that is important in multiresolution analysis applications. It is, however, possible to warp Cohen's class using the same power warping as in equation (33) to obtain the power warped Cohen's class,[41, 50] which is an example of a generalized warped Cohen's class in section 4.1.3 with $\xi(b) = \xi_{\kappa}(b)$ as shown in table 4. The κth power warped Cohen's class also satisfies the κth power time-shift covariance property, but it does not satisfy the scale covariance property. Thus, if an application does not require multiresolution analysis, but it is important to match the power group delay of a signal (as in the case of the analysis of power whistles), then either a power QTFR (power warped affine QTFR) or a power warped Cohen's class QTFR may be used.

In order to analyze some of the spotted-dolphin whistles, the short-time technique was implemented for the κth power QTFRs to enable large sections of the data to be analyzed in an on-line fashion. Using the short-time technique for power QTFRs, the long data was first divided into short sections, and then a power QTFR of each time section was computed using the warping approach in equation (33) by warping Cohen's class QTFRs or affine class QTFRs. When the power QTFR of the warped data section was obtained, only the center time slice was saved, which corresponded to the center of the window used to section the data. Similar to the short-time hyperbolic technique discussed in section 7.3, the computational time was also reduced to speed up processing. The resulting MATLAB algorithm for the short-time power smoothed pseudo-Wigner distribution (which is the power warped version of Cohen's class smoothed pseudo-Wigner distribution) is given in section A.9 in the appendix. Note that as the whistles of the spotted dolphins appear to start at much higher frequencies than the hyperbolic whistles of the long-finned pilot whales (tables 8 and 10), the data for the spotted dolphins cannot be decimated by a large factor for fear that high-frequency information would be lost. As a result, the number of samples for the spotted-dolphin whistles is very large, and although the computational savings have been applied to the short-time power QTFR, the computational time is still considerable. Using the short-time power QTFR implementation with a $\kappa = 2$ power smoothed pseudo-Wigner distribution, 125,000 samples were analyzed from a spotted-dolphin whistle (decimated by a factor of 2) from data file 83035024.kay. The computational time was 6.4 hours and the resulting analysis with a power group delay time-frequency characteristic is shown in figure 16.

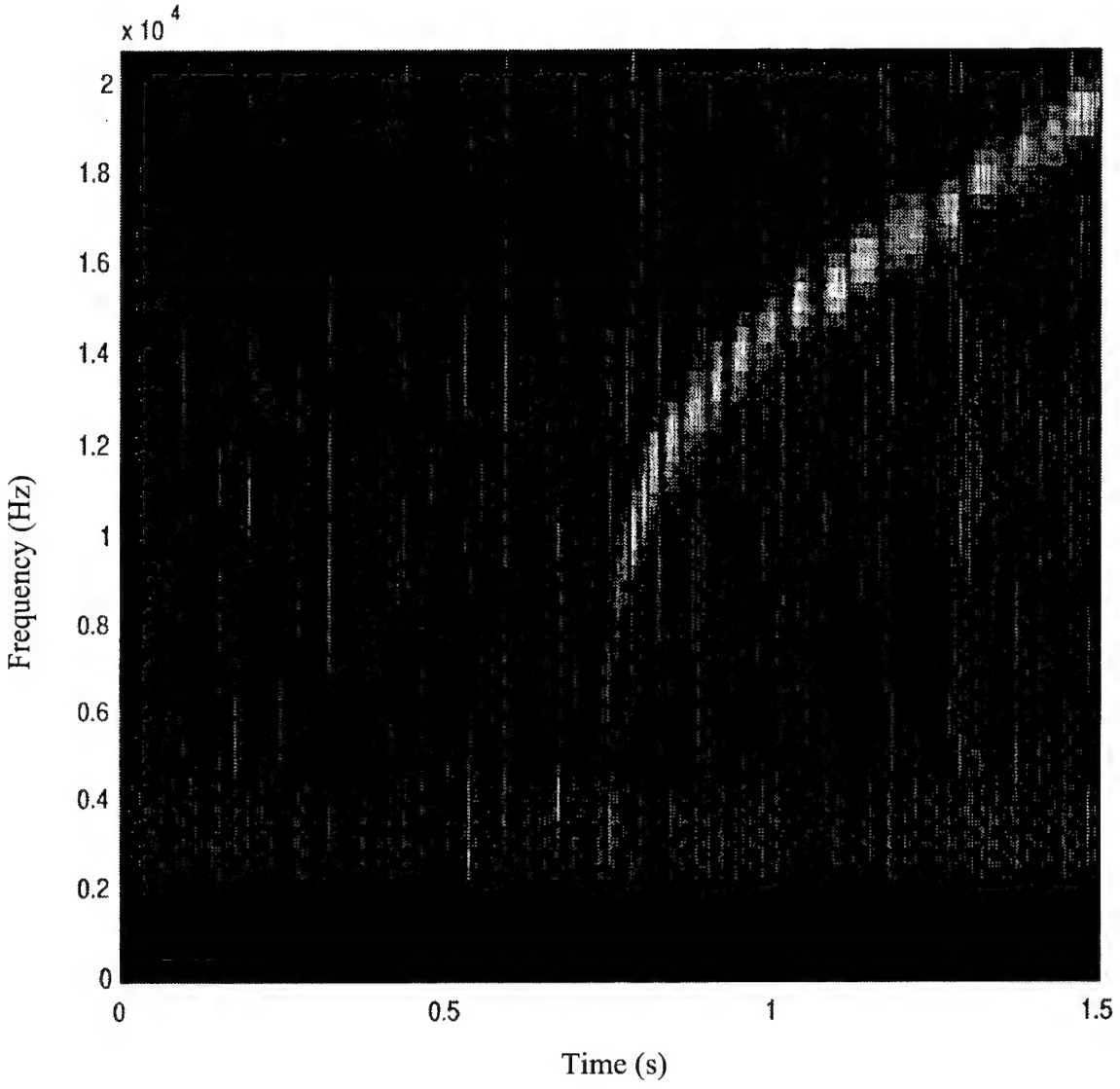

Figure 16. Short-Time Power Smoothed Pseudo-Wigner Distribution with $\kappa = 2$ of a Spotted-Dolphin Whistle from Data File 83035024.kay (Note that the power time-frequency structure of the whistle is matched to the power QTFR.)

7.5 ADAPTIVE OPTIMAL KERNEL QTFR ANALYSIS OF WHISTLES

In the analysis of whistles consisting of long data segments, short-time time-frequency techniques were used to enable computations of large data on-line, such as short-time Cohen, hyperbolic, and power QTFRs. These short-time techniques used QTFRs whose kernels were fixed for the whole signal analysis. However, when the signal characteristics change with time, new adaptive techniques that use QTFRs whose kernels change as the signal changes are used for a better time-frequency analysis. When combined with the short-time techniques, the adaptive, signal-dependent kernel QTFRs can compute various whistle characteristics in an on-line, fast fashion. In particular, the short-time adaptive radially Gaussian QTFR (AOK)[*62]adapts the kernel to each set of signal components, resulting in a highly concentrated time-frequency representation that is best matched to linear chirps. A copy of the author's C language program has been obtained for the AOK, and has been applied to the whistles from the marine mammal database. As expected, the compiled C program is very fast as compared to the interpreted MATLAB programs. The intention was to apply hyperbolic and power warping to the AOK program in order to match the AOK to hyperbolic and power impulses. It has been discovered, however, that for long data, the short-time characteristic of this method looks at segments of the data at a time that can be approximated to linear chirps. In other words, for a long section of data (corresponding to one whistle), even if the whistle has a hyperbolic time-frequency structure, each short segment in the short-time adaptive AOK appears linear. As a result, since the AOK is best matched to linear chirps, the results obtained are satisfactory. It is not believed that the warping will give any better results; on the contrary, it will try to analyze each short segment as a hyperbolic impulse (when it is actually a linear chirp) and the warping will increase the computational time. To demonstrate the analysis obtained by the AOK, three long-finned pilot whale whistles from data file 77035011.kay were considered. This file has been previously analyzed using the hyperbolic short-time smoothed pseudo-Altes Q-distribution in figure 14. Although good results have been obtained using the short-time smoothed pseudo-Altes Q-distribution, as the whistles have hyperbolic time-frequency structure, the computation took 1.5 hours as discussed in section 7.3. Using the C program for the short-time adaptive radially

---

[*] The radially Gaussian QTFR is not a member of Cohen's class of time-shift and frequency-shift covariant QTFRs, since its kernel depends on the analysis signal. However, similar to Cohen's class QTFRs, it is matched to signals with constant or linear group delay characteristics.

Gaussian kernel, similar results were obtained (figure 17) because the AOK is matched to linear portions of short segments of the hyperbolic curve. The advantage of using this method is that the computation now only takes 0.3 hours. The difference in resolution in figures 14 and 17 is due to the smoothed pseudo-Altes Q-distribution in figure 14 using two smoothing windows that limit the time-frequency resolution, whereas the AOK in figure 17 adapts to the signal changes.

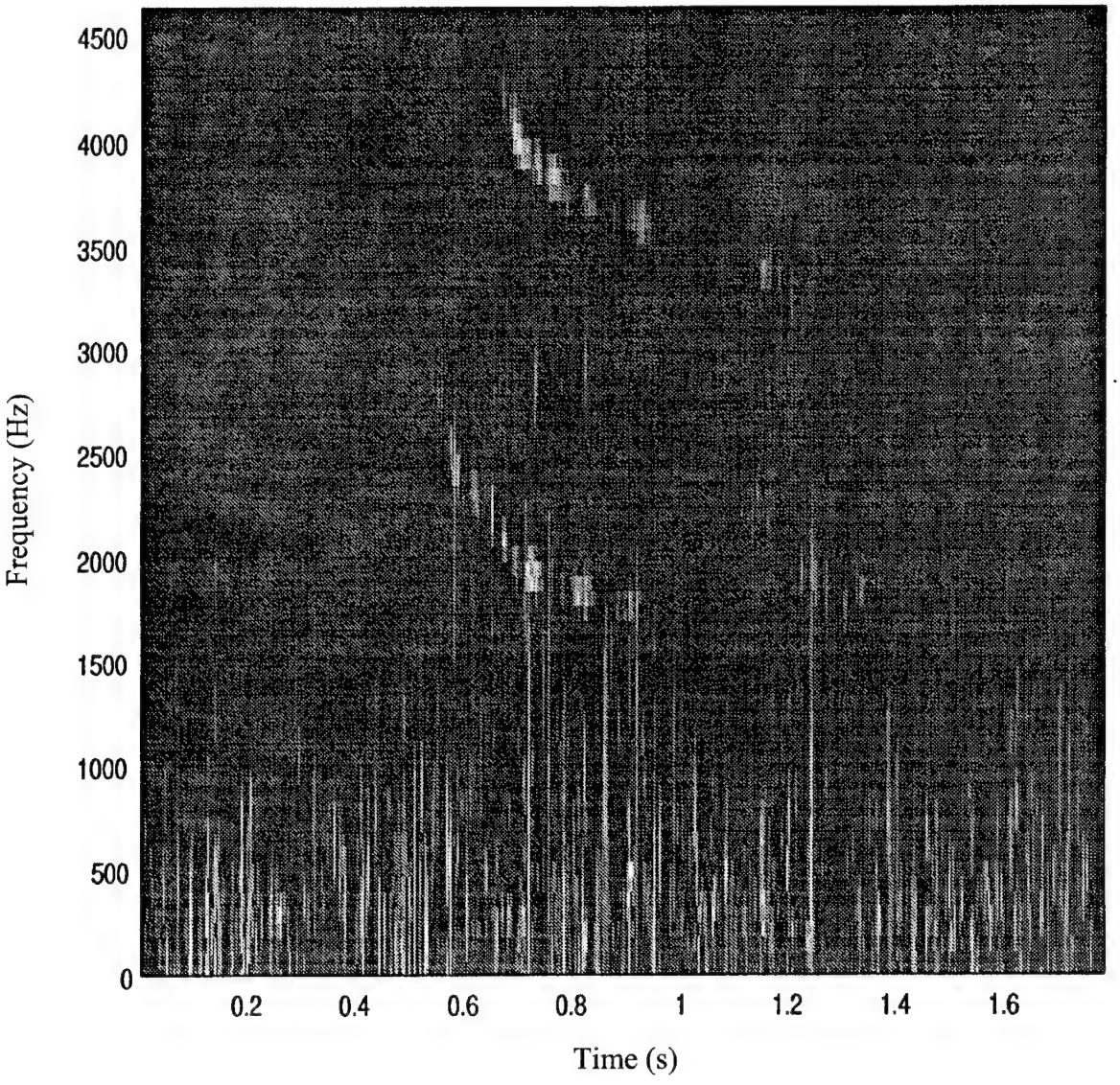

Figure 17. Short-Time Adaptive Radially Gaussian Kernel QTFR of Long-Finned Pilot Whale Whistles from Data File 77035011.kay

8. CONCLUSIONS

Marine mammal sounds are time-varying signals whose frequency content changes with time. As a result, time-frequency analysis techniques are ideal tools for analyzing such signals, since time-frequency representations provide temporal localization of the time-varying signal's spectral components. In this project, QTFRs were used to analyze the time-frequency structure of cetacean mammal sounds, such as clicks and whistles emitted by dolphins and whales. An investigation was proposed to determine signal types and their properties, and to investigate which types of QTFRs are best suited for analyzing these biological signals based on the properties of the signals.

As proposed, sonar signals (clicks) that are used by the marine mammals for echolocation were analyzed. The analysis tools used were Cohen's class QTFRs, such as the Wigner distribution, the pseudo-Wigner distribution, and the spectrogram. Cohen's class QTFRs were used because clicks were found to be short-duration, broadband, transient-like pulses with constant group delay characteristics and Cohen's class QTFRs are matched to signals with linear or constant group delay characteristics, as they preserve the signal's constant time shifts. As proposed, non-echolocation signals, called whistles, which are used by marine mammals for communication, were also analyzed. The whistles were found to be long-duration, narrowband, frequency-modulated, continuous tonal sounds that vary in frequency, duration, and in the shape of the whistle time-frequency structure, depending on the nature of the signal's frequency modulation. As a result, the marine mammals have different signature whistles whose group delay time-frequency characteristics included linear, hyperbolic, exponential, and power structures. Based on this, the generalized time-shift covariant QTFRs discussed in this report would be well-matched for analyzing the different types of whistles simply by choosing the corresponding group delay time-frequency structure of the whistle and matching it to the QTFR's time shift. In particular, it has been shown that many whistles of long-finned pilot whales have a $t = 1/f$ group delay characteristic that was successfully analyzed using hyperbolic QTFRs, i.e., QTFRs that preserve hyperbolic time shifts on the analysis signal. Initial analysis of some of the whistles of spotted dolphins show components with power function $t = f^{\kappa-1}$ time-

frequency characteristics. Thus, it has been shown that power QTFRs are matched to the analysis of these whistles as they preserve the signal's power changes in group delay. Given a marine mammal whistle, some preprocessing was necessary to determine its type of time-frequency structure. This preprocessing was usually performed with the spectrogram and was based on visual conclusions.

The MATLAB code needed for the analysis using Cohen's class QTFRs and hyperbolic class QTFRs already existed. But, as proposed, the MATLAB code for other QTFRs that were needed, such as the code for the power class QTFRs and the code for the exponential class QTFRs,[39, 42] were developed herein. During the duration of the project, the relevant theory that was developed in relation to the generalized time-shift covariant QTFRs was recorded.[39-44, 56, 57]

The major problem encountered was the fact that the sample duration of the whistles was very large, and the MATLAB code for the various QTFRs* suffered from memory management problems, with the system memory quickly consumed. This problem was addressed by using short-time time-frequency analysis techniques for Cohen's class, hyperbolic class, and power class QTFRs. The short-time technique yields a real-time, on-line operation that does not require the whole signal present in memory. Thus, the long data can be processed by the appropriate QTFRs without running out of system memory. Short-time data-adaptive QTFRs were also used, as they adapt to changes in the signal's time-frequency structure.

* The spectrogram implementation was relatively fast as a MATLAB built-in function was used for its computation.

REFERENCES

1. W. W. L. Au, *The Sonar of Dolphins*, Springer-Verlag, New York, NY, 1993.

2. P. E. Purves and G. Pilleri, *Echolocation in Whales and Dolphins,* London: Academic Press, London, England, 1983.

3. A. N. Popper, "Sound Emission and Detection in Delphinids," *Cetacean Behavior: Mechanisms and Functions*, Wiley-Interscience, New York, NY, 1980.

4. H. J. Diercks, R. T. Trochta, C. F. Greenlaw, and W. E. Evans, "Recording and Analysis of Dolphin Echolocation Signals," *Journal of the Acoustical Society of America*, vol. 49, 1971.

5. P. W. B. Moore, "Dolphin Echolocation and Audition," *Animal Sonar Processes and Performance,* Eds. P. E. Nachtigall and P. W. B. Moore, Plenum Press, New York, NY, 1988, pp. 161 – 168.

6. R. J. Schusterman, "Behavioral Methodology in Echolocation by Marine Mammals," Animal Sonar Systems, Eds. R. G. Busnel and J. F. Fish, Plenum Press, New York, NY, 1980, pp. 11 – 41.

7. C. W. Turl and R. H. Penner, "Differences in Echolocation Click Patterns of the Beluga (Delphinapterusleucas) and the Bottlenosed Dolphin (Tursiops truncatus)," *Journal of the Acoustical Society of America*, vol. 86, 1989, pp. 497 – 502.

8. L. M. Herman, *Cetacean Behavior: Mechanisms and Functions,* John Wiley & Sons, New York, NY, 1980.

9. P. Tyack, "Use of a Telemetry Device to Identify Which Dolphin Produces a Sound," *Dolphin Societies: Discoveries and Puzzles,* Eds. K. Pryor and K. Norris, University of California Press, Berkeley, CA, 1991.

10. *Dolphin Cognition and Behavior: A Comparative Approach*, Eds. R. J. Schusterman, J. A. Thomas, and F. G. Wood, Lawrence Erlbaum Associates, Mahwah, NJ, 1986.

11. W. W. Steiner II, "A Comparative Study of the Pure Tonal Whistle Vocalizations from Five Western North Atlantic Dolphin Species," Ph.D Dissertation, Oceanography Department, University of Rhode Island, Kingston, RI, 1980.

12. M. E. Cagan, "A Statistical Analysis of the Whistle Vocalizations of Delphinus Delphis and Pseudorca Crassidens: Between-Species and Within-Species Comparisons," MS Thesis, Oceanography Department, University of Rhode Island, Kingston, RI, 1981.

REFERENCES (Cont'd)

13. A. G. Taruski, "Whistles of the Pilot Whale (Globicephala spp.): Variations in Whistling Related to Behavioral/Environmental Context, Broadcast of Underwater Sound, and Geographic Location," Ph.D Dissertation, Oceanography Department, University of Rhode Island, Kingston, RI, 1976.

14. *Behavior of Marine Animals, Volume 3: Cetaceans,* Eds. H. E. Winn and B. L. Olla, Plenum Press, New York, NY, 1979.

15. W. Koenig, H. K. Dunn, and L. Y. Lacy, "The Sound Spectrograph," *Journal of the Acoustical Society of America*, vol. 17, 1946, pp. 19 – 49.

16. W. A. Watkins, "The Harmonic Interval: Fact or Artifact Spectral Analysis of Pulse Trains," *Marine Bio-Acoustics,* Ed. W. N. Tavolga, Pergamon Press, Tarrytown, NY, 1966, pp. 15 – 43.

17. P. L. Tyack, W. J. Williams, and G. Cunningham, "Time-Frequency Fine Structure of Dolphin Whistles," *Proceedings IEEE Symposium on Time-Frequency and Time-Scale Analysis*, Victoria, Canada, October 1992.

18. F. Hlawatsch and G. F. Boudreaux-Bartels, "Linear And Quadratic Time-Frequency Signal Representations," *IEEE Signal Processing Magazine*, vol. 9, April 1992, pp. 21 – 67.

19. P. Flandrin, *Temps-Frequence*, Paris: Hermes, Paris, France, 1993.

20. L. Cohen, *Time-Frequency Analysis,* Prentice-Hall, 1995.

21. B. Boashash, "Time-Frequency Signal Analysis," *Advances in Spectrum Estimation*, Ed. S. Haykin, Prentice-Hall, Englewood Cliffs, NJ, 1990.

22. T. A. C. M. Claasen and W. F. G. Mecklenbrauker, "The Wigner Distribution: A Tool For Time Frequency Signal Analysis, Part I: Continuous-Time Signals," *Phillips Journal of Research*, vol. 35, 1980, pp. 217 – 250.

23. L. R. Rabiner and R. W. Schafer, *Digital Processing of Speech Signals,* Prentice-Hall, Englewood Cliffs, NJ, 1978.

24. R. A. Altes, "Detection, Estimation, and Classification with Spectrograms," *Journal of the Acoustical Society of America*, vol. 67, 1980, pp. 1232 – 1246.

25. H. I. Choi and W. J. Williams, "Improved Time-Frequency Representation of Multicomponent Signals Using Exponential Kernels," *IEEE Transactions on Acoustics, Speech, and Signal Processing*, vol. 37, June 1989, pp. 862 – 871.

REFERENCES (Cont'd)

26. O. Rioul and P. Flandrin, "Time-Scale Energy Distributions: A General Class Extending Wavelet Transforms," *IEEE Transactions on Signal Processing*, vol. 40, July 1992, pp. 1746 – 1757.

27. R. A. Altes, "Wide-Band, Proportional-Bandwidth Wigner-Ville Analysis," *IEEE Transactions on Acoustics, Speech, and Signal Processing*, vol. 38, June 1990, pp. 1005 – 1012.

28. N. M. Marinovich, "The Wigner Distribution and the Ambiguity Function: Generalizations, Enhancement, Compression and Some Applications," Ph.D Dissertation, The City University of New York, New York, NY, 1986.

29. A. Papandreou, F. Hlawatsch, and G. F. Boudreaux-Bartels, "A Unifed Framework for the Bertrand Distribution and the Altes Distribution: The New Hyperbolic Class Of Quadratic Time-Frequency Distributions," *Proceedings of the IEEE-SP International Symposium on Time-Frequency and Time-Scale Analysis,* Victoria, Canada, October 1992, pp. 27 – 30.

30. L. Cohen, "Generalized Phase-Space Distribution Functions," *Journal of Mathematical Physics*, vol. 7, 1966, pp. 781 – 786.

31. J. Bertrand and P. Bertrand, "A Class of Affine Wigner Functions with Extended Covariance Properties," *Journal of Mathematical Physics*, vol. 33, 1992, pp. 2515 – 2527.

32. P. Flandrin and P. Goncalves, "From Wavelets to Time-Scale Energy Distributions," *Recent Advances in Wavelet Analysis,* Eds. L. L. Schumaker and G. Webb, Academic Press, San Diego, CA, 1994, pp. 309 – 334.

33. A. Papandreou, F. Hlawatsch, and G. F. Boudreaux-Bartels, "Quadratic Time-Frequency Distributions: The New Hyperbolic Class and Its Intersection with the Affine Class," *Proceedings Sixth SP Workshop on Statistical Signal and Array Processing,* Victoria, Canada, October 1992, pp. 26 – 29.

34. A. Papandreou, F. Hlawatsch, and G. F. Boudreaux-Bartels, "The Hyperbolic Class of Quadratic Time Frequency Representations, Part I: Constant-Q Warping, the Hyperbolic Paradigm, Properties, and Members," *IEEE Transactions on Signal Processing*, vol. 41, December 1993, pp. 3425 – 3444.

35. F. Hlawatsch, A. Papandreou-Suppappola, and G. F. Boudreaux-Bartels, "The Hyperbolic Class Of Quadratic Time-Frequency Representations, Part II: Subclasses, Intersection with the Affine and Power Classes, Regularity, and Unitarity," *IEEE Transactions on Signal Processing*, vol. 45, February 1997, pp. 303 – 315.

REFERENCES (Cont'd)

36. A. Papandreou-Suppappola, "New Classes of Quadratic Time-Frequency Representations with Scale Covariance and Generalized Time-Shift Covariance: Analysis, Detection, and Estimation," Ph.D Dissertation, Electrical Engineering Department, University of Rhode Island, Kingston, RI, May 1995.

37. F. Hlawatsch, A. Papandreou, and G. F. Boudreaux-Bartels, "The Power Classes of Quadratic Time Frequency Representations: A Generalization of the Hyperbolic and Affine Classes," *27th Asilomar Conference on Signals, Systems and Computers,* Pacific Grove, CA, November 1993, pp. 1265 – 1270.

38. A. Papandreou, F. Hlawatsch, and G. F. Boudreaux-Bartels, "A Unified Framework for the Scale Covariant Affine, Hyperbolic, and Power Class Quadratic Time-Frequency Representations Using Generalized Time Shifts," *Proceedings IEEE International Conference on Acoustics, Speech, and Signal Processing,* Detroit, MI, vol. 2, May 1995, pp. 1017 – 1020.

39. A. Papandreou-Suppappola, F. Hlawatsch and G. F. Boudreaux-Bartels, "Power Class Time-Frequency Representations: Interference Geometry, Smoothing, and Implementation," *IEEE-SP International Symposium on Time-Frequency and Time-Scale Analysis,* Paris, France, June 1996, pp. 193 – 196.

40. F. Hlawatsch, A. Papandreou-Suppappola, and G. F. Boudreaux-Bartels, "The Power Classes Quadratic Time-Frequency Representations with Scale Covariance and Dispersive Time-Shift Covariance," *IEEE Transactions on Signal Processing*, vol. 45, January 1997.

41. A. Papandreou-Suppappola and G. F. Boudreaux-Bartels, "The Exponential Class and Generalized Time-Shift Covariant Quadratic Time-Frequency Representations," *IEEE International Symposium on Time-Frequency and Time-Scale Analysis,* Paris, France, June 1996, pp. 429 – 432.

42. A. Papandreou-Suppappola, B. G. Iem, R. L. Murray, and G. F. Boudreaux-Bartels, "Properties and Implementation of the Exponential Class of Time-Frequency Representations," *30th Asilomar Conference on Signals Systems and Computers,* Pacific Grove, CA, November 1996.

43. A. Papandreou-Suppappola, R. L. Murray, and G. F. Boudreaux-Bartels, "Localized Subclasses of Quadratic Time-Frequency Representations," *Proceedings IEEE International Conference on Acoustics, Speech, and Signal Processing,* Munich, Germany, April 1997.

44. A. Papandreou-Suppappola, R. L. Murray, B. G. Iem, and G. F. Boudreaux-Bartels, "Generalized Time-Shift Covariant Quadratic Time-Frequency Representations," for submittal to *IEEE Transactions on Signal Processing*.

REFERENCES (Cont'd)

45. L. E. Freitag and P. L. Tyack, "Passive Acoustic Localization of the Atlantic Bottlenose Dolphin Using Whistles and Echolocation Clicks," *Journal of the Acoustical Society of America*, vol. 93, April 1993, pp. 2197 – 2205.

46. W. A. Watkins, K. Fristrup, M. A. Daher, and T. Howald, "SOUND Database of Marine Animal Vocalizations Structure and Operations," Woods Hole Oceanographic Institution Technical Report WHOI-92-31, Woods Hole, MA, August 1992.

47. K. Fristrup and W. A. Watkins, "Characterizing Acoustic Features of Marine Animal Sounds," Woods Hole Oceanographic Institution Technical Report WHOI-92-04, Woods Hole, MA, January 1992.

48. K. Fristrup and W. A. Watkins, "Marine Animal Sound Classification," Woods Hole Oceanographic Institution Technical Report WHOI-94-13, Woods Hole, MA, October 1993.

49. F. Hlawatsch and P. Flandrin, "The Interference Structure of the Wigner Distribution and Related Time Frequency Signal Representations," *The Wigner Distribution – Theory and Applications in Signal Processing*, Ed. W. Mecklenbrauker, Elsevier, to be published.

50. A. Papandreou-Suppappola, "Generalized Time-Shift Covariant Quadratic Time-Frequency Representations with Arbitrary Group Delays," *29th Asilomar Conference on Signals, Systems and Computers,* Pacific Grove, CA, October 1995, pp. 553 – 557.

51. A. Papandreou-Suppappola, F. Hlawatsch, and G. F. Boudreaux-Bartels, "Quadratic Time-Frequency Representations with Scale Covariance and Generalized Time-Shift Covariance: A Unified Framework for the Affine, Hyperbolic, and Power Classes," to be submitted to *Digital Signal Proceedings: A Review Journal.*

52. R. G. Baraniuk and D. L. Jones, "Warped Wavelet Bases: Unitary Equivalence and Signal Processing," *Proceedings IEEE International Conference on Acoustics, Speech, and Signal Processing,* Minneapolis, MN, vol. 3, April 1993, pp. 320 – 323.

53. R. G. Baraniuk, "Warped Perspectives In Time-Frequency Analysis," *IEEE International Symposium on Time-Frequency and Time-Scale Analysis,* Philadelphia, PA, October 1994, pp. 528 – 531.

54. R. G. Baraniuk and D. L. Jones, "Unitary Equivalence: A New Twist on Signal Processing," *IEEE Transactions on Signal Processing*, vol. 43, October 1995, pp. 2269 – 2282.

55. R. G. Baraniuk, "Covariant Time-Frequency Representations Through Unitary Equivalence," *IEEE Signal Processing Letters*, vol. 3, March 1996, pp. 79 – 81.

REFERENCES (Cont'd)

56. A. Papandreou-Suppappola and G. F. Boudreaux-Bartels, "Distortion that Occurs when the Signal Group Delay Does Not Match the Time-Shift Covariance of a Time-Frequency Representation," *30th Annual Conference on Information Sciences and Systems*, Princeton University, Princeton, NJ, March 1996, pp. 520 – 525.

57. A. Papandreou-Suppappola and G. F. Boudreaux-Bartels, "The Effect of Mismatching Analysis Signals and Time-Frequency Representations," *IEEE-SP International Symposium on Time-Frequency and Time-Scale Analysis,* Paris, France, June 1996.

58. R. A. Altes and E. L. Titlebaum, "Bat Signals as Optimally Doppler Tolerant Waveforms," *Journal of the Acoustical Society of America*, vol. 48, October 1970, pp. 149 – 152.

59. K. G. Canfield and D. L. Jones, "Implementing Time-Frequency Representations for Non-Cohen Classes," *27th Asilomar Conference on Signals, Systems and Computers,* Pacific Grove, CA, November 1993, pp. 1464 – 1468.

60. V. S. Praveenkumar, "Implementation of Hyperbolic Class Time-Frequency Distributions and Removal of Cross-Terms," MS Thesis, Electrical Engineering Department, University of Rhode Island, Kingston RI, 1995.

61. J. P. Ovarlez, "La Transformation de Mellin: Un Outil Pour L'Analyse Des Signaux a Large Bande," Ph.D Dissertation, These University, Paris, France, 1992.

62. D. L. Jones and R. G. Baraniuk, "An Adaptive Optimal-Kernel Time-Frequency Representation," *IEEE Transactions on Signal Processing*, vol. 43, October 1995, pp. 2361 – 2371.

APPENDIX
MATLAB PROGRAMS

This appendix comprises the essential MATLAB programs used for the project.

A.1 MATLAB FUNCTION TO EXTRACT SOUND DATABASE FILE HEADER AND READ THE DATA (loadkay.m)

```
function [y,header,Fs,Ns] = loadkay(filename,N,offset)
%     LOADKAY     Reads WHOI .kay files.  Reads N samples from filename starting at
%                 offset, returns the file header, the data vector y, the sampling rate Fs
%                 samples/sec and the total number of samples, Ns.

%  Antonia Papandreou-Suppappola, 22Jan96

%  Open file, return file descriptor
fid = fopen(filename,'r');
if fid < 0,
  error(sprintf('Unable to open file: %s', filename));
end

%  Read header in first 512 bytes of digitized file
header = fread(fid,512,'char');
%  Remove nulls
i=find(header==0); header(i)=30*ones(size(i));
%  Move each field to a separate line, they are separated by '_' in file
i=find(header=='_');
header(i)=10*ones(size(i));
i=find(header=='R');
header(i(1)-1)=10*ones(1,1);
%  Determine the sampling rate, Fs samples/sec
i=find(header=='S');   Fs=header(i(1)+3:i(1)+8);
Fs=setstr(Fs');   Fs=str2num(Fs);
%  Add the word 'Samples ' before the actual # of data samples
header(1:8)='Samples ';
%  Move the # of samples next to its field title
header(9:26)=header(27:44);   header(27:38)=15*ones(1,12);
%  Extract # of samples, Ns
Ns=str2num(setstr(header(9:14)'));
%  Display header in ASCII format
header = setstr(header');
%disp(' '); disp(header);
```

```
% Read N samples of data
if nargin==1,
  y=fread(fid,'short');
elseif nargin==2,
  y=fread(fid,N,'short');
elseif nargin==3,
  fseek(fid,offset*2,'cof');
  y=fread(fid,N,'short');
else
  error('Too many input arguments')
end

% close file
fclose(fid);
```

A.2 MATLAB FUNCTIONS TO IMPLEMENT THE POWER WIGNER DISTRIBUTION

A.2.1 Function power_WD.m

```
function [PWD] = power_WD(x,kappa);
% POWER_WD      This function computes the kappa power Wigner distribution (PWD) of
%               the time domain, analytic signal x (that is, the Fourier transform of x is
%               zero for negative frequency). The resulting PWD is an N x N matrix,
%               where N is the length of x. To increase computational speed, N must be a
%               power of 2.

% Antonia Papandreou-Suppappola 26April96

% Power warp the signal in the frequency domain
[warptimesig, M, df, dv, length2]=prewarp_PC(x,kappa);
% Compute the Wigner distribution, wd_warp, of the warped signal, warptimesig
wd_warp=wd(warptimesig);
% Transform the time and frequency axes of the Wigner distribution to obtain PWD
PWD=unwarp_PC(wd_warp, M, df, dv, length2, kappa);

% Plotting options
df=0.5/size(PWD,2); f=0:df:0.5-df;
m1=max(max(PWD)); contour_level=[0.1*m1:0.2*m1:0.9*m1];
% For contour plot
subplot(311); contour(1:size(PWD,2),f,flipud(PWD),contour_level);
title('Power Wigner distribution');
xlabel('time samples'); ylabel('norm. frequency');
% For mesh plot
subplot(312); mesh(1:size(PWD,2),f,flipud(PWD));
title('Power Wigner distribution');
xlabel('time samples'); ylabel('norm. frequency');
% For imagesc plot
subplot(313)
imagesc(1:size(PWD,2),f,flipud(PWD),contour_level); axis xy; colormap(jet);
title('Power Wigner distribution');
xlabel('time samples'); ylabel('norm. frequency');
```

A.2.2 Function prewarp_PC.m

```
function [warptimesig, M, df, dv, length2]=prewarp_PC(input,kappa);
% PREWARP_PC    Function that power warps with power kappa>1 the input time signal to
%               obtain the time signal, warptimesig. M is the number of samples in the
%               warped DFT of the input signal (before zeropadding), df is the frequency
%               sampling rate at which the input signal is assumed to be sampled, and dv
%               is the frequency sampling rate at which the warped signal is assumed to be
%               sampled. length2 is the length of warptimesig.

%  Antonia Papandreou-Suppappola March95 for power classes
%  Kyle Canfield 1991 for hyperbolic class

u = 8;          %  Set upsampling rate for DFT of input signal
L = length(input);      % Set length of input signal
N = u*L;        % Set length of zeropadded input signal
inputzero = [input zeros(size(1:N-L))];         % Initialize zeropadded input
fftinsig = fft(inputzero);        % Determine DFT of zeropadded input signal

%  Determine M, df, dv
df = 2/L;
M = 2*N/u;
dv = ( (df/u)*N/2 )^(1/kappa) / M;

%% To ensure that no aliasing occurs in the warped signal
%for m = 1:M-1,
%  test(m) = ((m+1)*dv)^(1/kappa) - (m*dv)^(1/kappa);
%  if test(m) > df
%       disp('THERE WILL BE ALIASING IN THE WARPED SIGNAL!!')
%       break
%  end
%end

%  Weight X(f) by inverse of square root of characteristic group delay function
group_delay = 0;
for count = 0:(N/2)-1
  group_delay(count+1) = kappa * (df* (count+1) )^(kappa-1);
  fftinsig(count+1) = fftinsig(count+1)/sqrt(group_delay(count+1));
end

%  Determine the samples of the warped DFT of the input signal
fftexpinsig(1) = fftinsig(1);
for count = 1:M-1
  est = ( ((count+1)*dv)^(1/kappa) )/df*u;
  estint = floor(est);
  dif = ( fftinsig(estint+1)-fftinsig(estint) )*(est-estint);
```

```
  fftexpinsig(count+1) = dif + fftinsig(estint);
end

%  Shift the samples of warped DFT of the input signal into an actual DFT form
%  and bandlimit to 1/4 of sampling rate
fftwarp=fftshift([zeros(1,M/2), fftexpinsig, zeros(1,M/2)]);
warptimesig = ifft(fftwarp);   % Find a time-domain version of the warped DFT
length2=(L/2)*4*2;
```

A.2.3 Function wd.m

```
function [W]=wd(x,NF)
%  WD  This function calculates the Wigner distribution (W) of the signal x where x must be
%         a column vector. W is a real N x NF matrix, where N=length(x).  If NF is not specified,
%         then NF = N provided that N is even; otherwise, NF = N + 1. For speed purposes,
%         NF should be a power of 2!

% Antonio H. Costa, April 2, 1992

[rows cols] = size(x);
N = length(x);
if cols ~= 1, x=x.'; end
if nargin == 1,
  if rem(N,2) == 1,
    NF = N + 1;
  else
    NF = N;
  end
elseif nargin == 2,
  if rem(N,2) == 0,
    if NF < N,
        error('Number of FFT points must be >= to the length(x)');
    end
  else
    if NF < N,
        error('Length(x) cannot be greater than the number of FFT points');
    end
  end
else
  error('Only 1 or 2 arguments allowed!...');
end
M = N - 1;
L = N / 2;
```

```
x = [zeros(L-1,1);x;zeros(L+1,1)];
q = zeros(N,N);
for j = 1:N,
  q(2:N,j) = x(j:M+j-1) .* conj(x(M+j-1:-1:j));
end
q=[q(fix(N/2)+1:N,:); zeros(NF-N,N); q(1:fix(N/2),:)];
W = 2 * fft(q);
W = real(fftswap(W));
W = flipud(W);
```

A.2.4 Function fftswap.m

```
function [r]=fftswap(A)
%  FFTSWAP        Swaps the order of the rows of matrix A.

[rows cols] = size(A); r = [A(fix(rows/2)+1:rows,:);A(1:fix(rows/2),:)];
```

A.2.5 Function unwarp_PC.m

```
function [PC_QTFR]=unwarp_PC(gg, M, df, dv, length2, kappa);
%  UNWARP_PC      % Function that transforms the time-frequency axes of the affine class
%                 QTFR of the warped signal, gg, for correct time-frequency localization to
%                 obtain the corresponding kappa power class QTFR, PC_QTFR.  M is the
%                 number of samples in the warped DFT of the  input signal (before
%                 zeropadding), df is the frequency sampling rate at which the input
%                 signal is assumed to be sampled, and dv is the frequency sampling rate
%                 at which the warped signal is assumed to be sampled. length2 is the length
%                 of the warped time signal.  Note that the affine QTFR of the warped
%                 signal has dimensions length 2 x length2 and the resulting PC_QTFR
%                 has dimensions length2/4 x length2/4.

%  Antonia Papandreou-Suppappola June95 for power classes
%  Kyle Canfield 1991 for hyperbolic class

L=length2/4; % Determine dimensions of power QTFR based on affine QTFR dimensions
start = 1; stop = L-1; % Initialize start and stop variables
```

```
% Find matrix alt with correct frequency locations of input signal components
for count=0:length2-1
  countd=count+1;     % Set up time sample counter from 1 to length2
  for count2=1:start
    count1=L-count2+1;
    alt(count1, countd)=0; % Zero out frequencies in alt not to be calculated, ones with index L
  end
  for count2=start:stop
    est=((count2*df/2)^kappa)/dv;     % Find the frequency sample on [1,M] to which
                                      % the frequency sample count2 in alt corresponds
    est=est+length2/4-M;       % Compensate for the frequency shifting done
                               % to the warped signal in PREWARP. As a result,
                               % est in on the interval [-length2/4, length2/4]
    est=est*2;     % Now est is on the interval [-length2/2, length2/2]
    est=est+length2/2;      % Now est is on the interval [0, length2] and
                            % corresponds to a frequency in gg
    estint=floor(est);       % Find the largest integer smaller than est
    est=length2-est+1;     % Correct est to correspond to the right frequency
                           % as indexed by Matlab
    estint=length2-estint+1;   % Determine two integers (estint and estint+1)
                               % between which est lies. These integers
                               % correspond to frequency samples of gg between
                               % which UNWARP will interpolate to get the
                               % correct value for the sample of interest in alt
    count1=L-count2+1; % Correct the frequency index of alt to correspond to
                       %  the indexing system used by Matlab
    alt(count1-1, countd) = 0;    % initialize the new matrix values to zero
                                  % note that countd is the current time sample
    if estint>0
      if estint<=length2    % Be sure estint is within the index limits of gg
        diff=(gg(estint-1, count+1)-gg(estint, count+1))*(est-estint);
        alt(count1-1, countd) = diff+gg(estint-1, count+1);
        % Interpolate between the two integers estint and estint+1 to find
        % the correct value for the sample of interest in alt
      end
    end
  end
end

%  Find a matrix PC_QTFR, the power QTFR, which shows the correct time and frequency
%  locations of signal components in the input signal
PC_QTFR=zeros(L,L);  %  Initialize PC_QTFR
for count1=1:L  %  time samples
  for count2=1:L  %  frequency samples
    freqcnt=L-count2+1;  % Correct the frequency index to correspond
                         %  to Matlab's indexing system; freqcnt=frequency row
```

```
    expand1=freqcnt/L;
    expand=kappa*expand1^(kappa-1);        % Determine amount to expand freqcnt
    expand=1/expand; % expand factor is inverted since time is inversely
                     % proportional with frequency relation
    arg = (count1-1)*expand+1;   % Find a sample in alt that corresponds
                                 % to the sample of interest in PC_QTFR
    intarg = floor(arg);   % Determine two integers (intarg and intarg+1)
                           % between which arg lies. These integers correspond
                           % to time samples of alt between which UNWARP will
                           % interpolate to get the correct value for the
                           % sample of interest in PC_QTFR
    if intarg>=1    % Be sure intarg is within the index limits of alt
      if intarg < length2
        diff2=(alt(count2,intarg+1)-alt(count2,intarg))*(arg-intarg);
        PC_QTFR(count2, count1) = diff2+alt(count2,intarg);
       % Interpolate between the two integers intarg, intarg+1 to find the
       % correct value for the sample of interest in PC_QTFR
      end
  end
  if intarg<1
    PC_QTFR(count2,count1)=alt(count2,1);
    % Use sample value at first time sample if intarg < 1, in which case
    % there is no sample at zero to use in interpolating between zero and one
    end
  end
end
```

A.3 MATLAB FUNCTION TO PLOT A SECTION OF THE DATA, ITS FOURIER TRANSFORM, WIGNER DISTRIBUTION, AND SPECTROGRAM (data_analysis.m)

```
function [y,Y,WD,SPEC] = data_analysis(filename,N,offset)
% DATA_ANALYSIS      Reads and plots data, computes and plots Fourier transform (FT),
%                    Wigner distribution (WD) and spectrogram. Reads N samples from
%                    filename starting at offset sample, returns the data y, its FT Y, its
%                    WD, and its spectrogram, SPEC. To start at the beginning
%                    of the data, offset is set to zero. To read all the data, omit N and
%                    offset. When all the data is read, the WD is not plotted. Instead,
%                    the data is decimated to a sampling frequency of 8,192 Hz to
%                    sound as actually recorded.
%                    The WD algorithm is not computationally efficient for N > 1024.

% Antonia Papandreou-Suppappola, 29Jan96

% Obtain the header information of the digitized file,
% read data vector y of length N and sampling rate, Fs
if nargin == 1,
  [ys,header,Fs,Ns]=loadkay(filename);
  N=length(ys);
  disp(' '); disp(header);
else
  [ys,header,Fs,Ns]=loadkay(filename,N,offset);
  disp(' '); disp(header);
end

% Reset axis
clf;subplot(111);gcf;

% To remove really low frequencies due to engine noise
b=fir1(40,0.08,'high');          % High pass filter
% To check frequency response
[h,w]=freqz(b,1,256); plot(w,abs(h));
y=conv(ys,b); y=y(20:N+20-1);

% Plot the data
Ts=1/Fs;
t=[offset:(N+offset-1)]*Ts;
subplot(411);
plot(t, y); xlabel('time, s'); ylabel('amplitude');
title(sprintf('Digitized %g data samples from %s', N, filename));
axis([offset*Ts (N+offset-1)*Ts min(y) max(y)]); figure(gcf)
```

```
%  Compute and plot the Fourier transform of the data
%  Plot only positive half of spectrum since symmetric FFT (real data)
Y=fft(y);
f=[0:((N/2)-1)]/N*Fs;
subplot(412);
plot(f,abs(Y(1:N/2))); ylabel('magnitude');
%plot(f,20*log10(abs(Y(1:N/2)))); ylabel('magnitude in dB');
xlabel('frequency in Hz'); title('Fourier transform of the data'); figure(gcf)

if N <= 1024,
  % Compute and plot the Wigner distribution provided data length is small
  WD=wd(y,N);
  WD=WD(N/2+1:N,:);        % Since real, keep only half the frequencies
  subplot(413);
  f=[0:N/2-1]/N*Fs/2;
  imagesc(t,fliplr(f),WD); title('Wigner distribution of the data')
  ylabel('frequency, Hz'); xlabel('time, s'); figure(gcf)
else
  %  Decimate to sampling frequency of 8,192 Hz to sound as actually recorded
  %  Resample data at a lower rate after lowpass filtering
  decimation_factor=round(Fs/8192);
  Dy=decimate(y,decimation_factor);
  DFs=Fs/decimation_factor; % DFs=8192;
  DTs=1/DFs;
  DN=N/decimation_factor;
  Dt=[0:(DN)]*DTs;
  subplot(413);
  plot(Dt, Dy); xlabel('time, s'); ylabel('amplitude');
  title(sprintf('Data decimated by a factor Fs/8192=%g', decimation_factor));
  figure(gcf)
end

%  Compute and plot the spectrogram of the data
%  If length of data is small, use smaller window length for better resolution
%  For clicks, use small window length (e.g. 4 or 8) since need better time res.
subplot(414)
if N <= 1024,
  SPEC=specgram(y,256,Fs,8,7);      % built-in Matlab program
else
  SPEC=specgram(y,256,Fs);
end
f=[0:N/2-1]/N*Fs;
imagesc(t,f,abs(SPEC));axis xy; colormap(jet);
title('Spectrogram of the data')
ylabel('frequency, Hz'); xlabel('time, s');
figure(gcf)
```

A.4 MATLAB FUNCTION TO COMPUTE THE PIECEWISE WIGNER DISTRIBUTION (piece_wd.m)

```
function [WD]=piece_wd(filename,N,decimation_factor,timeoffset)
%       PIECE_WD   Computes the Wigner distribution (WD) of Nwd blocks of data, each
%                  block 256 samples long such that the total section analyzed is N samples.
%                  The WDs of the various blocks are plotted consecutively. The section
%                  analyzed starts at time timeoffset. The data is first decimated by a factor
%                  decimation_factor.

%  Antonia Papandreou-Suppappola 24Feb1996

%  Load data
[ydata,header,Fs,Ns]=loadkay(filename);
disp(' '); disp(header); % Display header

% Duration of digitized cut
T=Ns/Fs; disp(' '); disp(sprintf('Signal duration in seconds: %g',T));

L=256;                          % Length of each block of Wigner distribution
Nwdmax=floor(Ns/L);             % Number of Wigner distributions to be computed for all data
Nwd=N/L;                % Number of Wigner distributions of length L that are computed

% Subtract dc value to remove initial frequencies due to recording equipment
ydata=ydata-mean(ydata);
% Highpass filter to remove really low frequencies due to engine noise
b=fir1(40,0.08,'high');
ydata=conv(ydata,b); Ndata=size(ydata);
ydata=ydata(20:Ns+20-1);      % since length increased by 40 samples

% Decimate the data to compute larger sections of WD
y=decimate(ydata,decimation_factor);
Fs=Fs/decimation_factor; Ns=Ns/decimation_factor;

%  Offset sample
offset=floor(timeoffset*Fs/L);

%  Compute the WD of each block and piece it together
WD=[];
for i=offset:(Nwd+offset)-1,
  WD=[WD wd_real(y(i*L+1:(i+1)*L))];
end

%  Plot piecewise WD
twd=[(offset*L+1):(offset+Nwd)*L]/Fs;
```

```
fwd=[0:L/2-1]/L*Fs/2; m2=max(max(WD));
imagesc(twd,fliplr(fwd),WD);axis xy; colormap(jet);
title('Piecewise Wigner distribution of the data')
ylabel('frequency, Hz'); xlabel('time, s');
hold on
for k=0:Nwd-1,
  plot([((offset+k)*L+1)/Fs ((offset+k)*L+1)/Fs], [min(fwd) max(fwd)],'red')
end
hold off

% Plot data analyzed
tsignal=[(offset*L+1):(offset+Nwd)*L]/Fs;
ysection=y(offset*L+1:(Nwd+offset)*L);
plot(tsignal,ysection);
axis([(offset*L+1)/Fs (offset+Nwd)*L/Fs min(ysection) max(ysection)])
title('Chosen section of time signal'); xlabel('time, s')

% Plot FT of data analyzed
K=L*Nwd;
fsignal=[0:K/2-1]/K*Fs;
Y=fft(y(offset*L+1:(Nwd+offset)*L));
plot(fsignal,abs(Y(1:K/2)));
title('FT of chosen section'); xlabel('frequency, Hz');

% Plot spectrogram of whole data
tspec=[1:Ns]/Fs;
fspec=[0:L/2-1]/L*Fs;
SPEC=specgram(y,256,Fs);
imagesc(tspec,fspec,abs(SPEC));axis xy; colormap(jet);
title('Spectrogram of the data')
ylabel('frequency, Hz'); xlabel('time, s');
hold on;
plot([(offset*L+1)/Fs (offset*L+1)/Fs], [min(fspec) max(fspec)],'red');
plot([(offset*L+Nwd*L)/Fs (offset*L+Nwd*L)/Fs], [min(fspec) max(fspec)],'red');
hold off

% Plot spectrogram of section of data only
tsignal=[(offset*L+1):(offset+Nwd)*L]/Fs;
f=[0:L-1]/L*Fs/2;
ysection=y(offset*L+1:(Nwd+offset)*L);
SPEC=specgram(ysection,256,Fs,64,23);
imagesc(tsignal,f,abs(SPEC));axis xy; colormap(jet);
title('Spectrogram of the section')
ylabel('frequency, Hz'); xlabel('time, s');
```

A.5 MATLAB FUNCTION TO COMPUTE VARIOUS QTFRS OF A SECTION OF THE DATA (various_tfrs.m)

```
function [WD,SPEC,PWD,SPWD,AD,PAD,power_WD,power_PWD]=various_tfrs(filename,N, offset);
% VARIOUS_TFRS  Computes various QTFRs of a block of data of length N starting at the
%               offset. The QTFRs include the Wigner distribution (WD), the spectrogram
%               (SPEC), the pseudo Wigner distribution (PWD), the smoothed pseudo
%               Wigner distribution (SPWD), the Altes Q-distribution (AD), the pseudo
%               Altes Q-distribution (PAD), the power Wigner distribution (power_WD),
%               and the power pseudo Wigner distribution (power_PWD).

%  Antonia Papandreou-Suppappola 24April1996

[y,header,Fs,Ns]=loadkay(filename,N,offset);
disp(' '); disp(header);

%  Duration of digitized cut
T=Ns/Fs;
disp(' '); disp(sprintf('Signal duration in seconds: %g',T));

%  Subtract dc offset due to recording equipment
%y=y-mean(y);
%  Highpass filter to remove really low frequencies due to engine noise
b=fir1(40,0.05,'high');
ysection=conv(y,b); ysection=ysection(20:N+20-1);

tsignal=[(offset+1):(offset+N)]/Fs;

% WD of section
f=[0:N/2-1]/N*Fs/2;
WD=wd(ysection); WD=flipud(WD);
WD=WD(N/2+1:N,:);          % Since real, keep only half the frequencies
imagesc(tsignal,f,WD);axis xy; colormap(jet);
title(sprintf('WD, filename = %s', filename))
ylabel('frequency, Hz'); xlabel('time, s');

% Spectrogram of section
f=[0:N/2-1]/N*Fs/2;
SPEC=spec(ysection,hamming(11),N);
SPEC=flipud(SPEC); SPEC=SPEC(N/2+1:N,:);
imagesc(tsignal,f,abs(SPEC));axis xy; colormap(jet);
title(sprintf('SPEC, filename = %s', filename))
ylabel('frequency, Hz'); xlabel('time, s');
```

```
% Pseudo WD of section
f=[0:N/2-1]/N*Fs/2;
PWD=pwd(ysection,hanning(11),N);
PWD=flipud(PWD); PWD=PWD(N/2+1:N,:);        % Since real, keep only half the frequencies
imagesc(tsignal,f,PWD);axis xy; colormap(jet);
title(sprintf('PWD, filename = %s', filename))
ylabel('frequency, Hz'); xlabel('time, s');

% Smoothed Pseudo WD of section
f=[0:N-1]/N*Fs/2;
SPWD=spwd(ysection,hanning(11),blackman(33),N);
SPWD=flipud(SPWD);
SPWD=SPWD(N/2+1:N,:);   % Since real, keep only half the frequencies
imagesc(tsignal,f,SPWD);axis xy; colormap(jet);
title(sprintf('SPWD, filename = %s', filename))
ylabel('frequency, Hz'); xlabel('time, s');

% Altes Q-distribution of section
input=hilbert(ysection); input=input.';          % to make data analytic
[warptimesig, M, df, dv, length2]=prewarp_HC(input);  % warp data
gg=wd(warptimesig.');          % compute WD of warped data
AD=unwarp_HC(gg, M, df, dv, length2);     % transform time and frequency axes
f=[0:N-1]/N*Fs/2;
imagesc(tsignal,f,flipud(AD));axis xy; colormap(jet);
title(sprintf('AD, filename = %s', filename))
ylabel('frequency, Hz'); xlabel('time, s');

% Pseudo Altes Q-distribution of section
input=hilbert(ysection); input=input.';          % to make data analytic
[warptimesig, M, df, dv, length2]=prewarp_HC(input); % warp data
gg=pwd(warptimesig.',hamming(11),length2);        % compute PWD of warped data
PAD=unwarp_HC(gg, M, df, dv, length2);   % transform time and frequency axes
f=[0:N-1]/N*Fs/2;
imagesc(tsignal,f,flipud(PAD));axis xy; colormap(jet);
title(sprintf('PAD, filename = %s', filename))
ylabel('frequency, Hz'); xlabel('time, s');
% Power WD of section
input=hilbert(ysection); input=input.';
kappa=2;        % kappa>1
[warptimesig, M, df, dv, length2]=prewarp_PC(input,kappa);        % warp data
gg=wd(warptimesig.');          % compute WD of warped data
power_WD=unwarp_PC(gg, M, df, dv, length2,kappa);      % transform time and frequency axes
f=[0:N-1]/N*Fs/2;
imagesc(tsignal,f,flipud(power_WD));axis xy; colormap(jet);
title(sprintf('Power %g WD, filename=%s', kappa, filename))
ylabel('frequency, Hz'); xlabel('time, s');
```

```
% Power pseudo WD of section
input=hilbert(ysection); input=input.';
kappa=2;        % kappa>1
[warptimesig, M, df, dv, length2]=prewarp_PC(input,kappa); % warp data
gg=pwd(warptimesig.',hamming(11),length2);        % compute PWD of warped data
power_PWD=unwarp_PC(gg, M, df, dv, length2,kappa); % transform time and frequency axes
f=[0:N-1]/N*Fs/2;
imagesc(tsignal,f,flipud(power_PWD));axis xy; colormap(jet);
title(sprintf('Power %g pseudo WD, filename=%s', kappa, filename))
ylabel('frequency, Hz'); xlabel('time, s')
```

A.6 MATLAB FUNCTION TO COMPUTE THE SMOOTHED PSEUDO-WIGNER DISTRIBUTION USING A DIRECT METHOD (spwd_dir.m)

```
function [SPWD] = spwd_dir(x,wf,wt)
%  SPWD_DIR      Computes the smoothed pseudo Wigner distribution (SPWD) of the time
%                domain signal x using a frequency window wf, and a time window wt. On
%                exit, the SPWD is an M x length(x) real matrix, where M is the length of
%                the longest window. The local autocorrelation function (LAF) of x
%                is first computed and then convolved with the time-smoothing window wt.
%                The LAF is updated so that the previous value can be used to compute the
%                next value. The result of the convolution then gets multiplied with the
%                squared magnitude of the frequency-smoothing window, and then the
%                Fourier transform of the product is obtained. Note that the length of the
%                windows must be smaller than that of the signal, and the length of wt must
%                be even.

%  Byeong-Gwan Iem, 21June1996; Antonia Papandreou-Suppappola, 27June1996

[rows cols] = size(x);
if cols ~= 1, x=x.'; end          % make column vector

N=length(wt); % size of window for time smoothing
M=length(wf);          % size of window for frequency smoothing
Lshift=(N-1);  % shifting amount for compensating the time delay in resulting QTFR
M1=M;
x=[x;zeros(Lshift,1)];
ndata=length(x);       % Number of samples in the time domain
wt=flipud(wt);         % Time reversal of the time domain window

if M > N       % Relocation of frequency smoothing window
  wf=[wf(fix(M/2)+1:M,1);wf(1:fix(M/2),1)];
else
  wf=[wf(fix(M/2)+1:M,1);zeros(N-M,1);wf(1:fix(M/2),1)];
  M1=N;
end
for k=1:N,
  wt1(:,k)=wt;   % Construction of window matrix by stacking the window vector
end
L=N/2;
q=zeros(N,N);  % Initialization of a block of LAF
x1=zeros(N,1);   % Initialization of a block of data
```

```
for k=1:ndata,
  q(2:N,:)=q(1:N-1,:);          % Shifting of LAF for updating it
  %  Calculation of local correlation vector at current time index
  x1=[x(k,1);x1(1:(N-1),1)];
  x2=[zeros(L-1,1);x1;zeros(L+1,1)];
  q(1,2:N)=conj(x2(L:1:(N+L-2))').*x2((N+L-2):-1:L)';
  %  Time domain smoothing
  q1=conj(sum(q.*wt1)');      % Convolution at current time index
  if N < M,
    q1=[q1(fix(N/2)+1:N,:);zeros((M-N),1);q1(1:fix(N/2),:)];
  else
    q1=[q1(fix(N/2)+1:N,:);q1(1:fix(N/2),:)];
  end
  %  Frequency domain smoothing
  q1 = q1.*(wf.^2);
  C = 2*fft(q1); C = real(fftswap(C));
  C1(:,k) = C(M1/2+1:M1);   % To only keep the high frequencies for real data
end
C1=[C1(:,Lshift:ndata) C1(:,1:(Lshift-1))];  % compensating for the time delay
SPWD=[C1(:,1:(ndata-Lshift))];       % compensating for the end effect
```

A.7 MATLAB FUNCTIONS TO COMPUTE THE SMOOTHED PSEUDO-WIGNER DISTRIBUTION USING THE SHORT-TIME TECHNIQUE

A.7.1 Function stafcet.m

```
function [SPWD] = stafcet(filename,decimation_factor,timeoffset,L,freq_window,time_window)
%  STAFCET        Computes the short-time smoothed pseudo-Wigner distribution (SPWD)
%                 using the short-time ambiguity function (STAF). It computes the
%                 ambiguity function of the windowed data, multiplies it with the fixed
%                 kernel, takes two-dimensional FFT, and keeps only the time-slice at the
%                 center of the windowed data for the resulting QTFR. The resulting QTFR
%                 has dimensions (Nw x N/Nw) where N is the data length, and Nw is length
%                 of the rectangular window used to segment the data. The sound data is
%                 decimated by a factor decimation_factor. The data starts at time timeoffset
%                 and has length L. The frequency  window of the SPWD is freq_window,
%                 and the time window of the SPWD is time_window.

% Antonia Papandreou-Suppappola, 17July1996

[y,header,Fs,Ns]=loadkay(filename);
disp(' '); disp(header);

T=Ns/Fs;        % Duration of digitized cut
disp(' '); disp(sprintf('Signal duration in seconds: %g',T));
t_y=[1:Ns]/Fs; plot(t_y, y);

% Highpass filter to remove low frequencies due to engine noise
b=fir1(40,0.05,'high');
y=conv(y,b); y=y(20:Ns+20-1);   %  since length of y increased by 40 samples

ydec=decimate(y,decimation_factor);   %  Decimate the data to reduce number of samples
Fsdec=Fs/decimation_factor; Nsdec=length(ydec);
%t_ydec=[1:Nsdec]/Fsdec; plot(t_ydec,ydec); specgram(ydec,256,Fsdec);

% Choose a section, starting at timeoffset secs
offset=floor(timeoffset*Fsdec);
tsection=[(offset+1):offset+L]/Fsdec;
ysection=ydec(offset+1:offset+L);     % From decimated signal
duration_signal_analyzed=max(tsection)-min(tsection);

% Start computation of short-time SPWD
Nw=256;   % length of windowed signal
time_sections=floor(L/Nw);    % number of signal sections
```

```
% examples of windows for SPWD
%freq_window=hamming(140); time_window=blackman(121);
%ker_WD=ones(Nw,Nw); % Compute Wigner distribution kernel
ker_SPWD=kerspwd(Nw,Nw,freq_window,time_window); % Compute SPWD kernel

for i=1:time_sections,
  ywindow=ysection((i-1)*Nw+1:i*Nw);    % shift rectangular window to segment data
  twindow=(i-1)*Nw+1:i*Nw;              % section of time covered
  % plot(twindow,abs(ywindow))
  AFwindow=af(ywindow);    % Compute AF of windowed data, STAF
  AFproduct=AFwindow.*ker_SPWD; % Obtain STAF and kernel product
  SPWD(:,i)=aftowd_section(AFproduct);  % Compute 2-D FFT and keep only center time of
window
end
SPWD=SPWD(Nw/2+1:Nw,:);        % For real data, keep only positive frequencies
f=[0:Nw/2-1]/Nw*Fsdec/2;  % frequency range depending on Fsdec
t=Nw/2:Nw:L-Nw/2;             % each time slice is the center of the xsection

% To obtain an image plot of the SPWD
m2=max(max(SPWD)); contour(tsection,f,flipud(SPWD),[0.1*m2:0.2*m2:0.9*m2]);
imagesc(tsection,fliplr(f),flipud(SPWD));axis xy; colormap(jet);
title(sprintf('SPWD, filename = %s', filename)); ylabel('frequency, Hz'); xlabel('time, s');
```

A.7.2 Function kerspwd.m

```
function [ker]=kerspwd(Ntau,Nnu,h,g)
%      KERSPWD    Computes the smoothed pseudo-Wigner distribution (SPWD) kernel in the
%                 ambiguity domain. ker is a Nnu x Ntau matrix with entries given by
ker(v,g) =
%                 n(g/2) * conj(n(-g/2)) * G(v) where G(v) represents the Fourier transform
of
%                 window function g, and h is a window function.

% Antonio H. Costa, March 13, 1993

ker=kerpwd(Ntau,Nnu,h); Lx=Ntau; Lg=length(g); Ng=(Lg - 1)/2; Nx=Lx / 2;
gx=zeros(Lx,1); gx(1:Ng+1)=g(Ng+1:Lg); gx(Lx-Ng+1:Lx)=g(1:Ng); gg=fft(gx);
gg=fftshift(gg);
for i = 1:Ntau,
  ker(:,i) = ker(:,i).*gg;
end
```

A.7.3 Function kerpwd.m

```
function [ker]=kerpwd(Ntau,Nnu,h)
%  KERPWD        Computes the pseudo Wigner distribution (PWD) kernel in the ambiguity
%                domain. ker is a Nnu x Ntau matrix with entries given by ker(v,g) = n(g/2)
%                * conj(n(-g/2)). h is the window function.

% Antonio H. Costa, March 13, 1993

h = h .* conj(h(length(h):-1:1)); Lh = length(h); Nh = round((Lh - 1) / 2); Nx = Ntau / 2;
hx = zeros(Ntau,1); hx(Nx - Nh + 1:Nx - Nh + Lh) = h; ker = zeros(Nnu,Ntau);
for j = 1:Nnu,
  ker(j,:) = hx.';
end
```

A.7.4 Function af.m

```
function [A]=af(x,NF)
% AF  This function calculates the ambiguity function (AF) of the signal x where x must be a
%     column vector. A is a complex NF x N matrix, where N=length(x). If NF is not specified,
%     then NF=N, provided that N is even; otherwise, NF=N+1. For speed purposes, NF should
%     be a power of 2!

% Antonio H. Costa, March 13, 1993

N = length(x); [rows cols] = size(x);
if cols ~= 1, x=x.'; end
if nargin == 1,
  if rem(N,2) == 1,
    NF = N + 1;
  else
    NF = N;
  end
elseif nargin == 2,
  if rem(N,2) == 0,
    if NF < N,
      error('Number of FFT points must be >= to the length(x)');
     end
  else
    if NF < N,
      error('Number of FFT points must be larger than length(x)');
     end
  end
else
```

```
  error('Only 1 or 2 arguments allowed!...');
end
M = N - 1; L = N / 2; x = [zeros(L-1,1);x;zeros(L+1,1)]; q = zeros(N,N);
for j = 1:N,
  q(2:N,j) = x(j:M+j-1).*conj(x(M+j-1:-1:j));
end
q=[q(:,N/2+1:N) zeros(N,NF-N) q(:,1:N/2)];
A = 2 * fft(q.',NF); A = fftswap(A); A = flipud(A);
```

A.7.5 Function aftowd_section.m

```
function [Wsection] = aftowd_section(A)
% AFTOWD_SECTION     Computes the two-dimensional FFT of A for only one time slice.
%                    The matrix A should be viewed as having "time lag" increasing as
%                    one progresses along each column, with column 1 representing
%                    time lag -K where K equals the number of columns of A.

%  Antonia Papandreou-Suppappola, 7July1996
%  Antonio H. Costa, March 13, 1993

[rows cols] = size(A);
if rows > cols,
  k = (rows - cols) / 2;
  A = [zeros(rows,k) A zeros(rows,k)];
end
A = fftshift(A);
A = fft(A.',rows);      % Take FT of each row
A = A.'; A = flipud(A);
W = ifft(A); W = W.'; W = flipud(W); W = real(W);
W = fftswap(W); W = fftswap(W.'); W = W.';
if rows > cols,
  W = W(:,k+1:k+cols);
end
W=fftswap(flipud(W));
Wsection=W(:,cols/2);   % keeping only the center time slice
```

A.8 MATLAB FUNCTION TO COMPUTE THE SMOOTHED PSEUDO-ALTES Q-DISTRIBUTION USINGTHE SHORT-TIME TECHNIQUE (hcstafcet.m)

```
function [SPAD] = hcstafcet(filename,decimation_factor,timeoffset,L,freq_window,time_window)
%    HCSTAFCET     Computes the hyperbolic class smoothed pseudo-Altes Q-distribution (SPAD)
%                  by hyperbolically warping the signal, computing Cohen's class smoothed
%                  pseudo-Wigner distribution (SPWD) of the warped signal, and transforming the
%                  axes for correct time-frequency localization. When the axes are transformed, only
%                  the time-slice at the center of the windowed data for the resulting QTFR is
%                  kept. The resulting SPAD has dimensions (Nw x N/Nw) where N is the length of
%                  the data, and Nw is length of the rectangular window used to segment the data.
%                  The sound data is decimated by a factor decimation_factor. The data to be
%                  analyzed starts at time timeoffset and has length L. The frequency window of the
%                  SPWD is freq_window, and the time window of the SPWD is time_window.

%  Antonia Papandreou-Suppappola, 27July1996

[y,header,Fs,Ns]=loadkay(filename);
disp(' ');disp(header);

% Duration of digitized cut
T=Ns/Fs; disp(' '); disp(sprintf('Signal duration in seconds: %g',T));
%t_y=[1:Ns]/Fs; plot(t_y, y);

% Highpass filter to remove low frequencies due to engine noise
b=fir1(40,0.05,'high');
y=conv(y,b); y=y(20:Ns+20-1); % since length of y increased by 40 samples

% Decimate the data to reduce number of samples
ydec=decimate(y,decimation_factor);
Fsdec=Fs/decimation_factor; Nsdec=length(ydec);
%t_ydec=[1:Nsdec]/Fsdec; plot(t_ydec,ydec); specgram(ydec,256,Fsdec);

% Choose a section, starting at timeoffset secs
offset=floor(timeoffset*Fsdec);
tsection=[(offset+1):offset+L]/Fsdec;
ysection=ydec(offset+1:offset+L);        % From decimated signal
duration_signal_analyzed=max(tsection)-min(tsection);

% Start computation of short-time SPAD
Nw=128;   % length of windowed signal
time_sections=floor(L/Nw); % Number of signal sections

% Examples of SPWD windows of warp signal
%freq_window=hamming(158); time_window=blackman(145);
ker_SPWD=kerspwd(Nw*4,Nw*4,freq_window,time_window);

for i=1:time_sections,
  ywindow=ysection((i-1)*Nw+1:i*Nw);          % shift rectangular window to segment data
  %twindow=(i-1)*Nw+1:i*Nw; plot(twindow,abs(ywindow));   % section of time covered
  [warptimesig, M, df, dv, length2]=prewarp_HC(ywindow.'); % warp signal
```

```
  % gg=wd(warptimesig);   % For Altes Q-distribution
  mm=af(warptimesig);C=mm.*ker_SPWD;gg=aftowd(C); % SPWD of warped signal
  % Keep positive frequencies and center time, and transform axes
  SPAD(:,i)=unwarp_HCsection(gg, M, df, dv, length2);
end
f=[0:Nw/2-1]/Nw*Fsdec/2; % frequency range depending on Fsdec
imagesc(tsection,f,flipud(SPAD));axis xy; colormap(jet);
title(sprintf('SPAD, filename = %s', filename))
ylabel('frequency, Hz'); xlabel('time, s');          % Max frequency is Fs/dec_factor/4
```

A.9 MATLAB FUNCTION TO COMPUTE THE κ TH POWER SMOOTHED PSEUDO-WIGNER DISTRIBUTION USING THE SHORT-TIME TECHNIQUE (pcstafcet.m)

```
function [PSPWD] = pcstafcet(filename,decimation_factor,timeoffset,L,kappa,freq_window,time_window)
%    PCSTAFCET      Computes the kappa power smoothed pseudo-Wigner distribution (PSPWD) of
%                   the power class by power warping the signal, computing Cohen's class smoothed
%                   pseudo-Wigner distribution (SPWD) of the warped signal, and transforming the
%                   axes for correct time-frequency localization. When the axes are transformed, only
%                   the time-slice at the center of the windowed data for the resulting QTFR is kept.
%                   The resulting PSPWD has dimensions (Nw x N/Nw) where N is the length of the
%                   data, and Nw is the length of the rectangular window used to segment the data.
%                   The sound data is decimated by a factor decimation_factor. The data to be
%                   analyzed starts at time timeoffset and has length L. The frequency window of the
%                   SPWD is freq_window, and the time window of the SPWD is time_window.

%  Antonia Papandreou-Suppappola, 17Oct1996

[y,header,Fs,Ns]=loadkay(filename);
disp(' '); disp(header);

% Duration of digitized cut
T=Ns/Fs; disp(' '); disp(sprintf('Signal duration in seconds: %g',T));
%t_y=[1:Ns]/Fs; plot(t_y, y);

% Highpass filter to remove low frequencies due to engine noise
b=fir1(40,0.05,'high');
y=conv(y,b); y=y(20:Ns+20-1); % since length of y increased by 40 samples

% Decimate the data to reduce number of samples
ydec=decimate(y,decimation_factor);
Fsdec=Fs/decimation_factor; Nsdec=length(ydec);
%t_ydec=[1:Nsdec]/Fsdec; plot(t_ydec,ydec); specgram(ydec,256,Fsdec);

% Choose a section, starting at timeoffset secs
offset=floor(timeoffset*Fsdec);
tsection=[(offset+1):offset+L]/Fsdec;
ysection=ydec(offset+1:offset+L);        % From decimated signal
duration_signal_analyzed=max(tsection)-min(tsection);

% Start computation of short-time power smoothed pseudo Wigner distribution
Nw=128;                          % length of windowed signal
time_sections=floor(L/Nw);       % Number of signal sections

% Examples of SPWD windows of warp signal
%freq_window=hamming(158); time_window=blackman(145);
ker_SPWD=kerspwd(Nw*4,Nw*4,freq_window,time_window);

for i=1:time_sections,
  ywindow=ysection((i-1)*Nw+1:i*Nw);          % shift rectangular window to segment data
  %twindow=(i-1)*Nw+1:i*Nw; plot(twindow,abs(ywindow)); % section of time covered
  [warptimesig, M, df, dv, length2]=prewarp_PC(ywindow.',kappa); % warp signal
```

```
  % gg=wd(warptimesig);   % For power Wigner distribution
  mm=af(warptimesig);C=mm.*ker_SPWD;gg=aftowd(C); % SPWD of warped signal
  % Keep positive frequencies and center time, and transform axes
  PSPWD(:,i)=unwarp_PCsection(gg, M, df, dv, length2);
end
f=[0:Nw/2-1]/Nw*Fsdec/2; % frequency range depending on Fsdec
imagesc(tsection,f,flipud(PSPWD));axis xy; colormap(jet);
title(sprintf('PSPWD, filename = %s', filename))
ylabel('frequency, Hz'); xlabel('time, s');   % Max frequency is Fs/dec_factor/4
```

INITIAL DISTRIBUTION LIST

Addressee	No. of Copies
Office of Naval Research (ONR 342 - R. Gisiner)	1
Arizona State University (Dr. A. Papandreou-Suppappola)	1
Defense Technical Information Center	2
Center for Naval Analyses	1